Separation and Purification Technology 276 (2021) 119363

Contents lists available at ScienceDirect

Separation and Purification Technology

journal homepage: www.elsevier.com/locate/seppur

Absorption separation of fluorinated refrigerant gases with ionic liquids: Equilibrium, mass transport, and process design

Salvador Asensio-Delgado, Fernando Pardo, Gabriel Zarca, Ane Urtiaga *

Department of Chemical and Biomolecular Engineering, Universidad de Cantabria, Av. Los Castros 46, Santander 39005, Spain

ARTICLE INFO

Keywords:
Hydrofluorocarbons
Hydrofluoroolefins
Ionic liquids
Solubility
Diffusivity
Membrane separation

ABSTRACT

Interest in recovering and reclaiming refrigerant gases is growing as a consequence of increasing concern about the high global warming potential of some hydrofluorocarbons (HFCs). However, advanced separation processes, like extractive distillation, are required to selectively separate azeotropic and close-boiling refrigerant mixtures. In this regard, ionic liquids (ILs) arise as promising entrainers because of their favorable properties, including nonvolatility and good HFC solubility selectivity. The aim of this review is to become a reference text for the research and design of novel separation processes for mixtures of fluorinated gases based on the use of ILs. We include an extensive compilation of publications on equilibrium, mass transport, and absorption and membrane separation related to the use of ILs to selectively separate, not only the most relevant refrigerants employed nowadays, namely, HFCs, hydrofluoroolefins, and hydrochlorofluoroolefins, but also other relevant refrigerant families, such as chlorofluorocarbons, hydrochlorofluorocarbons, and perfluorocarbons. The UC-RAIL database provided as Supplementary Information compiles more than 5000 data points that are comprehensively analyzed in the review focusing on process design. Finally, we provide a set of directions that lead to the recovery of fluorinated refrigerant gases, to shift the refrigeration and air conditioning sector towards a more circular economy.

1. Introduction

Hydrofluorocarbons (HFCs) are synthetic compounds used primarily as refrigerant gases, but also as foam blowing agents, aerosols, and fire extinguishers [1,2]. The HFC family of refrigerants rapidly universalized after ratification of the Montreal Protocol (1987), an international agreement aimed at avoiding the depletion of stratospheric ozone by phasing out the use of chlorofluorocarbons (CFCs) and hydrochlorofluorocarbons (HCFCs) [3–5].

The implementation of HFCs in various sectors of the refrigeration and air conditioning (RAC) market led to a consequent increase in their emissions to the atmosphere. Fig. 1 presents a summary of the data collected from inventory reports published recently by the US and European Union environmental agencies, considering the main sources of HFC emissions, among which refrigeration and air conditioning applications clearly predominate [6,7].

Despite their zero ozone depletion potential (ODP), HFCs are still greenhouse gases (GHGs) of very high concern, with global warming potential (GWP) values of up to 12,400 CO_2 equivalents. The contribution of HFCs to global GHG emissions was estimated as being 0.46, 0.73, and 1.1 Gt CO_2-eq in 2005, 2010, and 2015, respectively [8]. In fact, while the average emissions of all other GHGs decreased in the European Union between 1990 and 2018, fluorinated gases were the only group whose emission increased, up to 77.6% [9]. Furthermore, different scenarios predict a further rise of HFCs global emissions up to more than 8 Gt CO_2-eq·yr^{-1} by 2050, if mitigation or abatement policies are not enacted [10].

The international consensus on the negative contribution of HFCs to climate change led to the promulgation of the Kigali Amendment to the Montreal Protocol (2016), a global agreement aimed at reducing emissions of fluorinated gases. The Kigali Amendment defined a schedule for phasing down the production and consumption of HFCs by 85% of the 2011–2013 average by the late 2040s [11,12]. In line with this, some regions and nations have already implemented regulations for meeting the objectives of this agreement. For example, the European F–Gas Regulation (EU 517/2014) aims to achieve a 79% reduction in the 2009–2012 HFC sales by 2030 [13], and the USA has implemented incentive credits for the use of low-GWP refrigerants according to the US

* Corresponding author.
E-mail address: urtiaga@unican.es (A. Urtiaga).

https://doi.org/10.1016/j.seppur.2021.119363
Received 26 May 2021; Received in revised form 23 July 2021; Accepted 23 July 2021
Available online 26 July 2021

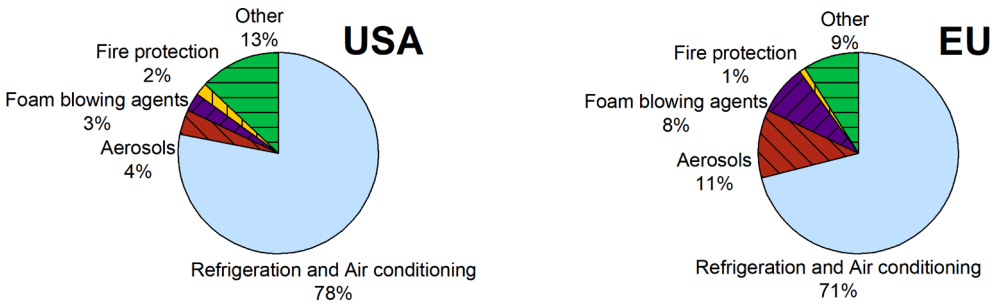

Fig. 1. Main sources of F-gases emissions in the USA and the European Union in 2018. This figure has been produced using data collected from references [6] and [7].

Environmental Protection Agency's Significant New Alternatives Policy (SNAP). Other countries, including Australia, Norway, Switzerland, and Turkey, have also put into effect new policies that will enable full compliance with the requirements of the Kigali Amendment [8]. Most of these rules define stages of progressive restrictions that are adapted to HFC applications and GWP. Fig. 2 summarizes the prohibitions for introducing HFCs into the European market [13,14]. As can be seen, from 2020 on, movable air-conditioning equipment and foams must contain refrigerants with a maximum GWP of 150, and stationary and commercial use equipment cannot contain with a GWP of more than 2500.

These limitations on the use of HFCs have drastically affected refrigeration, air conditioning, and heat pump (RACHP) equipment, as well as foam and aerosol production, and, in the short term, new low-GWP refrigerants are being adopted to substitute the high-GWP HFC blends [15]. It is clear, therefore, that low GWP is a new environmental constraint that must be considered in the formulation of refrigerants in addition to ODP, flammability, stability, energy efficiency, and system complexity [4,16,17]. In response to this need, hydrofluoroolefins (HFOs) have emerged as a new family of refrigerants with zero ODP and very low GWP. HFO molecules have a carbon–carbon double bond that increases their reactivity, reducing their atmospheric lifetimes and, thus, their GWP. Unfortunately, the greater reactivity also translates into slightly increased flammability [3,4]. Hydrochlorofluoroolefins (HCFOs) are also considered for the same reasons as HFOs, with the caveat of their small ODP, as the molecule contains chlorine. At present, there is no pure compound that satisfies all these constraints simultaneously, for which reason new refrigerants are actually formed by mixing HFCs with moderate GWP and HFOs, sometimes even including small proportions of hydrocarbons and CO_2 [18].

In addition, the new regulations establish a new paradigm in the RACHP sector by including the term "reclamation" of fluorinated refrigerants, referring to the reprocessing of a fluorinated greenhouse gas recovered during maintenance or prior to disposal, to match the equivalent performance of a virgin substance [13]. Therefore, recovering the HFC blends from end-of-life equipment and separating these into their pure components allows the reuse of those with lower environmental impacts in new, more eco-friendly blends. Furthermore, some of these HFC/HFO blends that have recently been introduced into the RAC market will be short-lived because of the staggered reduction in the

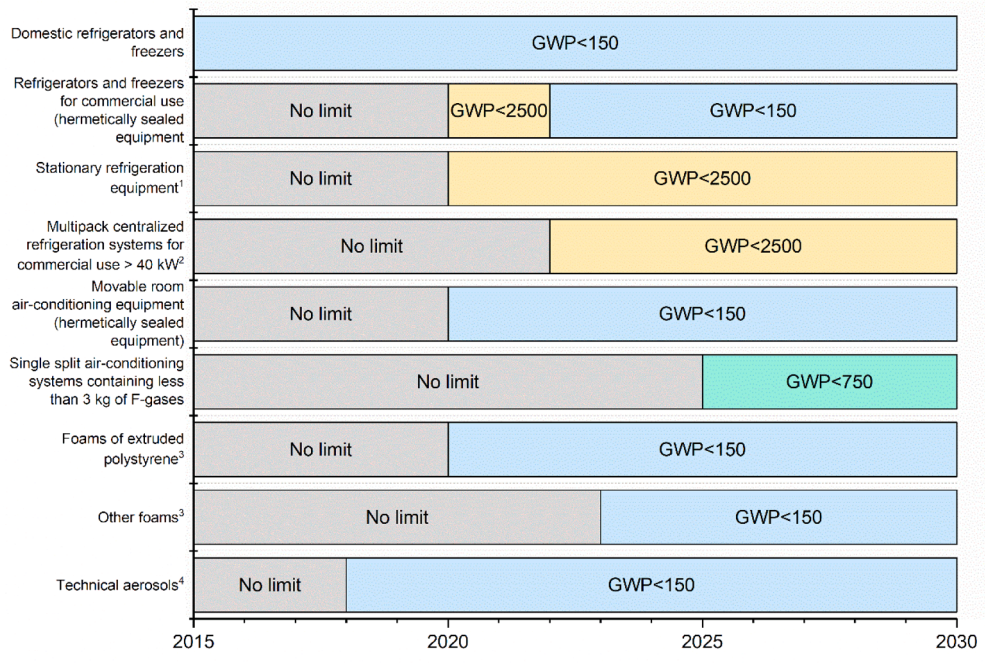

Fig. 2. Prohibitions on HFCs market placing in the European Union. This figure has been prepared with data collected from reference [13].

GWP limits established by some regulations. The recovery, reclamation and reuse of refrigerants is a promising approach that increases their lifetime while minimizing the amount of new HFCs introduced into the market and their subsequent release to the atmosphere, shifting the RACHP market towards a more circular economy.

However, separating most refrigerant blends using conventional gas separation processes like distillation is not straightforward, as these are close-boiling mixtures that often exhibit azeotropic behavior, as shown in Section 3 [19]. For these systems, only advanced separation processes present a real alternative for recovering refrigerant blends. In this context, absorption in liquid entrainers, adsorption on particulate materials, and membrane separation technologies emerge as candidates for separating fluorocarbon mixtures. A recent review analyzed the use of metal organic frameworks (MOFs) as adsorbent materials [20], and there is some pioneering work on the use of polymer membranes [21,22]. However, it is absorption in ionic liquids (ILs) that has attracted the most research attention. ILs are compounds comprising highly asymmetric cations and anions, and these have attracted attention in many different fields, including separation [23,24], synthesis and catalysis [25,26], energy [27], analytical applications [28], and as building blocks for advanced materials [29]. Their unique properties explain their spread among so many disciplines, including the separation and recovery of refrigerant compounds from mixtures: they present good chemical and thermal stability, they are non-flammable, have a wide liquid range, the ability to solubilize both polar and nonpolar compounds through various mechanisms, and they have negligible vapor pressure [30,31]. In the design of absorption or extractive distillation processes, the use of ILs is advantageous as there are no trace amounts of these in the distillate, the bottoms stream can be easily regenerated, and the selectivity of the separation is potentially high if the cation–anion combination is carefully selected to suit the mixture of interest [32].

Given the level of interest in developing novel separation processes for refrigerant mixtures, this review comprehensively analyzes the research carried out over the last two decades in terms of the absorption of different fluorocarbon gases (F-gases) into ILs. Knowing the vapor–liquid equilibrium (VLE) of the systems of interest is crucially important for the design of refrigerant separations using advanced absorption and extractive distillation processes. Moreover, other properties like mixture viscosity and gas diffusivity have important effects on process operation, as these can determine whether equilibrium is reached, therefore impacting the equipment sizing and the operating costs of a real separation facility. For that reason, this review includes a number of studies that consider these mass transport properties. In summary, we provide a complete compilation and analysis of equilibrium and transport data for a wide number of F-gas—IL systems containing 4444 vapor–liquid equilibrium points (193 absorption pairs formed by 52 ILs and 26 F-gases), 86 vapor–liquid-liquid equilibrium (VLLE) points (25 absorption pairs formed by 3 ILs and 16 gases), 908 diffusion coefficients (81 absorption pairs formed by 31 ILs and 14 F-gases), and 249 mixture viscosity points (4 systems). All these data are collected in the extensive UC-RAIL (Refrigerant Absorption in Ionic Liquids) database provided as Supplementary Information.

The review is organized as follows: firstly, we explain the refrigerant coding system with considerations regarding gas mixture characteristics followed by a general classification of the phase behavior of refrigerant systems and their separation challenges. After that, we present and analyze F-gas—IL equilibrium and mass transport experimental data. Finally, the solubility selectivity of ILs is assessed using the Regular Solution Theory to determine the ideal characteristics an IL should have to yield efficient separations, and we review examples of recovery systems that could be used to introduce a circular economy model to the refrigerant market, including the use of ILs with polymer materials in membrane technology.

2. Fluorinated refrigerants

2.1. Pure compounds

Refrigerant fluids are designated according to the American Society of Heating, Refrigerating and Air-Conditioning Engineers (ASHRAE) [3,33]. Fig. 3 describes the ASHRAE code used to name refrigerants, in which four figures describe the molecular structure, followed by letters that distinguish between isomers. The first digit is the number of unsaturated bonds in the molecule, the second is the number of carbon atoms minus one, the third is the number of hydrogen atoms plus one, and the last digit accounts for the number of fluorine atoms. Chlorine atoms, if any, are calculated from the available carbon bonds after subtracting the number of fluorine and hydrogen atoms present in the molecule. For instance, R22 is a one-carbon molecule with two fluorine atoms, one hydrogen atom, and one chlorine atom, i.e., R22 stands for chlorodifluoromethane. In the event that the molecule has atoms of other elements, the refrigerant code indicates the element and the number of atoms at the end [34]. For example, this review includes information on bromodifluoromethane, whose refrigerant name is R22B1 (notice that the letter is just “B” instead of “Br” for its chemical symbol).

Isomer designations depend on the molecule chain length. In the case of ethane-based molecules, no letter at the end of the name refers to the most symmetrical molecule in terms of the distribution of mass around each carbon atom. For instance, 1,1,2,2-tetrafluoroethane is R134, while R134a designates 1,1,1,2-tetrafluoroethane. The isomer coding becomes more complicated for longer chain molecules, with different letters depending on the carbon segment substitution as shown in Table 1 [3]. Table S1 in the Supplementary information gives the list of gases in this review including their name, code, and chemical formula.

Other considerations include the safety classification of refrigerants. F-gases are nontoxic, so they receive the letter A. Moreover, the flame propagation behavior of refrigerants means they are nonflammable, low flammable, and mildly flammable compounds (designated as A1, A2L, and A2, respectively). As a reference point, HFO R1234ze(E), classified as A2L, requires approximately 250 000 times more energy to ignite than its equivalent hydrocarbon [3].

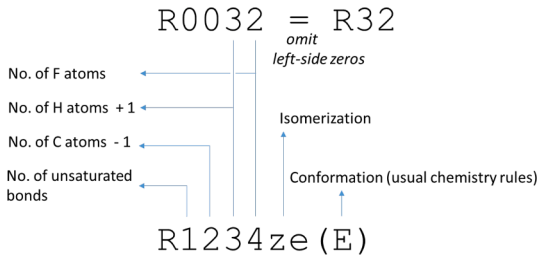

Fig. 3. ASHRAE refrigerant code system.

Table 1
ASHRAE designations for isomer differentiation.

Segment	Letter	Segment	Letter
CCl_2	a	$CHCl_2$	n
CClF	b	CH_2Cl	o
CF_2	c	CHF_2	p
CHCl	d	CH_2F	q
CHF	e	CHClF	r
CH_2	f	CH_3	s
CCl_3	j	C	t
CCl_2F	k	CCl	x
$CClF_2$	l	CF	y
CF_3	m	CH	z

Table 2
Selection of some common commercial refrigerant blends.

ASHRAE mixtures		ASHRAE safety classification	GWP	Application	Composition (wt%)					
					R32	R143a	R134a	R125	R1234yf	R1234ze(E)
Phase-out subject mixtures	R404A	A1	3922	medium and low temperature commercial refrigeration		52.0	4.0	44.0		
	R407C	A1	1774	air-conditioning units heat-pumps, chillers, industrial and commercial medium temperature refrigeration	23.0		52.0	25.0		
	R410A	A1	2088	air-conditioning units heat pumps; cold storage; industrial and commercial and low temperature refrigeration	50.0			50.0		
	R507A	A1	3985	medium and low temperature commercial refrigeration		50.0		50.0		
Alternative blends	R447A	A2L	583	replacement for R410A in stationary air-conditioners	68.0			3.5		28.5
	R448A	A1	1387	non-flammable replacement for R404A in low and medium temperature commercial and transport refrigeration	26.0		21.0	26.0	20.0	7.0
	R449A	A1	1397	non-flammable replacement for R404A in low and medium temperature commercial and transport refrigeration	24.3		25.7	24.7	25.3	
	R452B	A2L	698	replacement for R410A in chillers	67.0			7.0	26.0	
	R454A	A2L	239	replacement for R404A in low and medium temperature commercial refrigeration	35.0				65.0	
	R454B	A2L	466	replacement for R410A	68.9				31.1	
	R454C	A2L	148	replacement for R404A in low and medium temperature commercial refrigeration (hermetic units)	21.5				78.5	
	R513A	A1	631	non-flammable replacement for R134a in medium temperature commercial refrigeration and chillers			44.0		56.0	

2.2. Refrigerant mixtures

Nowadays, most refrigeration systems employ F-gas mixtures. ASHRAE classifies refrigerant blends as zeotropic mixtures, codified as the 400 series, and azeotropic mixtures, with code numbers in the 500 series. For all mixtures, the numeric code is followed by an uppercase letter denoting the different mixture compositions of the same refrigerant compounds [33]. However, for separation purposes, it should be noted that a mixture of compounds belonging to the series 400 may also present azeotropic behavior with a different composition. One example of this is R410A, an equimass mixture of R32 and R125 with an azeotropic point at 92 mol % of R32.

Table 2 is a list of some of the most important third- and fourth-generation mixtures of fluorinated refrigerants together with their ASHRAE safety classification and composition. As can be seen, binary, ternary, quaternary, and even more complicated mixtures exist currently. New mixture formulations that are being introduced into the market include HFOs (namely, R1234yf and R1234ze(E)), driven by the need to reduce the GWP of refrigerants and achieve higher refrigeration efficiencies, whereas the proportion of high-GWP HFCs, such as R125, is dropping [35]. Further insights can be extracted from Table 2, where it can be seen that when blending HFOs with the HFCs R134a and R125, the resulting mixtures have no flame propagation (A1 safety classification) but at the expense of achieving only a moderately reduced GWP. On the other hand, blending HFOs and R32 provides mixtures with a significantly lower GWP than the phased-out HFC mixtures, yet with low flammability (A2L) [4]. In addition, the presence of HFCs such as R32, R134a, and R125 in new blends highlights the importance of recovering compounds from end-of-life equipment as a way of reducing the environmental impact of this sector and advancing towards a sustainable production and consumption model in harmony with current environmental protection and GWP mitigation policies.

3. Mixture separation challenges

Refrigerant mixtures show different behaviors in their VLE. Usually, the RACHP sector leans towards the design of azeotropic (R500 series) and near-azeotropic blends because in refrigeration systems these mixtures behave as if they were pure fluids [19]. Although R400 series blends are near-azeotropic mixtures, they exhibit a very low temperature glide, that is, the difference in the dew and bubble points of the mixture is very narrow at a constant pressure. In addition to their pure-fluid behavior, another advantage of using azeotropic or near-azeotropic blends is that their heat transfer coefficients are higher than those of zeotropic mixtures [36]. Furthermore, in the event of leaks during the operation of a refrigeration system, zeotropic mixtures undergo compositional changes that can decrease the efficiency of the cycle [37–39]. In general, refrigeration systems with azeotropic mixtures use less energy, and have higher refrigeration capacity and a better coefficient of performance [40].

Overall, using the best refrigerants for RACHP equipment is disadvantageous for the recycling and recovery of individual gases from the mixture because their behavior is very close to that of a single fluid. In this article, we classify the phase behavior of binary refrigerant mixtures into five different types posing separation challenges of increasing difficulty. This classification does not intend to describe the global phase behavior [41], as its purpose is to provide a simplified view of the separation requirements of the refrigerant mixtures. For a clear explanation, Fig. 4 shows the pressure-molar fraction diagram of five representative binary mixtures of the third-generation HFC commercial blends that are to be phased out. Other examples that appear with the launch of HFOs in the market are also disclosed. Two lines represent each mixture, describing the pressure dependence of the liquid- and vapor-phase composition at a fixed temperature. The different behaviors are described below:

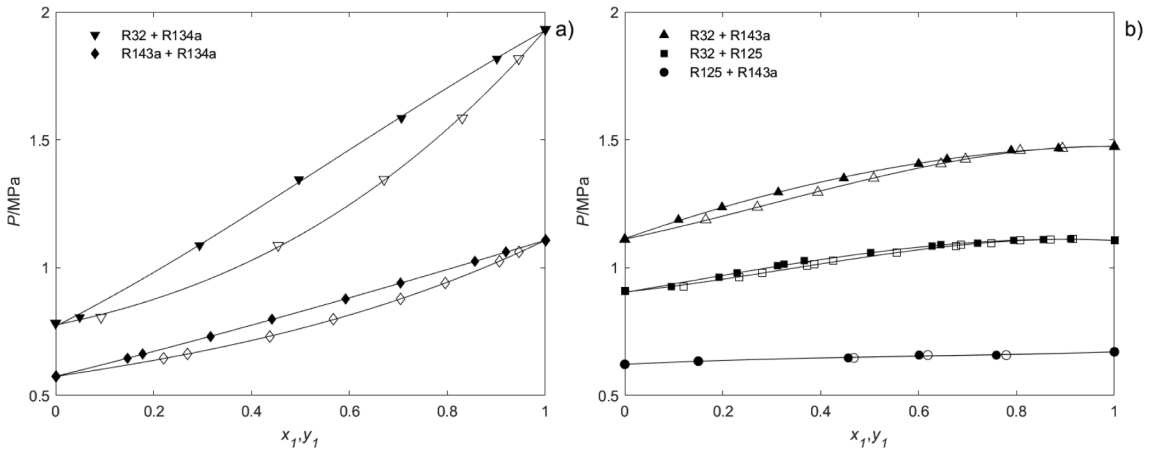

Fig. 4. Examples of vapor–liquid equilibrium behaviors of third-generation refrigerant mixtures. Type 1: R32 (1) + R134a (2) at 303 K (▼), Type 2: R143a (1) + R134a (2) at 293 K (◆), Type 3: R32 (1) + R143a (2) at 293 K (▲), Type 4: R32 (1) + R125 (2) at 275 K (■), and Type 5: R125 (1) + R143a (2) at 273 K (●). Filled and empty symbols are the molar liquid and vapor phase composition, respectively [42,44,45,50,55].

1. Zeotropic mixtures with a high temperature glide. These mixtures are easy to separate using conventional vapor–liquid equilibrium technologies, as the phase change significantly increases the proportion in which one of the components is found with respect to the other. Fig. 4a shows the VLE of the system R32 + R134a, and other examples of interest are the systems R32 + R1234ze(E) and R134a + R125 [42–44].
2. Zeotropic mixtures with a very low temperature glide. These close-boiling mixtures can be separated using distillation, but at the cost of an excessive number of equilibrium stages. Fig. 4a shows the VLE of R134a + R143a [45]. Other examples are the mixtures of R1234ze (E) and R1234yf with R161, which seem attractive for formulating new blends thanks to their low GWP and extremely low temperature glide [46,47].
3. Zeotropic mixtures showing the "pinch effect" or "bird's beak", in other words, the bubble and dew lines tend to overlap when approaching pure compound composition [48,49]. Fig. 4b presents the case of R32 + R143a, which is encountered in mixtures such as R427A [50]. Another example is the system R32 + R1234yf (e.g., the R454C mixture) [51].
4. Azeotropic mixtures at a certain composition. This is the case of the system of R32 + R125, which presents an azeotrope at around 92 mol % of R32 [52–54], and the vapor and liquid compositions are very close throughout the entire range of composition (Fig. 4b) [44].
5. Azeotropic mixtures over the entire range of composition. This behavior usually occurs in mixtures of compounds with very similar vapor pressures. Fig. 4b shows the R125 + R143a system [55]. The mixture of R134a + R1234yf is another example of an azeotrope among the fourth-generation blends. The commercialization of mixtures based on R134a and R1234yf is currently gaining importance, so it is expected that these azeotropic mixtures will be collected as residual gas from end-of-life RACHP equipment in the near future [18,51,56].

Accordingly, the recovery, reclamation and reuse of refrigerants from end-of-life RACHP equipment requires in most cases the use of advanced separation technologies to break the azeotropic behavior or enhance the separation of near-azeotropic mixtures. For this purpose, ILs are interesting solvents that present promising properties enabling the successful separations of F-gases and allowing the design of new reclamation technologies and processes.

4. Experimental methods

This section summarizes the main experimental techniques employed to determine the VLE and VLLE as well as to characterize mixture viscosity and gas diffusivity. The methods are divided into analytical and synthetic methods. Analytical methods analyze the phases by taking samples or using gravimetric methods at different pressures and temperatures. Conversely, in synthetic methods the exact total composition is known, and the change in pressure, temperature and volume are used to calculate the composition of each of the phases [57].

4.1. Phase equilibrium

Two methods are predominant in the studies of F-gas solubility in ILs: the gravimetric microbalance (GM) method and the isochoric saturation (IS) method. These two methods measure the VLE and allow the calculation of the diffusion coefficients in the same measurement.

The GM method is an analytical technique based on monitoring the mass of the sample in the balance, which increases as gas dissolves into the liquid [57,58]. Initially, the IL sample is loaded into a balance with a counterweight inside a pressure vessel. Two different modes of operation can be applied. In one mode, with temperature and pressure control, gas is admitted and the exhaust valves open and close to adjust the pressure to the set point for a sufficiently long time (3 to 8 h) to ensure proper equilibrium [59]. Another option consists of a temperature controlled stepwise supply of gas where the pressure falls during the absorption process and both the mass and pressure variations are recorded in equilibrium [60]. The IL swells when absorbing gas, making buoyancy corrections necessary to determine the actual mass of gas absorbed [59].

The IS method is a synthetic pressure-decay technique based on putting known amounts of gas in contact with a mass of IL in a constant volume vessel. The system is formed of two parts: a reservoir where the gas is stored, and the equilibrium cell where the IL and the gas are in contact under continuous stirring. The temperature and pressure of both chambers are recorded at initial and equilibrium conditions to determine the amount of gas in each condition, and the difference between the two quantities is the amount of gas absorbed. Volume expansion effects should also be considered with this technique. However, the effect of IL expansion may be negligible in systems employing sufficiently large gas volumes relative to the IL sample volume.

In the synthetic isochoric method (SI), the gas reservoir is replaced by a syringe pump that allows the amount of gas absorbed to be determined from the difference between the volume injected by the pump and the final volume in the system calculated from the temperature and pressure readings [61].

There is a further synthetic method, known as the synthetic isobaric method (SIP) that allows direct readings of the volume change during

the absorption process. The pressure of the system remains constant thanks to the control of a linear actuator that adjusts the position of a piston, and its displacement represents the volume of gas dissolved [62].

Lastly, one study used an analytical method referred to as the weight method (WM). The gas enters the solvent-loaded equilibrium cell from a syringe pump and pressure decays to its equilibrium value. The solute and solvent mole fractions are determined from the mass increase of the liquid. Unlike the GM method, the WM does not use buoyancy corrections [63].

Vapor-liquid-liquid equilibrium (VLLE) methods are visual. One of the methods uses the same equipment as the synthetic isochoric method, i.e., uses a syringe pump for determining the VLLE. In this case, to determine the VLLE, the gas is added to the IL until a droplet of a very thin film of condensed refrigerant (with a negligible mass) is seen through a view cell in the apparatus at the vapor pressure of the F-gas [61].

The other technique is a visual volumetric method based only on mass and volume measurements. In the case of a non-volatile IL, two sample containers with different quantities of F-gas and IL are prepared. The VLLE is reached in each container when three separated phases form and their heights remain constant, a process that normally takes several days. The height of each phase can then be related to the phase compositions in the two containers using linear algebra [64].

4.2. Viscosity of gas-ionic liquid mixtures

Determining the viscosity of gas-IL mixtures requires the sample to be in equilibrium conditions. Two methods have been used to study the viscosity of ILs as a function of the concentration of gas absorbed. One consists of letting the refrigerant and the IL reach equilibrium conditions in a vessel and then introducing the mixture into the viscometer with a constant flow pump under saturated pressure [65]. In the other method, the liquid phase continuously circulates from the equilibrium cell to the viscometer, which accelerates the mixing with the F-gas; once the pressure stops decaying the mixture is isolated in the viscometer to measure its viscosity [66].

4.3. Diffusion coefficients

As previously mentioned, both the GM and IS methods allow the diffusion coefficients to be determined at the same time the VLE data are obtained. With the IS method, the semi-infinite volume model can be applied to obtain the diffusion coefficients at infinite dilution [67,68], while the GM allows the measurement of concentration-dependent diffusion coefficients [69].

5. Refrigerant absorption in ionic liquids

The refrigerant gases in this review are synthetic fluorocarbons, namely, HFCs and HFOs, but we also report the data available for HCFOs, CFCs, HCFCs, and perfluorocarbons (PFCs). Most articles focus on describing the VLE of binary mixtures where one IL dissolves one refrigerant gas. In addition, a few articles study the three-phase VLLE that is achieved when the IL reaches its maximum absorption capacity, and the refrigerant gas starts to condense in a separate phase. Most articles examine the absorption of gases in imidazolium-based ILs, as this cation is the most commonly known and readily available. Other cations considered in a lesser extent are pyridinium, phosphonium, and ammonium. Table 3 lists the name of the cations and anions of the ILs found in this review, and Table S2 in the UC-RAIL database in the Supporting Information also discloses their structure. The colored matrix in Fig. 5 provides a complete overview of the studied pairs and indicates whether the information comprises many different temperatures and pressures or just a limited set of conditions. In this matrix, fluorinated gases are grouped according to their family, showing that the available information on HFCs is more extensive both in number of gases considered and total absorption pairs studied.

5.1. Hydrofluorocarbons

Table 4 summarizes the experimental absorption pairs formed by an HFC and an IL found in the literature together with the experimental method, the number of data points and the range of experimental conditions (*T-P-x*). In addition, the complete UC-RAIL database containing all the data series has been constructed and this is provided in Table S3 as Supporting Information. These tables present ILs with imidazolium cations first, followed by pyridinium and phosphonium cations, and finally ammonium cations. Within each cation group, ILs with fewer and shorter alkyl chains in the cation appear first. The order for ILs with the same cation is alphabetical with respect to the short name of their anions. When there is information on the absorption of several refrigerant gases in one IL, the gas solutes appear according to their increasing number of carbon atoms. Within each of these groups, refrigerants with the lowest molar masses come first. If several authors have studied the

Table 3
List of IL cations and anions.

Cation	Cation name	Anion	Anion name
$[C_2mim]^+$	1-ethyl-3-methylimidazolium	$[Ac]^-$	acetate
$[C_4mim]^+$	1-butyl-3-methylimidazolium	$[BEI]^-$	bis(pentafluoroethylsulfonyl)imide
$[C_6mim]^+$	1-hexyl-3-methylimidazolium	$[BF_4]^-$	tetrafluoroborate
$[C_7mim]^+$	1-heptyl-3-methylimidazolium	$[Cl]^-$	chloride
$[C_8mim]^+$	3-octyl-1-methylimidazolium	$[Et_2PO_4]^-$	diethylphosphate
$[(C_8)_2im]^+$	1,3-dioctylimidazolium	$[FEP]^-$	tris(pentafluoroethyl)trifluorophosphate
$[C_8H_4F_{13}mim]^+$	1-(3,3,4,4,5,5,6,6,7,7,8,8,8-tridecafluorooctyl)-3-methylimidazolium	$[FS]^-$	2-(1,2,2,2-tetrafluoroethoxy)-1,1,2,2-tetrafluoroethanesulfonate
$[C_{12}mim]^+$	1-dodecyl-3-methylimidazolium	$[HFPS]^-$	1,1,2,3,3,3-hexafluoropropanesulfonate
$[(C_1)_2C_3im]^+$	1,2-dimethyl-3-propylimidazolium	$[I]^-$	iodide
$[C_2mpy]^+$	1-ethyl-3-methylpyridinium	$[MeSO_4]^-$	methylsulfate
$[C_3mpy]^+$	3-methyl-1-propylpyridinium	$[OTf]^-$	trifluoromethanesulfonate
$[C_4mpy]^+$	1-butyl-3-methylpyridinium	$[Pe]^-$	pentanoate
$[P_{4441}]^+$	tributyl(methyl)phosphonium	$[PF_6]^-$	hexafluorophosphate
$[P_{4442}]^+$	tributyl(ethyl)phosphonium	$[Pr]^-$	propionate
$[P_{44414}]^+$	tributyl(tetradecyl)phosphonium	$[PFBS]^-$	perfluorobutanesulfonate
$[P_{66614}]^+$	trihexyl(tetradecyl)phosphonium	$[PFP]^-$	perfluoropentanoate
$[m\text{-}2\text{-}HEA]^+$	N-methyl-2-hydroxyethylammonium	$[SCN]^-$	thiocyanate
		$[Tf_2N]^-$	bis(trifluoromethylsulfonyl)imide
		$[TFES]^-$	1,1,2,2-tetrafluoroethanesulfonate
		$[TMeM]^-$	tris(trifluoromethylsulfonyl)methide
		$[TMPP]^-$	bis(2,4,4-trimethylpentyl)phosphinate
		$[TPES]^-$	1,1,2-trifluoro-2-(perfluoroethoxy)ethanesulfonate
		$[TTES]^-$	1,1,2-trifluoro-2-(trifluoromethoxy)ethanesulfonate

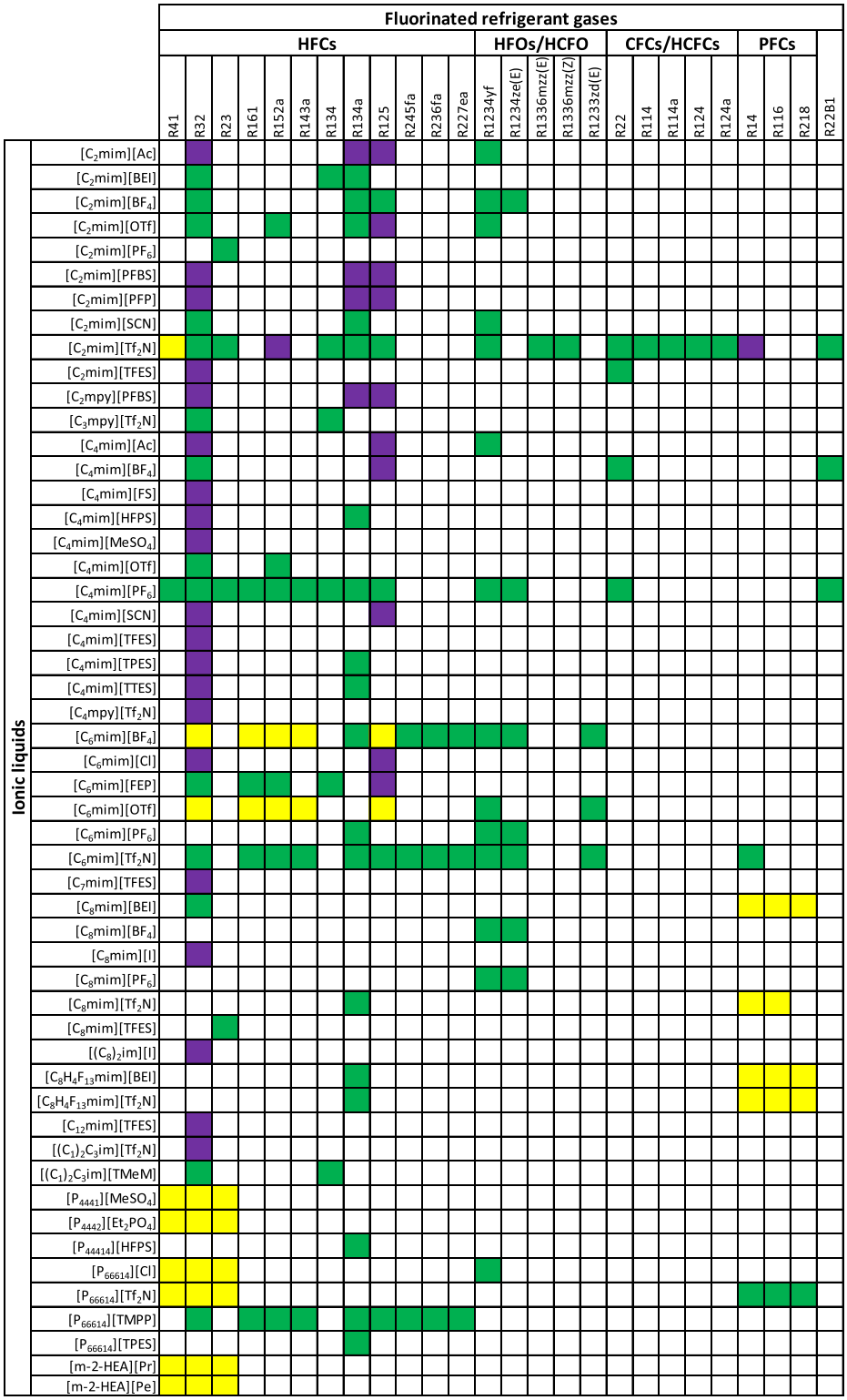

Fig. 5. F-gas—IL VLE pairs studied. Green color stands for systems studied in a wide set of pressure and temperature conditions, purple color marks absorption pairs studied at a single temperature, and yellow color indicates systems studied at a single pressure. (For interpretation of the references to color in this figure legend, the reader is referred to the web version of this article.)

same absorption pair, they appear in chronological order of publication.

The data on HFCs—IL VLE range from 273.13 to 353.15 K and 0.0094 to 2.16 MPa. The most common temperature range is from 295 to 305 K, which accounts for 37% of the total volume of solubility data. The next temperature range, in order of available experimental solubility data (19%), is from 315 to 325 K, while the other temperatures ranges distribute more or less equally. In terms of pressure, 78% of the data was obtained at less than 0.5 MPa, and 44% at less than 0.2 MPa, the main reason being that some of the refrigerant gases are highly condensable, so they liquefy at moderate pressures. Currently, there are data available for the absorption of 12 HFCs in 50 different ILs. Almost 50% of the data provides information on the solubility of R32 or R134a. The outstanding

Table 4
Summary of solubility data of HFCs in ILs. Table S3 of the UC-RAIL database collects all the data.

Ionic liquid	Gas	Method*	T/K	P/MPa	x/mol·mol^{-1}	No.	Ref.
[C_2mim][Ac]	R32	GM	303.15	0.0294–0.5246	0.0117–0.2229	9	[60]
	R134a	GM	303.15	0.0259–0.5007	0.0111–0.2851	11	[60]
	R125	GM	303.15	0.0486–0.4940	0.0168–0.3067	10	[60]
[C_2mim][BEI]	R32	GM	283.15–348.15	0.0096–1.0005	0.001–0.802	31	[70]
	R134	GM	283.12–348.16	0.010–0.350	0.010–0.980	31	[71]
	R134a	GM	283.10–348.10	0.0103–0.3505	0.006–0.795	32	[72]
[C_2mim][BF_4]	R32	IS	283.15–323.15	0.0369–0.8753	0.0132–0.5245	32	[73]
	R134a	IS	283.15–323.15	0.0374–0.4946	0.0104–0.4266	36	[73]
	R125	WM	313.15–353.15	0.072–0.835	0.0076–0.0773	25	[74]
[C_2mim][OTf]	R32	IS	273.14–348.16	0.097–0.857	0.029–0.630	27	[75]
	R32	GM	303.15	0.0402–0.5093	0.0229–0.2689	8	[60]
	R32	IS	298.15	0.0492–0.4404	0.0296–0.2469	6	[73]
	R152a	IS	273.16–348.17	0.040–0.848	0.048–0.473	24	[75]
	R134a	GM	303.15	0.0460–0.4994	0.0369–0.3518	10	[60]
	R134a	IS	283.15–323.15	0.0308–0.4216	0.0185–0.4208	31	[73]
	R125	GM	303.15	0.0245–0.6173	0.0068–0.1904	8	[60]
[C_2mim][PF_6]	R23	GM	332.90–348.00	0.0097–1.9999	0.001–0.151	17	[76]
[C_2mim][PFBS]	R32	GM	303.15	0.0283–0.5025	0.0244–0.3276	11	[60]
	R134a	GM	303.15	0.0155–0.4928	0.0271–0.4791	12	[60]
	R125	GM	303.15	0.0266–0.6084	0.0284–0.3835	10	[60]
[C_2mim][PFP]	R32	GM	303.15	0.0402–0.5093	0.0315–0.3299	8	[60]
	R134a	GM	303.15	0.0460–0.4994	0.0674–0.5277	10	[60]
	R125	GM	303.15	0.0245–0.6173	0.0266–0.4548	8	[60]
[C_2mim][SCN]	R32	IS	283.15–313.15	0.0578–0.7396	0.0130–0.2411	22	[77]
	R134a	IS	283.15–313.15	0.0648–0.4342	0.0071–0.1276	20	[77]
[C_2mim][Tf_2N]	R41	SIP	288.15–308.19	0.10128–0.10763	0.03988–0.05714	5	[78]
	R32	GM	283.15–348.05	0.0096–1.0005	0.002–0.786	31	[70]
	R32	SIP	288.11–308.19	0.10203–0.10447	0.07150–0.1135	5	[78]
	R32	GM	303.15	0.0283–0.5025	0.0228–0.3225	11	[60]
	R32	IS	303.15	0.024–0.208	0.0129–0.145	9	[79]
	R23	GM	298.0–323.2	0.0265–1.9993	0.007–0.481	35	[80]
	R23	SIP	288.13–308.17	0.09897–0.10659	0.02542–0.03627	5	[78]
	R23	IS	303.15	0.100–0.302	0.0451–0.127	6	[79]
	R152a	GM	298.1–298.2	0.025–0.550	0.041–0.823	35	[81]
	R134	GM	282.9–348.1	0.0099–0.3505	0.006–0.964	31	[82]
	R134a	GM	282.7–348.1	0.0100–0.3503	0.000–0.755	32	[82]
	R134a	SI	298–348	0.028–2.160	0.0087–0.8183	47	[83]
	R134a	GM	303	0.0249–0.3499	0.0308–0.3708	6	[84]
	R134a	GM	303.15	0.0155–0.4928	0.0257–0.4420	12	[60]
	R134a	IS	303.15	0.018–0.155	0.0147–0.156	7	[79]
	R125	GM	283.10–348.20	0.0100–1.0001	0.004–0.681	36	[85]
	R125	GM	303.15	0.0266–0.6084	0.0201–0.2787	10	[60]
[C_2mim][TFES]	R32	GM	298.05–298.15	0.0099–1.0016	0.006–0.477	8	[70]
[C_4mim][Ac]	R32	GM	289.05–298.25	0.0099–1.0004	0.010–0.518	8	[70]
	R32	GM	298.15	0.05–1.0	0.054–0.510	7	[86]
	R125	GM	298.15	0.05–1.0	0.060–0.692	7	[86]
[C_4mim][BF_4]	R32	GM	283.0–348.2	0.0097–0.9999	0.002–0.759	31	[69]
	R32	GM	298.15	0.05–1.0	0.024–0.545	7	[86]
	R125	GM	298.15	0.05–1.0	0.008–0.378	7	[86]
[C_4mim][FS]	R32	GM	298.15	0.0100–1.0005	0.009–0.638	8	[70]
[C_4mim][HFPS]	R32	GM	298.15	0.0095–1.0004	0.010–0.670	8	[70]
	R134a	GM	283.10–348.10	0.0099–0.3506	0.003–0.677	32	[72]
[C_4mim][$MeSO_4$]	R32	GM	298.15	0.0099–1.0006	0.012–0.489	8	[70]
[C_4mim][OTf]	R32	IS	273.13–348.24	0.098–0.902	0.033–0.683	26	[75]
	R152a	IS	273.22–348.18	0.056–0.879	0.060–0.536	24	[75]
[C_4mim][PF_6]	R41	GM	283.09–348.18	0.0097–1.9995	0.002–0.637	34	[87]
	R32	GM	283.20–348.20	0.0097–0.9999	0.003–0.815	31	[69]
	R32	GM	298.15	0.05–1.0	0.039–0.574	7	[86]
	R23	GM	282.6–348.1	0.0096–2.0002	0.000–0.535	34	[69]
	R161	GM	283.06–348.16	0.0099–0.7005	0.003–0.575	30	[87]
	R152a	GM	283.1–348.2	0.0097–0.4505	0.005–0.799	28	[69]
	R143a	GM	284.9–348.2	0.0095–1.0004	0.000–0.241	36	[69]
	R134	GM	283.11–348.16	0.0101–0.3505	0.006–0.789	30	[87]
	R134a	GM	283.0–348.2	0.0097–0.3500	0.000–0.724	32	[69]
	R125	GM	283.1–348.3	0.0098–0.9998	0.000–0.660	36	[69]
	R125	GM	298.15	0.05–1.0	0.012–0.323	7	[86]
[C_4mim][SCN]	R32	GM	298.15	0.0095–0.9992	0.004–0.379	8	[70]
	R32	GM	298.15	0.05–1.0	0.004–0.349	7	[86]
	R125	GM	298.15	0.05–1.0	0.001–0.105	7	[86]
[C_4mim][TFES]	R32	GM	298.15	0.0097–0.9989	0.007–0.556	8	[70]
[C_4mim][TPES]	R32	GM	298.15	0.0095–0.9994	0.010–0.674	8	[70]
	R134a	GM	283.05–348.10	0.0102–0.3505	0.006–0.798	32	[72]
[C_4mim][TTES]	R32	GM	298.15	0.0095–0.9992	0.010–0.650	8	[70]
	R134a	GM	282.10–348.15	0.0102–0.3505	0.005–0.748	32	[72]

(*continued on next page*)

Table 4 (*continued*)

Ionic liquid	Gas	Method*	*T*/K	*P*/MPa	*x*/mol·mol^{-1}	No.	Ref.
[C_6mim][BF_4]	R32	IS	303.2–343.2	0.0406–0.0603	0.01795–0.02800	5	[88]
	R161	IS	303.2–343.2	0.0457–0.0640	0.01662–0.02787	5	[88]
	R152a	IS	303.2–343.2	0.0326–0.0529	0.02011–0.03196	5	[88]
	R143a	IS	303.2–343.2	0.1076–0.1569	0.01501–0.02196	5	[88]
	R134a	SI	298–348	0.081–1.970	0.0000–0.7071	17	[89]
	R125	IS	303.2–343.2	0.0954–0.1294	0.01592–0.02953	5	[88]
	R245fa	IS	303.15–343.15	0.011–0.125	0.0213–0.1358	25	[90]
	R236fa	IS	303.15–343.15	0.039–0.263	0.0285–0.1462	25	[90]
	R227ea	IS	303.15–343.15	0.073–0.332	0.0201–0.1150	25	[90]
[C_6mim][Cl]	R32	GM	298.15	0.05–1.0	0.021–0.410	7	[86]
	R125	GM	298.15	0.05–1.0	0.040–0.654	7	[86]
[C_6mim][FEP]	R32	IS	293.1–343.2	0.051–0.493	0.0467–0.3493	36	[91]
	R32	GM	298.15	0.05–1.0	0.067–0.720	7	[86]
	R161	IS	293.0–343.2	0.036–0.548	0.0615–0.4895	36	[91]
	R152a	IS	293.0–343.2	0.031–0.525	0.0691–0.5225	36	[91]
	R134	GM	283.07–348.14	0.010–0.350	0.009–0.959	31	[71]
	R125	GM	298.15	0.05–1.0	0.038–0.578	7	[86]
[C_6mim][OTf]	R32	IS	303.2–343.2	0.0522–0.0683	0.02015–0.03263	5	[88]
	R161	IS	303.2–343.2	0.0405–0.0587	0.02466–0.03932	5	[88]
	R152a	IS	303.2–343.2	0.0329–0.0563	0.02843–0.04113	5	[88]
	R143a	IS	303.2–343.2	0.0646–0.0837	0.01426–0.02307	5	[88]
	R125	IS	303.2–343.2	0.0609–0.0804	0.01393–0.02486	5	[88]
[C_6mim][PF_6]	R134a	SI	298–348	0.081–2.057	0.0295–0.7677	21	[89]
[C_6mim][Tf_2N]	R32	IS	302.5–344.1	0.1144–1.2208	0.0923–0.4972	35	[92]
	R161	IS	302.2–344.3	0.0300–0.6730	0.0305–0.3878	49	[93]
	R152a	IS	302.3–343.4	0.0376–0.3074	0.0573–0.2528	30	[92]
	R143a	IS	302.7–343.0	0.130–1.545	0.0434–0.3561	42	[93]
	R134a	SI	298–348	0.042–2.075	0.0247–0.8572	29	[89]
	R134a	SI	343.15	0.084–2.075	0.0397–0.9440	11	[66]
	R125	IS	302.6–343.2	0.1091–1.0592	0.0530–0.3282	30	[92]
	R245fa	IS	303.15–343.15	0.016–0.144	0.049–0.196	30	[94]
	R236fa	IS	303.15–343.15	0.030–0.315	0.046–0.279	30	[94]
	R227ea	IS	303.15–343.15	0.058–0.485	0.042–0.284	30	[94]
[C_7mim][TFES]	R32	GM	298.15	0.0099–0.9980	0.008–0.592	8	[70]
[C_8mim][BEI]	R134a	GM	303–343	0.0248–0.3495	0.0191–0.4523	18	[84]
[C_8mim][I]	R32	GM	298.0–298.2	0.01007–1.00022	0.004–0.416	8	[76]
[C_8mim][Tf_2N]	R134a	GM	303–343	0.0248–0.3496	0.0161–0.3976	18	[84]
[C_8mim][TFES]	R23	GM	298.1–323.2	0.0501–2.0007	0.007–0.462	37	[95]
[$(C_8)_2$im][I]	R32	GM	297.9–298.0	0.01002–1.00024	0.007–0.468	8	[76]
[$C_8H_4F_{13}$mim][BEI]	R134a	GM	303–343	0.0248–0.3499	0.0208–0.4761	18	[84]
[$C_8H_4F_{13}$mim][Tf_2N]	R134a	GM	303–343	0.0248–0.3493	0.0210–0.4586	18	[84]
[C_{12}mim][TFES]	R32	GM	298.15	0.0096–1.0010	0.006–0.569	8	[70]
[$(C_1)_2C_3$im][Tf_2N]	R32	GM	298.05–298.15	0.0099–1.0011	0.008–0.651	8	[70]
[$(C_1)_2C_3$im][TMeM]	R32	GM	283.15–348.15	0.0094–1.0005	0.000–0.805	31	[70]
	R134	GM	283.03–348.14	0.010–0.350	0.006–0.963	31	[71]
[C_2mpy][PFBS]	R32	GM	303.15	0.0294–0.5246	0.0248–0.3634	9	[60]
	R134a	GM	303.15	0.0259–0.5007	0.0330–0.4989	11	[60]
	R125	GM	303.15	0.0486–0.4940	0.0361–0.3587	10	[60]
[C_3mpy][Tf_2N]	R32	GM	283.15–348.05	0.0095–1.0004	0.003–0.782	31	[70]
	R134	GM	283.00–348.14	0.010–0.350	0.005–0.925	31	[71]
[C_4mpy][Tf_2N]	R32	GM	298.15	0.0096–1.0000	0.010–0.654	8	[70]
[P_{4441}][$MeSO_4$]	R41	SIP	288.15–308.33	0.09953–0.10633	0.03176–0.04397	5	[96]
	R32	SIP	288.15–308.39	0.10054–0.10356	0.08052–0.11740	5	[96]
	R23	SIP	288.15–308.45	0.09981–0.10401	0.05197–0.09487	5	[96]
[P_{4442}][Et_2PO_4]	R41	SIP	288.15–308.15	0.10086–0.10228	0.03891–0.05634	5	[96]
	R32	SIP	288.15–308.21	0.09993–0.10344	0.1306–0.1950	5	[96]
	R23	SIP	288.15–308.27	0.09908–0.10363	0.1942–0.2512	5	[96]
[P_{44414}][HFPS]	R134a	GM	283.05–348.10	0.0099–0.3504	0.009–0.763	32	[72]
[P_{66614}][Cl]	R41	SIP	288.15–308.55	0.10081–0.10600	0.04901–0.06752	5	[96]
	R32	SIP	288.15–308.15	0.09997–0.10589	0.1210–0.1705	5	[96]
	R23	SIP	288.17–308.17	0.09976–0.10759	0.1704–0.2299	5	[96]
[P_{66614}][Tf_2N]	R41	SIP	288.15–308.15	0.09911–0.10313	0.06653–0.09092	5	[78]
	R32	SIP	288.15–308.23	0.10249–0.10686	0.1004–0.1330	5	[78]
	R23	SIP	288.15–308.39	0.09704–0.10168	0.04360–0.05886	5	[78]
[P_{66614}][TMPP]	R32	IS	302.4–343.6	0.1347–1.0693	0.1030–0.4629	30	[97]
	R161	IS	302.2–343.3	0.097–0.595	0.139–0.479	30	[98]
	R152a	IS	302.2–343.2	0.055–0.561	0.067–0.413	30	[98]
	R143a	IS	302.3–343.8	0.169–1.136	0.087–0.385	30	[98]
	R134a	IS	302.9–343.6	0.164–0.801	0.199–0.488	30	[98]
	R125	IS	302.4–343.6	0.114–0.847	0.180–0.536	25	[98]
	R245fa	IS	292.5–333.4	0.0216–0.1750	0.0803–0.2583	30	[97]
	R236fa	IS	292.9–333.4	0.0109–0.2945	0.0338–0.3807	30	[97]
	R227ea	IS	292.5–333.2	0.0134–0.3211	0.1017–0.4570	25	[97]
[P_{66614}][TPES]	R134a	GM	282.80–348.10	0.0098–0.3505	0.003–0.799	32	[72]
[m-2-HEA][Pr]	R41	SIP	288.15–308.23	0.09993–0.10449	0.01095–0.01542	5	[78]
	R32	SIP	288.15–308.23	0.10005–0.10571	0.02435–0.03624	5	[78]

(*continued on next page*)

Table 4 (*continued*)

Ionic liquid	Gas	Method*	*T*/K	*P*/MPa	*x*/mol·mol^{-1}	No.	Ref.
	R23	SIP	288.15–308.23	0.10005–0.10571	0.01035–0.01444	5	[78]
[m-2-HEA][Pe]	R41	SIP	288.15–308.17	0.10023–0.10414	0.01678–0.02153	5	[78]
	R32	SIP	283.15–308.21	0.10268–0.10650	0.03055–0.04684	5	[78]
	R23	SIP	288.15–308.36	0.10043–0.10556	0.01549–0.02040	5	[78]

* GM: gravimetric microbalance. IS: isochoric saturation. SI: synthetic isochoric. SIP: synthetic isobaric. WM: weight method.

research effort of Shiflett's group makes [C_2mim][Tf_2N] and [C_4mim][PF_6] the most well-studied ILs, followed by [C_6mim][Tf_2N] and [P_{66614}][TMPP], studied by He's group.

The UC-RAIL database compiled in this review permits a deeper analysis of the solubility of fluorinated gases in ILs. The solubility assessment is made in terms of mole fraction, x (mol·mol^{-1}), which is the most widely used composition expression in articles evaluating the VLE. However, we also compare the solubility according to molality, m (mol·kg^{-1}), for two different reasons. Firstly, because the dependence on the molar mass of the ILs is eliminated; the wide range of IL molar masses (149–781 g·mol^{-1}) can lead to misleading conclusions when comparing the F-gas solubility between ILs with a large difference. As will be shown, in some extreme cases an IL with a high molar fraction absorption capacity results in one of the lowest molality capacities. Furthermore, expressing the solubility in molality helps process design as it is a useful engineering unit to compare the mass of solvent required for a given separation.

Knowing what determines the solubility of F-gases in ILs is helpful for selecting the optimal IL for the intended application. However, many different factors affect the solubility of F-gases, so there is no single driving mechanism that can describe the solubility of all gases in every IL. Both enthalpic and entropic effects are present in the solvation process, and it seems that the predominance of either one mechanism or the other depends on the type of absorbed gas. For example, Lepre et al. [84] showed that the absorption capacity for the polar R134a increases when the [C_8mim]$^+$ cation is replaced by its fluorinated analogue [$C_8H_4F_{13}$mim]$^+$ due to the more favorable entropy of solvation. On the other hand, for the case of apolar PFCs, they found that the higher solubility in the IL with fluorinated cation can be attributed to a more favorable enthalpy of solvation [99], the difference being related to the polarity of the solutes and the existence of polar and apolar regions in the nanosegregated domains of the ILs. These facts were further confirmed by means of molecular dynamics simulations, which showed that the polar R134a dissolves in the polar domain of [C_8mim][Tf_2N], but in the apolar domain of [$C_8H_4F_{13}$mim][Tf_2N] due to a shielding effect observed on R134a fluorine atoms that occurs upon fluorination of the cation alkyl side chain; while apolar PFCs dissolve in the apolar domain of both ILs [84,99].

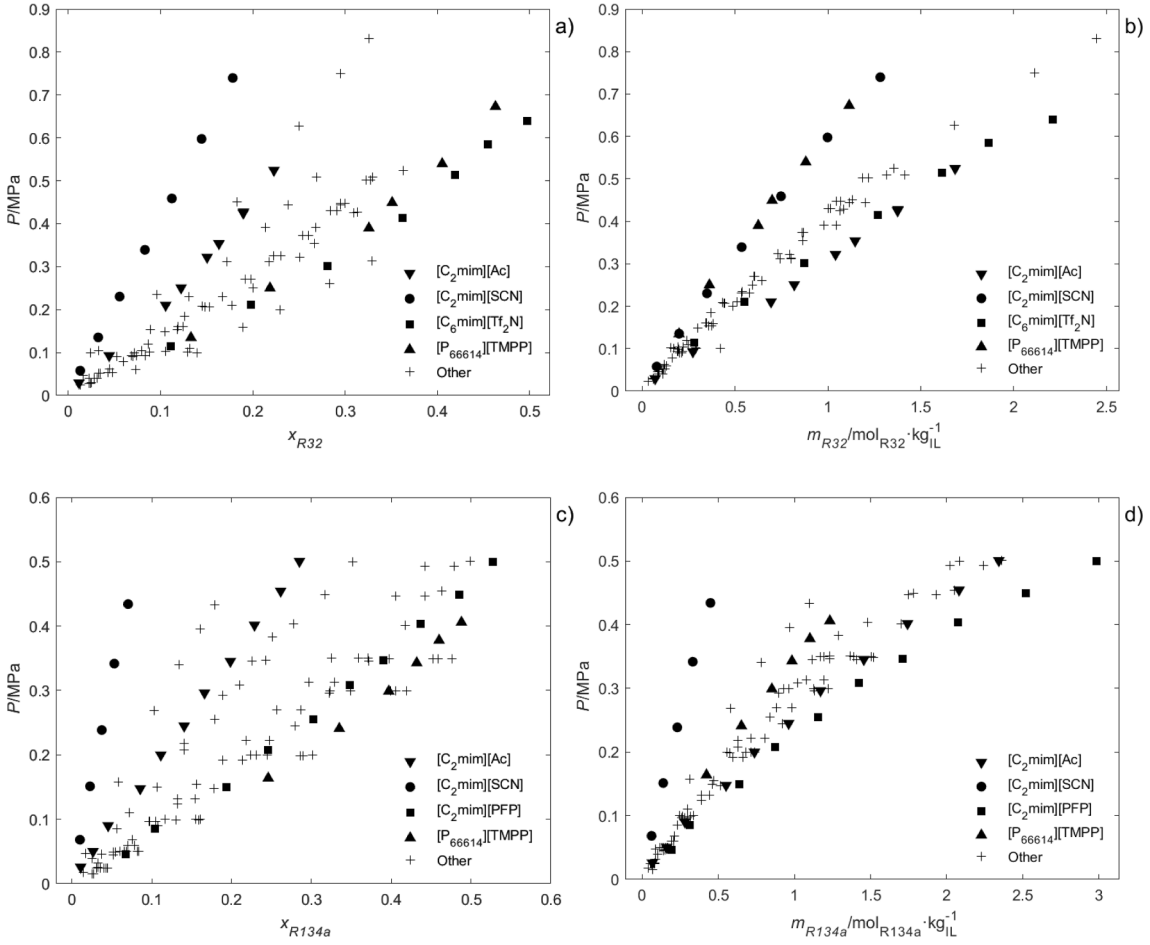

Fig. 6. Solubility of HFCs in different ILs at 303 K: R32 in (a) mole fraction, x/mol·mol^{-1}, and (b) molality, m/mol·kg^{-1}; and R134a in (c) mole fraction, x/mol·mol^{-1}, and (d) molality, m/mol·kg^{-1}. Data from references [60,73,77–79,84,88,91,92,96–98].

Enthalpic effects relate to different gas–liquid interactions, such as ion–dipole interactions or the H-bonding capability of the compounds. The dipole moment of the solute was proposed as a possible driver for F-gas solubility in ILs, but there is not clear correlation between the electric dipole moment of a series of F-gases and their solubility in a given IL because other interactions also affect solubility [69,97]. Moreover, HFCs form clusters that increase their effective dipole moment, further hindering the analysis of the dipole effect in solubility [100–102]. On the other hand, the H-bonding interaction makes the solubility of F-gases in fluorinated anions higher than in non-fluorinated anions [60,70,72,90–92]. In that sense, Fig. 6 shows the absorption isotherms at 303 K for R32 and R134a, two HFC gases of interest in current refrigeration mixtures for which abundant datasets are available (see Table 4 and Fig. 5). For R32 the lowest solubility occurs with a non-fluorinated anion, $[SCN]^-$, while the highest is seen with the most common fluorinated anion, $[Tf_2N]^-$. In the case of R134a, $[SCN]^-$ again presents the lowest capacity, while the highest solubility of this gas occurs with $[PFP]^-$, a heavily fluorinated perfluoroanion. In addition, it is worth noticing the solubility of gases in [C_2mim][Ac]. Contrary to what is expected, the absorption capacity of this low-molecular-weight IL is comparably high when expressed in molality (Fig. 6b and 6d), even analogous to that of [C_6mim][Tf_2N]. A possibility for the high absorption capacity of [C_2mim][Ac] is that the two resonant oxygen atoms of acetate act as electron donors in forming H-bonds (as happens in its mixtures with water [103]), making the anion highly polar, but this hypothesis needs to be confirmed.

Entropic effects relate to the degree of order achieved in the solvation process and the free volume available in the IL. In general, the solvation entropy determines the absorption capacity in such a way that the gas solubility is higher for less negative values of the solvation entropy [60,73,77,84]. The available free volume therefore plays a key role in determining the solubility of F-gases in ILs [104,105]. For this reason, solubility (in the mole fraction basis) increases with increasing IL molar volume [106]. Additionally, fluorinated ILs have higher free volumes because of the greater rigidity of the fluorinated chains [84]. The effect of IL size and degree of fluorination becomes clear in Fig. 6a and 6c. [C_2mim][SCN], a small IL with no fluorine atoms, presents the lowest R32 and R134a solubility values, while the large [P_{66614}][TMPP] and the very fluorinated [C_6mim][Tf_2N] display high solubility values for these two gases.

However, the solubility range of ILs narrows when expressed in molality basis, as previously noted by Carvalho et al. [107] for the case of CO_2 solubility in ILs, and leads to a fairer comparison between solvents. For example, some studies support the idea that phosphonium-ILs have a higher absorption capability than imidazolium-ILs. Nevertheless, although [P_{66614}][TMPP] seems to have a high R32 absorption capacity in mole fraction (Fig. 6a), it actually exhibits the lowest capacity per unit mass of solvent, similar to that of [C_2mim][SCN] (Fig. 6b). A similar, yet less-pronounced decrease in the [P_{66614}][TMPP] capacity is observed for the absorption of R134a when expressed in mass units (Fig. 6c and d).

For a fixed cation, the solubility of polar F-gases is reported to scale with increasing anion size and charge density, as larger anions can have a more dispersed negative charge [89]. This effect is depicted in Fig. 7a, which shows that the solubility of R32 at 303 K increases in the order [C_2mim][BF_4] < [C_2mim][OTf] < [C_2mim][Tf_2N]. However, Fig. 7b shows that, when represented in molality, the three ILs have a very similar absorption capacity. In this manner, while Fig. 6 shows that IL fluorination has an important effect on the F-gas solubility, Fig. 7 suggests that the size of similarly fluorinated anions has little effect on the solubility of a given F-gas.

An interesting analysis of the solubility of HFCs in ILs comes from the assessment of the Henry's law constants. These constants relate the fugacity of gases with the absorbed molar fraction at low concentrations:

$$k_H(T) = \lim_{x\to 0} \frac{f(p,T)}{x} \tag{1}$$

where f is the refrigerant fugacity and x is the absorbed gas molar fraction. To unify the criteria, we have recalculated Henry's law constants from the experimental data compiled from the literature in the UC-RAIL database. To this end, refrigerant fugacity is calculated using the Peng-Robinson equation of state (EoS) and Eq. (1) is simplified to obtain the Henry's law constants as the first derivative of a second-order polynomial fit evaluated at zero composition [69,73,77,84]:

$$k_H \approx \left(\frac{df}{dx}\right)_{x=0} \tag{2}$$

Considering that the critical temperature of pure compounds is a property closely related to the intermolecular potential well depth, and that the Henry's law constants are directly related to the excess chemical potential of a solute at infinite dilution, Shiflett and Yokozeki [87] postulated that, for a given solvent, the Henry's law constants must be related to the solute critical temperature. They demonstrated that $\ln k_H$ is linearly correlated to the critical temperature of pure HFCs, which exhibit different slopes for the methane and ethane series of HFCs. In other words, the solubility increases as the well depth (or the attractive interaction) becomes greater [87]. In 2006, the authors speculated whether the relationship holds for other compounds in a given IL [87], a hypothesis that can now be tested given the amount of new experimental data. In this review, we extend this analysis to other ILs, to propene fluorinated derivatives, as well as the methane series of HCFCs and halons (R22 and R22B1). Fig. 8 shows the results for two different ILs, [C_4mim][PF_6] and [C_6mim][Tf_2N], demonstrating that the relationship holds when extending the mentioned systems, and that varying slopes are obtained for different families of compounds.

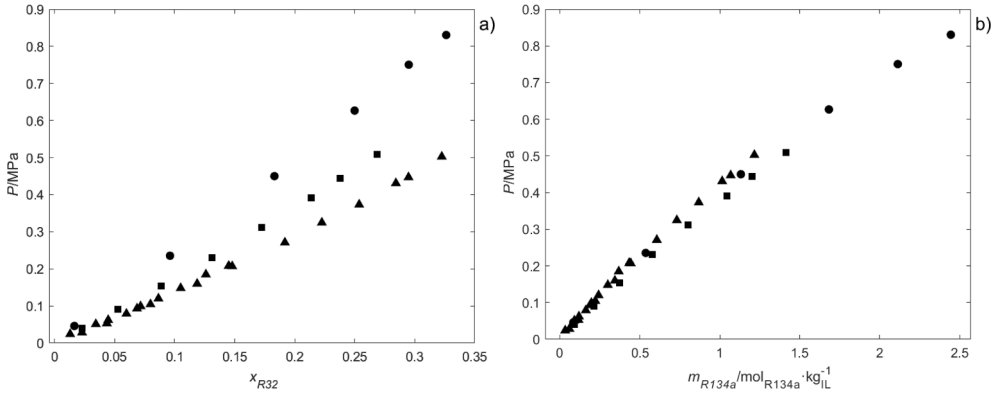

Fig. 7. Solubility of R32 at 303 K in [C_2mim][BF_4] (●), [C_2mim][OTf] (■), and [C_2mim][Tf_2N] (▲) in (a) mole fraction, x/mol·mol^{-1}, and (b) molality, m/mol·kg^{-1}. Data from references [60,73].

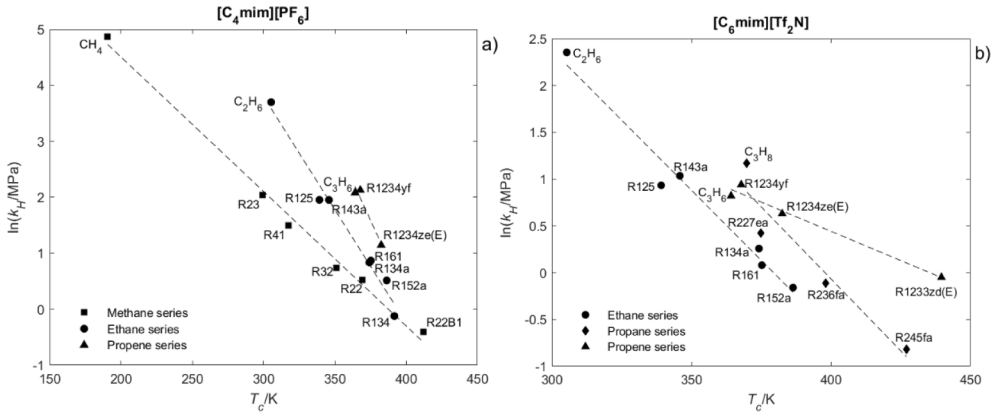

Fig. 8. Correlation between solute critical temperature and their Henry's law constants for absorption of fluorinated refrigerants at 323 K in (a) [C_4mim][PF_6] and (b) [C_6mim][Tf_2N]. The Henry's law constants for F-gases are calculated fitting data from references [69,81,87,89,92–94,108–112] to Eq. (2), and the Henry's law constants for hydrocarbons come from various references [113–116].

Table 5
Summary of solubility data of HFOs and HCFOs in ILs. Table S4 of the UC-RAIL database collects all the data.

Ionic liquid	Gas	Method*	*T*/K	*P*/MPa	*x*/mol·mol^{-1}	No.	Ref.
[C_2mim][Ac]	R1234yf	IS	283.15–343.15	0.073–0.568	0.003–0.060	49	[121]
[C_2mim][BF_4]	R1234yf	IS	283.15–343.15	0.0592–0.4399	0.0019–0.0398	49	[118]
	R1234yf	IS	303.15	0.0607–0.4223	0.0038–0.0277	5	[73]
	R1234ze(E)	IS	283.15–343.15	0.050–0.438	0.0063–0.1814	49	[119]
[C_2mim][OTf]	R1234yf	IS	283.15–323.15	0.0511–0.4825	0.0051–0.1577	25	[73]
[C_2mim][SCN]	R1234yf	IS	283.15–313.15	0.0635–0.4593	0.0007–0.0366	20	[77]
[C_2mim][Tf_2N]	R1234yf	IS	283.15–323.15	0.0499–0.4796	0.0134–0.3602	25	[73]
	R1336mzz(E)	N.A.	293.1–353.8	0.194–0.800	0.093–0.173	11	[123]
	R1336mzz(Z)	N.A.	293.1–353.8	0.05–0.41	0.280–0.589	12	[123]
[C_4mim][Ac]	R1234yf	IS	283.15–343.15	0.078–0.811	0.007–0.133	66	[121]
[C_4mim][PF_6]	R1234yf	IS	283.15–343.15	0.0460–0.4339	0.0063–0.0954	49	[110]
	R1234ze(E)	IS	283.15–343.15	0.0854–0.4347	0.0289–0.2969	42	[108]
[C_6mim][BF_4]	R1234yf	IS	303.2–343.2	0.1109–0.1587	0.01530–0.02515	5	[88]
	R1234yf	IS	283.15–343.15	0.0548–0.4384	0.0063–0.1388	49	[118]
	R1234yf	IS	303.20–353.23	0.109–0.660	0.012–0.149	30	[122]
	R1234ze(E)	IS	283.15–343.15	0.044–0.434	0.0160–0.3241	49	[119]
	R1233zd(E)	IS	303.07–343.19	0.007–0.142	0.004–0.081	30	[111]
[C_6mim][OTf]	R1234yf	IS	303.2–343.2	0.0619–0.0824	0.01629–0.02866	5	[88]
	R1234yf	IS	303.02–353.7	0.127–0.752	0.019–0.151	30	[122]
	R1233zd(E)	IS	303.15–343.17	0.009–0.139	0.006–0.103	30	[111]
[C_6mim][PF_6]	R1234yf	IS	283.15–343.15	0.0506–0.4303	0.0100–0.1366	49	[110]
	R1234yf	IS	303.05–353.27	0.138–0.747	0.012–0.138	30	[122]
	R1234ze(E)	IS	283.15–343.15	0.0847–0.4342	0.0344–0.3472	42	[108]
[C_6mim][Tf_2N]	R1234yf	IS	292.29–353.21	0.0993–0.9251	0.0376–0.3536	35	[112]
	R1234ze(E)	IS	292.98–353.23	0.0497–0.6937	0.0228–0.3312	35	[112]
	R1233zd(E)	IS	303.12–343.17	0.009–0.130	0.010–0.113	30	[111]
[C_8mim][BF_4]	R1234yf	IS	283.15–343.15	0.0548–0.4379	0.0108–0.1847	49	[118]
	R1234ze(E)	IS	283.15–343.15	0.045–0.433	0.0200–0.3614	49	[119]
[C_8mim][PF_6]	R1234yf	IS	283.15–343.15	0.0538–0.4377	0.0125–0.1894	49	[110]
	R1234ze(E)	IS	283.15–343.15	0.0850–0.4340	0.0403–0.3877	42	[108]
[P_{66614}][Cl]	R1234yf	IS	283.15–343.15	0.064–0.825	0.061–0.641	66	[121]

* GM: gravimetric microbalance. IS: isochoric saturation. SI: synthetic isochoric. SIP: synthetic isobaric. WM: weight method.

5.2. Hydrofluoroolefins and hydrochlorofluoroolefins

Table 5 lists the experimental absorption pairs formed by HFO or HCFO and an IL found in the literature, with information on the method, number of data points and experimental conditions. Table S4 in the UC-RAIL database in the Supporting Information contains all the composition data. The organization of the information contained in the two tables is the same as for HFCs.

The study of HFOs and HCFO-1233zd(E) solubility in ILs started later than work on HFCs. Some information appeared in the early 2010s, but the quantity of data in the literature increases most significantly from 2017 on. The VLE data are reported for temperature and pressure ranges from 283.15 to 353.27 K and 0.0070 to 0.9251 MPa. The solubility data are distributed uniformly within that temperature range, while most data are reported at low pressures (90% of the data at 0.5 MPa or less). R1234yf is the most widely studied refrigerant in this group, and accounts for 62% of the data. In general, the solubility of R1234yf is lower than the solubility of R32 or R134a, but higher than other HFCs like R143a. On the other hand, R1234ze(E) is more soluble than its isomer R1234yf, at least with the studied ILs. The solubility of R1233zd(E) in the same ILs is higher [111] than that of the two R1234 isomers, as shown in Fig. 8, behavior that is attributed to the increased attractive interaction when the terminal fluorine is substituted by the more polar chlorine atom. Additionally, temperature affects the solubility of HFOs more than that of HFCs with higher absolute values of solvation enthalpy [112], and the solvation entropy determines the absorption capacity as it does for HFCs [73,77].

Fig. 9 compiles the absorption isotherms of R1234yf at 303 K.

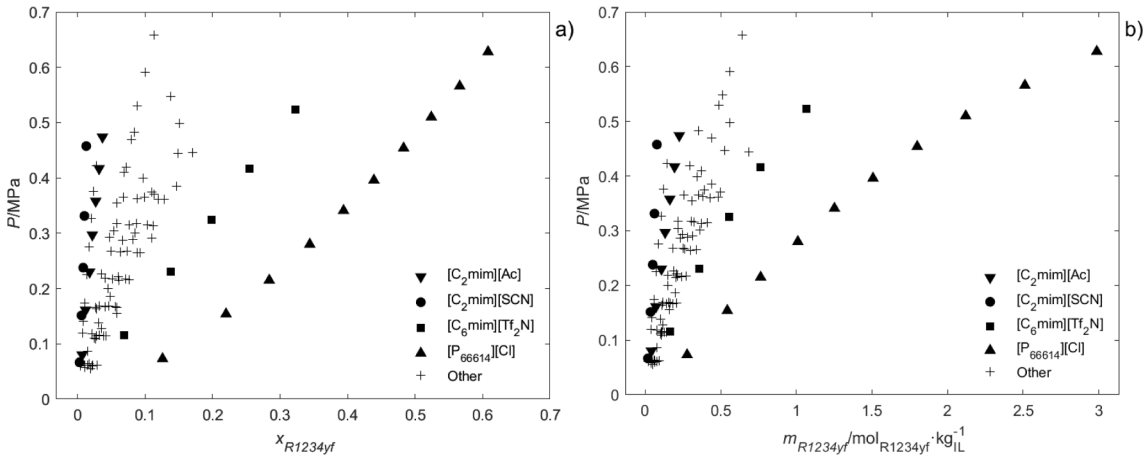

Fig. 9. Solubility of R1234yf in different ILs at 303 K in (a) mole fraction, x/mol·mol^{-1}, and (b) molality, m/mol·kg^{-1}. Data from references [73,77,88,110,112,118,121,122].

Similarly to the results shown for R32 and R134a in Fig. 6, the solubility of R1234yf in most of the absorption pairs falls between the non-fluorinated $[SCN]^-$ and the fluorinated $[Tf_2N]^-$. The only exception is the solubility in $[P_{66614}][Cl]$, which presents a very high absorption capacity (both in molar and mass basis), which can be attributed to the electronegative anion and the high free volume of the IL [117].

The influence of the cation alkyl chain length has scarcely been studied in the literature. Fig. 10 shows that the solubility of R1234yf is enhanced with increasing alkyl chain length [77,118,119], which has been attributed to stronger van der Waals interactions between the IL and R1234yf [118,120].

A comparison between the solubility of HFCs and HFOs permits preliminary screening for a suitable G-L absorption system to selectively separate HFOs from their mixtures with HFCs. Fig. 9b shows that the solubility of R1234yf in $[C_2mim][Ac]$ is very low, unlike the absorption of R32 and R134a in this same IL (Fig. 6b and 6d). This initial assessment therefore suggests that $[C_2mim][Ac]$ is a good possibility for separating mixtures of R1234yf and R32 or R134a such as, for example, the azeotropic R513A (R134a + R1234yf).

5.3. Other refrigerant gases

Table 6 lists the experimental absorption pairs formed by CFCs, HCFCs, PFCs, or R22B1 and an IL found in the literature. Table S5 in the Supporting Information is a database containing all the composition data as a function of temperature and pressure.

CFCs and HCFCs are compounds of interest in the current context of F-gas emissions control, as they still appear in waste mixtures of refrigerant gases, from old RACHP equipment that is reaching its end of life. However, the phase down of ozone-depleting substances retired CFCs and HCFCs from the market, and the availability of absorption data in ILs for these substances is very scarce. Research efforts should also focus on these as they appear in residual gases from equipment that is nearing its end of life, and they are often intermediates in the synthesis routes to HFOs or HCFOs [3].

Shiflett and Yokozeki [82] related the solubility and miscibility differences when mixing CFCs, HCFCs and HFCs with $[C_2mim][Tf_2N]$ to the dipole moments of the refrigerants as chlorine atoms are substituted by hydrogen atoms. They found that the solubility of CF_3-$CFCl_2$ in $[C_2mim][Tf_2N]$ is lower than the solubility of CF_3-CHFCl and much lower than the solubility of CF_3-CH_2F. Furthermore, refrigerant gases with increasingly electronegative and polar groups, like chloride, show higher solubility in $[C_2mim][Tf_2N]$. Thus, the order of solubility is CHF_2-Cl>CHF_2-F>CHF_2-CH_3>CHF_2-CF_3 when represented against normalized pressure to remove any bias due to the different saturation pressures of the gases [81].

The solubility of bromodifluoromethane (R22B1), which also appears in F-gases collected from end-of-life equipment, has been reported in some ILs. The authors state that fluorocarbon molecules with polar, electronegative groups like bromide are more soluble in ILs than those with an alkyl functionality [109].

PFCs are used in ultra-low temperature applications (below −50 °C)

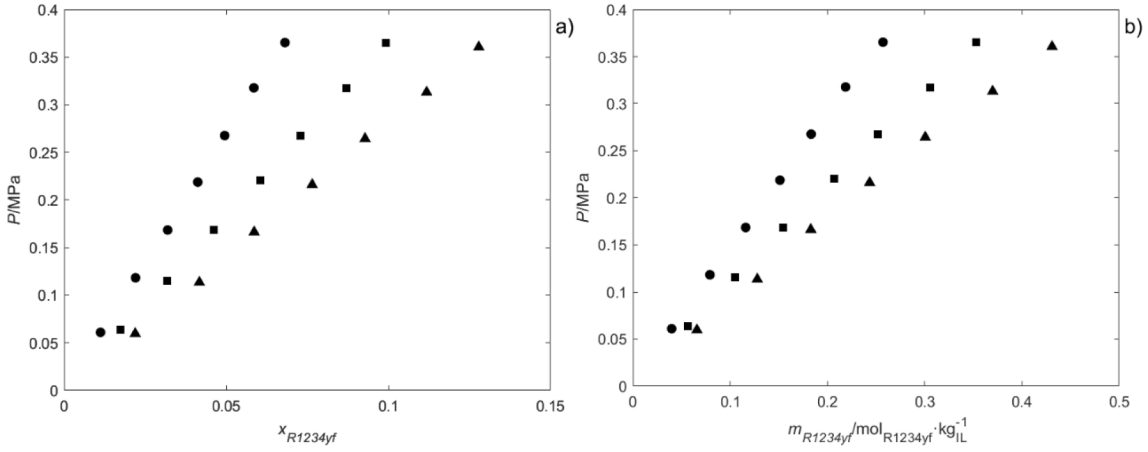

Fig. 10. Solubility of R1234yf in $[C_4mim][PF_6]$ (●), $[C_6mim][PF_6]$ (■), and $[C_8mim][PF_6]$ (▲) in (a) mole fraction, x/mol·mol^{-1}, and (b) molality, m/mol·kg^{-1}. Data from reference [110].

Table 6
Summary of solubility data of CFCs, HCFCs, PFCs, and R22B1. Table S5 of the UC-RAIL database collects all the data.

Ionic liquid	Gas	Method*	*T*/K	*P*/MPa	*x*/mol·mol^{-1}	No.	Ref.
[C_2mim][Tf_2N]	R22	GM	283.1–348.2	0.0500–0.9000	0.024–0.835	46	[81]
	R14	IS	303.15	0.044–0.474	0.0034–0.0583	6	[79]
	R22B1	GM	283.2–348.2	0.0249–0.4000	0.025–0.788	45	[109]
	R114	GM	283.0–348.1	0.0103–0.1504	0.000–0.126	22	[82]
	R114a	GM	283.1–348.1	0.0102–0.1504	0.001–0.142	22	[82]
	R124	GM	283.0–348.1	0.0101–0.3004	0.001–0.757	26	[82]
	R124a	GM	283.1–348.1	0.0103–0.3001	0.001–0.759	26	[82]
[C_2mim][TFES]	R22	GM	283.1–348.2	0.0498–0.8999	0.016–0.810	46	[81]
[C_4mim][BF_4]	R22	GM	283.1–348.2	0.0500–0.9000	0.017–0.827	46	[81]
	R22B1	GM	283.1–348.2	0.0250–0.4000	0.019–0.785	45	[109]
[C_4mim][PF_6]	R22	GM	283.2–348.2	0.0500–0.9001	0.017–0.814	46	[81]
	R22B1	GM	283.1–348.2	0.0249–0.4000	0.017–0.759	45	[109]
[C_6mim][Tf_2N]	R14	IS	293.3–413.3	1.127–9.582	0.0122–0.0889	27	[126]
	R14	IS	303.42–343.44	0.11465–0.12991	0.00106–0.00150	5	[125]
[C_8mim][BEI]	R14	IS	303.16–343.20	0.07073–0.08203	0.00228–0.00328	10	[99]
	R116	IS	303.15–343.18	0.06335–0.07466	0.00310–0.00589	14	[99]
	R218	IS	303.17–343.12	0.06632–0.08028	0.00681–0.01198	10	[99]
[C_8mim][Tf_2N]	R14	IS	303.18–342.76	0.06945–0.08352	0.00117–0.00165	12	[99]
	R116	IS	303.17–343.19	0.06675–0.07594	0.00219–0.00318	10	[99]
[$C_8H_4F_{13}$mim][BEI]	R14	IS	318.15–343.07	0.07261–0.07827	0.00419–0.00526	7	[99]
	R116	IS	318.16–343.24	0.06339–0.07963	0.00662–0.01097	11	[99]
	R218	IS	318.18–343.17	0.06927–0.07872	0.01403–0.02508	7	[99]
[$C_8H_4F_{13}$mim][Tf_2N]	R14	IS	303.16–343.16	0.06824–0.07794	0.00319–0.00455	9	[99]
	R116	IS	303.15–343.19	0.06280–0.07412	0.00528–0.01048	16	[99]
	R218	IS	303.16–343.21	0.06181–0.07168	0.01132–0.02538	9	[99]
[P_{66614}][Tf_2N]	R14	IS	303.41–343.49	0.10459–0.12410	0.00163–0.00297	13	[125]
	R116	IS	303.19–343.23	0.10554–0.13135	0.00296–0.00545	8	[125]
	R218	IS	303.43–343.70	0.04120–0.11984	0.00690–0.0116	10	[125]

* GM: gravimetric microbalance. IS: isochoric saturation. SI: synthetic isochoric. SIP: synthetic isobaric. WM: weight method.

either alone or in mixtures with R23 (mixtures R508A and R508B) and in the manufacture of electronic semiconductors. The use of PFCs is not restricted by the F-gas regulations due to the limited number of units in operation [124], but their high-GWP makes them GHGs of concern that may well be regulated in the future. The little data available in the literature show that the solubility of PFCs in ILs is very low, the order of solubility being perfluoromethane<perfluoroethane<perfluoropropane. For these gases, Pison et al. [125] found that the solubility in [P_{66614}][Tf_2N] increases with the molecular size due to a more favorable entropy of solvation given that the enthalpy of solvation was similar for all gases. However, for ILs with different cations, the solubility becomes larger as the apolar domains in the IL increase, for example, the solubility of perfluoromethane is higher in [P_{66614}][Tf_2N] than in [C_6mim][Tf_2N] due to a more favorable enthalpic contribution.

5.4. Global phase behavior

Most of the information on the equilibrium of F-gases with ILs that is available in the literature has already been covered in the previous sections in relation to VLE. The global phase behavior (VLLE, cloud points, critical fluid-liquid equilibrium) is much less well studied, but it can still provide meaningful insights of the phase equilibrium of F-gases and ILs mixtures. To illustrate the type of equilibrium, Fig. 11 presents the global phase behavior of the mixture of R134a and [C_4mim][PF_6]. Compared to previous figures, this covers the entire range of composition up to the pure refrigerant and shows that when the saturation pressure of the refrigerant is reached, it condenses in a separate phase if the IL does not have enough absorption capacity (which may only occur at sufficiently high temperatures). The global phase behavior is organized according to the van Konynenburg and Scott classification, which labels the binary phase behavior as types I through VI. For the case of HFC—IL mixtures, the behavior is usually a type V, that is, there is a VLE region at low pressures, followed by the VLLE region with a lower critical solution temperature (LCST) point where only one liquid phase exists, such as that illustrated in Fig. 11. In some cases, the behavior falls into a type III, where there is no LCST and the VLLE region exists at low

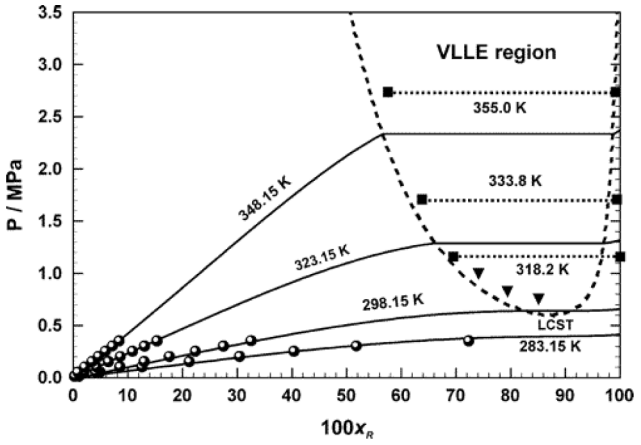

Fig. 11. Pressure-composition phase diagram for R134a + [C_4mim][PF_6]. Solid and dashed lines represent the modeling of a modified-RK equation of state, and symbols are experimental data: VLE (●), VLLE (■), and cloud-points (▼). Reprinted with permission from reference [129]. Copyright 2006 American Chemical Society.

temperatures until the IL freezing point is reached [64,127–129].

The studies that consider VLLE cover different families of gases such as HFCs (R41, R23, R161, R152a, R143a, R134a, and R125), HCFCs (R124, R124a, R123, and R123a), and CFCs (R11, R114, R114a, R113 and R113a) in the ILs [C_2mim][Tf_2N] and [C_4mim][PF_6] [64,82,85,128–130]. The VLLE of binary mixtures of R134a with [C_6mim][BF_4], [C_6mim][PF_6] and [C_6mim][Tf_2N] has also been reported [66,89]. Table S6 in the Supporting Information presents these data. The studies show that the miscibility of HFCs with ILs is higher and much higher than the miscibility of HCFCs and CFCs with ILs, respectively, as evidenced by a much wider VLLE region in the phase diagram of the latter compounds.

Cloud points have been reported in studies dedicated to VLLE for mixtures of [C_2mim][Tf_2N] with R123, R123a, R124, R124a, R134,

R134a, and R125 [82,85], and mixtures of [C_4mim][PF_6] with the refrigerants R23, R123, R152a, R134a, and R125 [64,128–130]. Moreover, some articles consider the phase behavior of supercritical R23 with ILs to gain insights into the use of this gas as an extractant of solutes from the IL; these are compiled in Table S7 of the Supporting Information [131,132].

6. Mass transport properties

Mass transfer influences the operation of equilibrium-based separation processes [133], therefore affecting both the chemical and economic design [134]. If the diffusion of the gaseous species is slow, column stages will likely operate in non-equilibrium conditions. For example, the CO_2 absorption completion in [C_2mim][Tf_2N] in flow conditions has been determined to be around 70% of the equilibrium concentration [135]. Diffusion is slower in more viscous solvents, thus decreasing mass transfer rates [133]. Also, if the viscosity is too high, pumping costs go up and the separation target may not be achievable [136]. Mass transport properties that influence the kinetics of the separation process therefore require further assessment.

6.1. Viscosity of gas-ionic liquid mixtures

Mixture viscosity is one of the key properties to consider when applying ILs to gas separations [120]. Some screening and design studies constrain the maximum IL viscosity to 100 mPa·s at 298.15 K in order to consider it a feasible solvent [137,138]. Then, an IL like [C_2mim][Ac], which we noted in previous sections as a promising candidate for separating the constituents of the R513A mixture would simply not be considered due to its high viscosity (143.6 mPa·s at 298.15 K [139]). However, the viscosity of the IL-gas mixture may be considerably lower than that of the pure IL, and this mixed viscosity property could make the operation viable.

In line with this thinking, the viscosity of [C_6mim][Tf_2N] mixed with various HFCs and HFOs has recently been published, as summarized in Table 7. A compilation of all the data from the literature is included in Table S8 of the UC-RAIL database in the Supplementary Information. [C_6mim][Tf_2N] is an IL with a relatively low viscosity, between 153 mPa·s at 283.15 K and 14.6 mPa·s at 343.15 K for the pure IL [140], so the effects discussed in this section may be more pronounced for more viscous ILs.

The data in the literature show that the viscosity of the IL [C_6mim][Tf_2N] decreases sharply as the gas pressure increases, in other words, at increased F-gas content absorbed in the IL. This effect is particularly remarkable at low temperatures that promote gas absorption, so process design stages should consider this carefully. For example, the viscosity of the mixture of R152a with [C_6mim][Tf_2N] at 283.15 K and 1 bar is 66 mPa·s, one third of the viscosity of the pure IL. Fig. 12 shows the viscosity data of mixtures of refrigerants with [C_6mim][Tf_2N] as a function of molar fraction of gas dissolved at 323.15 K [65,66,141]. The viscosity of pure refrigerants is calculated using CoolProp 6.4.0 [142]. The viscosity of refrigerants in their liquid phase is in the range 0.10–0.15 mPa·s, two orders of magnitude lower than [C_6mim][Tf_2N], explaining why the viscosity of the mixture is so low in comparison with the pure IL. Fig. 12 also includes the mixture viscosity predicted with the Arrhenius (Eq. (3)) and the Kendall and Monroe's (Eq. (4)) models considering

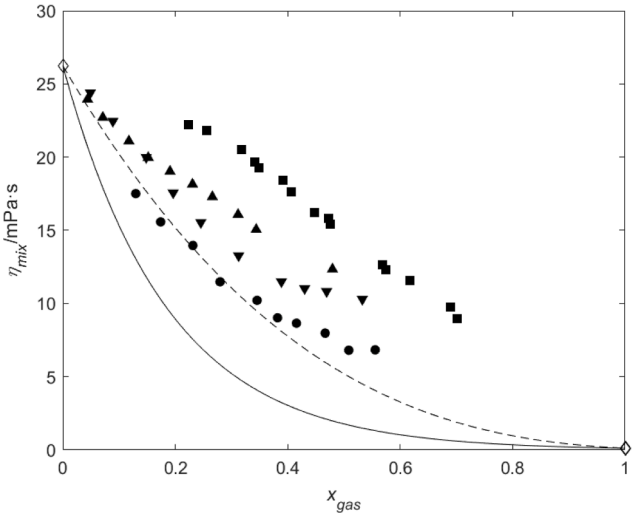

Fig. 12. Viscosity of mixtures of [C_6mim][Tf_2N] with refrigerant gases at 323.15 K. Experimental points for different F-gases: R152a [65] (●), R134a [65,66] (■), R1234yf [141] (▲), and R1234ze(E) [141] (▼). Pure [C_6mim][Tf_2N] viscosity [140] and pure refrigerant viscosity [142] presented as diamonds (◇). The lines represent the Arrhenius (solid line, —) and Kendall-Monroe (dashed line, –) ideal behaviors of mixture viscosity.

ideal mixture behavior [143]:

$$\ln\eta_{mix} = x_1\ln\eta_1 + x_2\ln\eta_2 \tag{3}$$

$$\eta_{mix} = \left(x_1\cdot\eta_1^{1/3} + x_2\cdot\eta_2^{1/3}\right)^3 \tag{4}$$

It can be observed that, although the Kendall-Monroe model performs better than the Arrhenius model, the mixture viscosity of all systems present positive deviations for the ideal behavior that are particularly significant for R134a and almost negligible for R152a. To account for these deviations, the variation of the viscosity with the mixture composition has been described using both empirical correlations, like the Setschenow equation [65], and more accurate semi-theoretical models based on Eyring's viscosity theory, like the Eyring-NRTL and Eyring-modified two-suffix Margules (Eyring-MTSM) models [141,144], that include a nonideal term based on the excess Gibbs free energy (G^E) of the mixture.

$$\ln(\eta_{mix}) = x_1\ln(\eta_1) + x_2\ln(\eta_2) + \frac{G^E}{RT} \tag{5}$$

6.2. Diffusion coefficients

Gas separations with ILs are driven by differences in solubility, rather than diffusivity differences [145]. However, diffusion coefficients are one of the most important transport properties, necessary for calculating mass transfer rates [146,147]. In the case of fluorinated refrigerant gases, the research has mainly focused on assessing the diffusion coefficients of R32, as shown in the summary presented in Fig. 13, followed by those of R134a, R125, and R1234yf. Diffusion coefficients have been determined either using a GM method or through the IS

Table 7
Summary of the viscosity (η) of mixtures of HFCs and HFOs with [C_6mim][Tf_2N]. Table S8 of the UC-RAIL database collects all the data.

Gas	T/K	P/MPa	x/mol·mol^{-1}	η/mPa·s	No.	Ref.
R152a	283.15–343.15	0.053–0.786	0.1143–0.6978	118.24–4.92	70	[65]
R134a	298.15–343.15	0.29–2.03	0.148–0.813	55.8–3.24	15	[66]
R134a	298.15–343.15	0.158–1.930	0.127–0.768	66.435–4.301	24	[65]
R1234yf	283.15–343.15	0.086–1.301	0.0286–0.4796	145.28–10.31	70	[141]
R1234ze(E)	283.15–343.15	0.096–1.420	0.0302–0.5510	119.21–9.34	70	[141]

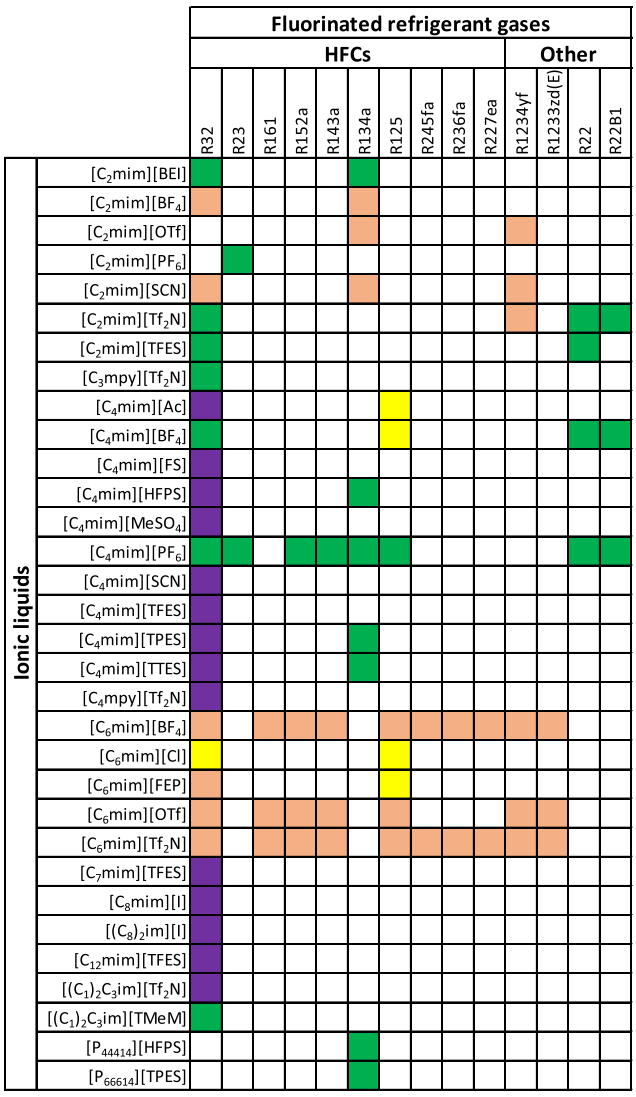

Fig. 13. F-gas—IL diffusion coefficient pairs studied. Green color stands for pressure-dependent data at several temperatures, purple color marks pressure-dependent diffusion studied at a single temperature and yellow color indicates systems studied at a single pressure with the same method, while light orange are systems studied using the semi-infinite dilution model. (For interpretation of the references to color in this figure legend, the reader is referred to the web version of this article.)

method with a semi-infinite volume model. The former provides data at different concentrations (Table 8), while the latter only determines the diffusion coefficients at infinite dilution (Table 9). A compilation of all the data from the literature is included in Table S9 of the UC-RAIL database in the Supplementary Information.

The number of systems for which the diffusion coefficients have been studied is much lower than for the characterization of the VLE, so it is difficult to find trends and correlations in the data. A comparison of the different diffusion coefficients at infinite dilution shows that the relationship of diffusivity with viscosity is not clear. In fact, strong deviations occur with $[OTf]^-$ and $[Tf_2N]^-$ anions, something that was also observed for CO_2 and which led to the formulation of different correlations for those anions [148]. In general, the published data on diffusivity of fluorinated gases are not yet sufficient to infer any family behavior. Future studies should focus on assessing the impact of alkyl chain length in 1-alkyl-3-methylimidazolium ILs for different anion families, to achieve a deeper understanding of diffusion coefficients behavior.

Self-diffusion of refrigerant gases and IL mixtures has been studied in two recent articles. One of these experimentally assessed the self-diffusion of R134a + $[C_6mim][Tf_2N]$ [66], while the other used molecular dynamics simulations to calculate the self-diffusion of R1234yf + $[C_4mim][Tf_2N]$ [149]. When compared with data for the pure compound, the refrigerant self-diffusion coefficient is lower, while the cation and anion of the IL diffuse faster. This is attributed to the fact that the solution reduces the free volume of the refrigerant and increases the IL free volume.

7. Fluorinated gas separation analysis

The wide range of ILs makes it complicated to select the optimal entrainer, due to the heterogeneity of the cations and anions available. For that reason, this section first applies the Regular Solution Theory (RST) as a screening tool for elucidating trends in IL solubility selectivity and setting meaningful guidelines for selecting optimal entrainers. After that, we analyze the available information on modeling and process design for the separation of F-gases using ILs and, finally, we present the process intensification strategy through the synthesis of mixed matrix membranes formed by an IL and a polymer, with the aim of improving the selectivity and reducing the equipment size.

7.1. Prediction of ionic liquid selectivity using the Regular solution Theory

The RST is a simple model used to describe the solubility of gases in ILs [150]. A simplified version of the RST relates the Henry's law constant to the squared difference between the solubility parameters of the solvent (δ_{IL}) and solute (δ_{F-gas}). These solubility parameters can be estimated from the lattice energy density of the IL using the Kapustinskii equation [116], which can be solved to relate the Henry's law constants to the molar volume of the IL (V_m^{IL}), as shown in Eq. (6) [145,151]:

$$\ln(k_H(bar)) = \alpha + \frac{\beta}{\left(V_m^{IL}\left(cm^3 \cdot mol^{-1}\right)\right)^{4/3}} \tag{6}$$

The parameters α and β in Eq. (6) are constants that depend only on the gas being absorbed and the temperature. In Fig. 14a we have adjusted the Henry's law constants of R32, R134a, R1234yf and R1234ze(E) at 303 K to $V_m^{IL\,-4/3}$ to determine the α and β parameters. The good fit of the data to Eq. (6) shows that the RST provides a reasonable description of the absorption of fluorinated gases in ILs, and ILs with increasing molar volume present lower Henry's law constants, i.e., higher solubility. Table 10 presents the values of α and β calculated from the y-intersect and the slope of the linear fitting in Fig. 14a. The Henry's law constants have been calculated from absorption data included in the UC-RAIL database, as explained in Section 5.1. We focus on two HFCs (R32 and R134a) and two HFOs (R1234yf and R1234ze(E)) as these are widely applied in current RACHP equipment, and there is interest in developing separation processes to selectively recover these refrigerant gases.

The absorption capacity of ILs at 1 bar can be predicted as a function of the IL molar volume by rearranging of Eq. (6) [145] as

$$Absorption\ capacity\left(\frac{mol\ gas}{L\ IL}\right) = \frac{1}{\left[\exp\left(\alpha + \frac{\beta}{\left(V_m^{IL}\right)^{4/3}}\right) - 1\right] V_m^{IL}} \tag{7}$$

Fig. 14b shows the gas absorption capacity of ILs as predicted by Eq. (7) for a wide range of IL molar volumes. As can be seen, the absorption capacity increases with the IL molar volume until it reaches a maximum, after which the absorption capacity tends to descend or stabilize. The prediction of the CO_2 absorption capacity of ILs is also presented as a reference [145].

The definition of the RST used in this work considers only the IL molar volume as the solubility driving factor [145], although enthalpic effects can also exert an important influence, as previously explained in

Table 8
Summary of diffusion coefficients of refrigerants in ILs data from a gravimetric microbalance. Table S9 in the UC-RAIL database collects all the data.

Ionic liquid	Gas	T/K	P/MPa	x/mol·mol^{-1}	D/10^{-11} m^2·s^{-1}	No.	Ref.
[C_2mim][BEI]	R32	283.15–348.15	0.0096–0.8505	0.010–0.802	3.8–35	25	[70]
	R134a	283.10–348.10	0.0103–0.3005	0.006–0.673	1.9–17	27	[72]
[C_2mim][PF_6]	R23	332.9–348.0	0.00965–1.99990	0.001–0.151	10.2–72.2	15	[76]
[C_2mim][Tf_2N]	R22B1	283.2–348.2	0.0499–0.4000	0.051–0.760	13.1–73.7	22	[109]
	R22	283.1–348.2	0.0500–0.9000	0.024–0.835	4.5–86	15	[81]
	R32	283.15–348.05	0.0096–0.8504	0.005–0.672	4.1–48	24	[70]
[C_2mim][TFES]	R22	283.2–348.2	0.0498–0.8999	0.016–0.810	1.7–47	15	[81]
	R32	298.05	0.2484–1.0016	0.133–0.477	2.9–12	6	[70]
[C_3mpy][Tf_2N]	R32	283.15–348.05	0.0095–1.0002	0.003–0.782	5.7–55	25	[70]
[C_4mim][Ac]	R32	298.05–298.25	0.0099–1.0004	0.010–0.518	2.2–21	8	[70]
	R32	298.15	0.05	0.054	0.5	1	[86]
	R125	298.15	0.05	0.060	0.4	1	[86]
[C_4mim][BF_4]	R22B1	283.1–348.2	0.0500–0.4000	0.039–0.763	6.14–119	22	[109]
	R22	283.1–348.2	0.0500–0.9000	0.017–0.827	3.1–160	15	[81]
	R32	283.0–348.2	0.0097–0.9999	0.002–0.759	1.7–19	31	[69]
	R32	298.15	0.05	0.024	7.8	1	[86]
	R125	298.15	0.05	0.008	2.4	1	[86]
[C_4mim][FS]	R32	298.15	0.0100–1.0005	0.009–0.638	4.3–28	7	[70]
[C_4mim][HFPS]	R32	298.15	0.0095–1.0004	0.010–0.670	3.3–17	8	[70]
	R134a	283.10–348.10	0.0099–0.3506	0.003–0.677	0.9–8.1	25	[72]
[C_4mim][$MeSO_4$]	R32	298.15	0.0099–1.0006	0.012–0.489	2.1–12	8	[70]
[C_4mim][PF_6]	R22B1	283.1–348.2	0.0500–0.4000	0.037–0.732	4.18–119	22	[109]
	R22	283.2–348.2	0.0500–0.9001	0.017–0.814	1.5–76	15	[81]
	R32	283.2–348.2	0.0099–0.9999	0.003–0.815	1.7–12	28	[69]
	R32	298.15	0.05	0.039	8.5	1	[86]
	R23	282.6–348.1	0.0098–2.0000	0.000–0.419	1.5–23	28	[69]
	R152a	283.1–348.2	0.0099–0.4505	0.005–0.577	1.1–15	22	[69]
	R143a	285.1–348.2	0.1000–1.0003	0.009–0.241	0.8–14	26	[69]
	R134a	283.0–348.2	0.0097–0.3500	0.000–0.724	0.4–8.4	29	[69]
	R125	283.1–348.3	0.0996–0.9998	0.007–0.660	0.6–11	31	[69]
	R125	298.15	0.05	0.012	1.7	1	[86]
[C_4mim][SCN]	R32	298.15	0.0095–0.9992	0.004–0.379	8.1–21	7	[70]
[C_4mim][TFES]	R32	298.15	0.0999–0.9989	0.072–0.556	1.5–14	7	[70]
[C_4mim][TPES]	R32	298.15	0.0095–0.9994	0.010–0.674	4.5–21	8	[70]
	R134a	283.05–348.10	0.0102–0.3505	0.006–0.673	0.9–15	29	[72]
[C_4mim][TTES]	R32	298.15	0.0095–0.9992	0.010–0.650	4.3–25	8	[70]
	R134a	282.10–348.15	0.0102–0.3502	0.005–0.630	1.0–14	30	[72]
[C_4mpy][Tf_2N]	R32	298.15	0.0096–1.0000	0.010–0.654	6.8–23	6	[70]
[C_6mim][Cl]	R32	298.15	0.05	0.021	1.5	1	[86]
	R125	298.15	0.05	0.040	0.4	1	[86]
[C_6mim][FEP]	R32	298.15	0.05	0.067	19.6	1	[86]
	R125	298.15	0.05	0.038	5.5	1	[86]
[C_7mim][TFES]	R32	298.15	0.0099–0.9980	0.008–0.592	3.9–16	8	[70]
[C_8mim][I]	R32	298.0–298.2	0.01007–1.00022	0.004–0.416	1.75–6.37	8	[76]
[$(C_8)_2$im][I]	R32	297.9–298.0	0.01002–1.00024	0.007–0.468	1.78–5.77	8	[76]
[C_{12}mim][TFES]	R32	298.15	0.0995–1.0010	0.074–0.569	4.7–13	7	[70]
[$(C_1)_2C_3$im][Tf_2N]	R32	298.05–298.15	0.0099–1.0011	0.008–0.651	6.3–23	8	[70]
[$(C_1)_2C_3$im][TMeM]	R32	283.15–348.05	0.0099–1.0005	0.004–0.805	1.4–21	25	[70]
[P_{44414}][HFPS]	R134a	283.05–348.10	0.0100–0.3504	0.009–0.763	1.3–20.2	30	[72]
[P_{66614}][TPES]	R134a	282.85–348.10	0.0098–0.3505	0.003–0.718	1.7–23	30	[72]

Section 5.1 and 5.2. Despite the good fit of the data to the RST, Fig. 14a contains some points that deviate significantly from the model. The R32 and R134a absorption data in three ILs with molar volumes of around 150 cm^3·mol^{-1}, [C_2mim][Ac], [C_2mim][BF_4], and [C_2mim][SCN], may shed some light on the solubility of fluorinated gases, so the differences between the experimental and predicted values are presented in Fig. 15. The RST accurately describes the capacity of [C_2mim][BF_4], but fails for the other two ILs. In the case of [SCN]$^-$, the lower absorption capacity may be related to a lower electron donor capacity. Conversely, [Ac]$^-$ may have a higher capacity to form hydrogen bonds as discussed previously, favoring the absorption capacity. In fact, the highest R134a capacity is observed for the [PFP]$^-$ anion, reinforcing the idea that carboxylate-based ILs provide increased F-gas solubility, higher than expected. Interestingly, the solubility of R1234yf in the three ILs with a molar volume of around 150 cm^3·mol^{-1} is very low, so that all three are expected to enhance the solubility selectivity when separating this HFO from its mixtures with HFCs.

Some of these deviations from the RST may be a result of chemical interactions and should be explored further. For example, the [Ac]$^-$ and [Cl]$^-$ anions present such a high R125 absorption capacity [60,86] that their behavior strongly deviates from the RST predictions. Table 10 presents the α and β parameters for R125. Fig. 15 shows the differences between the RST prediction and the experimental Henry's law constant for R125 in [C_4mim][Ac] and [C_6mim][Cl] at 298 K and [C_2mim][Ac] at 303 K, where deviations become clear: the ILs with [Ac]$^-$ and [Cl]$^-$ anions have very low Henry's law constant values and therefore a higher absorption capacity (at low pressure) than expected from the physical solubility description of the RST.

Using the RST, it is possible to infer the expected trend in solubility selectivity of gas–liquid absorption separation, which is calculated as the ratio of absorption capacities [145]. In this work, we have calculated the selectivity for some interesting mixtures that present the azeotropic or pinch behaviors discussed in Section 3. Fig. 16a shows the absorption selectivity of R32 over R1234yf and R134a over R1234yf and R1234ze (E); Fig. 16b shows the absorption selectivity of R32 over R125. The lines were obtained from the model (Eq. (7)) and the α and β parameters in Table 10, and the points are calculated from the experimental data reported in the UC-RAIL database.

Table 9
Summary of diffusion coefficients of refrigerants in ILs data calculated with a semi-infinite volume model. Table S9 in the UC-RAIL database collects all the data.

Ionic liquid	Gas	*T*/K	$D/10^{-10}$ m^2·s^{-1}	No.	Ref.
[C_2mim][BF_4]	R32	283.15–323.15	1.67–10.04	5	[73]
	R134a	283.15–323.15	1.27–9.57	5	[73]
[C_2mim][OTf]	R134a	283.15–323.15	1.06–5.42	5	[73]
	R1234yf	283.15–323.15	0.97–8.01	5	[73]
[C_2mim][SCN]	R32	283.15–313.15	5.1–13.3	4	[77]
	R134a	283.15–313.15	1.5–13.2	4	[77]
	R1234yf	283.15–313.15	0.5–9.8	4	[77]
[C_2mim][Tf_2N]	R1234yf	283.15–323.15	0.36–5.14	5	[73]
[C_6mim][BF_4]	R32	303.2–343.2	1.29–4.76	5	[88]
	R161	303.2–343.2	1.23–4.20	5	[88]
	R152a	303.2–343.2	0.74–2.56	5	[88]
	R143a	303.2–343.2	0.77–3.39	5	[88]
	R125	303.2–343.2	0.63–3.66	5	[88]
	R245fa	303.15–343.15	0.53–4.87	5	[90]
	R236fa	303.15–343.15	0.56–6.24	5	[90]
	R227ea	303.15–343.15	1.26–7.79	5	[90]
	R1234yf	303.2–343.2	0.69–3.59	5	[88]
	R1233zd(E)	303.2–343.2	3.3–16.8	5	[111]
[C_6mim][FEP]	R32	293.5–343.2	1.75–11.42	6	[91]
	R161	293.2–343.2	0.56–8.78	6	[91]
	R152a	293.2–343.2	0.41–6.36	6	[91]
[C_6mim][OTf]	R32	303.2–343.2	3.01–8.35	5	[88]
	R161	303.2–343.2	2.08–5.91	5	[88]
	R152a	303.2–343.2	1.48–4.73	5	[88]
	R143a	303.2–343.2	1.96–6.13	5	[88]
	R125	303.2–343.2	2.38–6.19	5	[88]
	R1234yf	303.2–343.2	1.46–4.97	5	[88]
	R1233zd(E)	303.2–343.2	5.2–26.2	5	[111]
[C_6mim][Tf_2N]	R32	303.0–343.2	1.55–4.78	5	[88]
	R161	303.2–343.2	1.28–4.13	5	[88]
	R152a	302.8–343.0	0.99–3.16	5	[88]
	R143a	303.4–342.8	1.84–5.10	5	[88]
	R125	303.1–342.9	1.02–4.21	5	[88]
	R245fa	303.15–343.15	0.84–3.47	5	[94]
	R236fa	303.15–343.15	1.55–8.42	5	[94]
	R227ea	303.15–343.15	2.72–12.6	5	[94]
	R1234yf	303.1–343.2	1.39–5.96	5	[88]
	R1233zd(E)	303.2–343.2	2.9–8.3	5	[111]

In general, Fig. 16 shows that ILs with a small molar volume offer greater solubility selectivity for separating of HFC/HFO mixtures, so research efforts in the design of separation processes should be directed towards characterizing ILs with a molar volume near to 150 cm^3·mol^{-1}. [C_2mim][Ac] would provide the greatest selectivity because it dissolves small amounts of R1234yf while presenting a high solubility for R32 and R134a, as shown in Fig. 6. In contrast, the selectivity of [C_2mim][Ac] for separating mixtures of R32 and R125 is very low, behavior attributed to its strong interaction with R125 (Fig. 16b). In the same manner, [C_4mim][Ac] and [C_6mim][Cl] display a selectivity value lower than one for separating the gas pair R32 and R125, meaning that both ILs absorb more R125 than R32. Recovering R32 from R410A (the commercial equimass mixture of R32 and R125) would therefore need an IL that interacts with R125 strongly enough to give a high selectivity of R125 over R32. Finally, Fig. 16a shows that separating R134a and R1234ze(E) using G-L absorption may be cumbersome because the predicted selectivity is close to one for a wide range of IL molar volumes, so in this case, the efforts should be focused on systems that deviate from the RST.

The assessment would also require further information relating to the description of the solubility mechanism, in order to explain the solubility selectivity deviations from the RST, as observed for the IL with the [SCN]$^-$ and [Ac]$^-$ anions, where the former presents a low absorption capacity and the latter provides high solubility as discussed in Section 5.1. Another interesting deviation from the RST is the case of [C_6mim][FEP], which offers much greater selectivity than predicted for the separation of R32 and R125 mixtures; this may be related to repulsive interactions between the large number of fluorine atoms in R125 and the IL anion [FEP]$^-$.

7.2. Thermodynamic models

A barrier identified for the implementation of ILs in industrial applications is the lack of fundamental understanding of their performance in relation with their compositional structure [152]. Accurate models for the description of thermodynamic properties and phase behavior are tools whose use is fundamental to advance in the design of novel separation processes. In the field of F-gases mixtures with ILs there is a good number of publications interested in describing the thermodynamic behavior of these complex mixtures, a challenge that has been addressed through the different approaches reviewed in this section, namely, activity coefficient models, cubic EoS, statistical mechanics EoS, quantum chemistry calculations and artificial intelligence models.

In the previous section, we modeled the absorption of refrigerant gases in ILs using RST and showed that it does not capture the real behavior of these binary mixtures because the molecular interactions between the IL and the F-gases are neglected. Furthermore, the RST analysis is based on Henry's law constants, which are defined at infinite dilution. To consider the Henry's law constant dependence on pressure, some authors have applied empirical correlations based on the Krichevsky-Kasarnovsky and Krichevsky-Ilinskaya equations [92,93,97,98,108,112,118,153].

Most frequently, the VLE is described using activity coefficient approaches based on excess Gibbs free energy models [23], among which the nonrandom two-liquid (NRTL) model is the most widely applied. Despite being developed for nonelectrolyte solutions, a total of 91 F-gas—IL systems have been modeled using NRTL with good accuracy [69–73,75,77,81,82,85,87,90,91,108–111,118,119,122,130,154,155]. Other activity coefficient models have also been evaluated providing

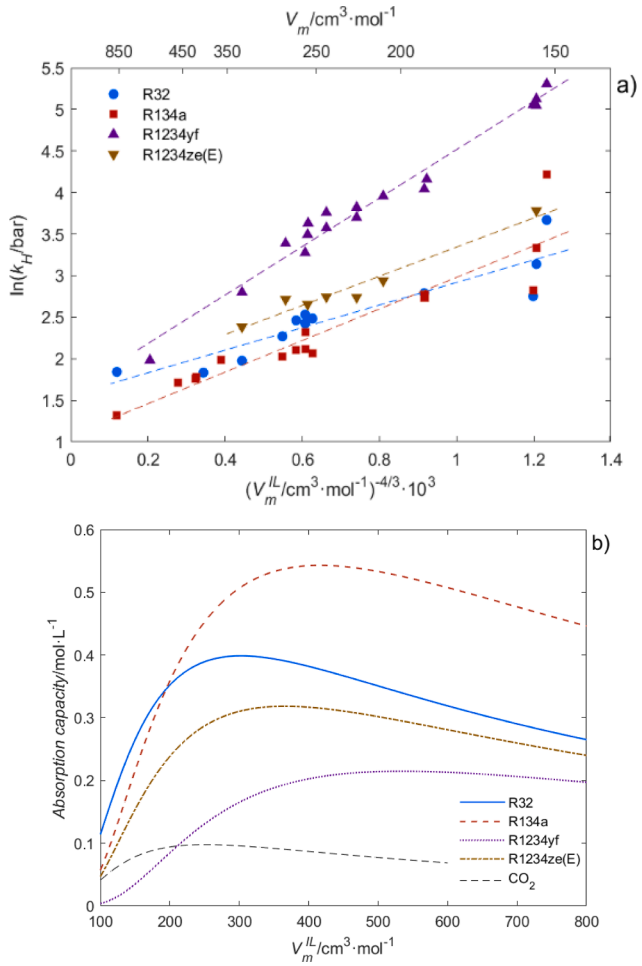

Fig. 14. RST applied to HFC/HFO absorption in ILs: (a) regression plot to Eq. (4), (b) predicted absorption capacity of ILs (Eq. (5)). Symbols represent each of the gases: R32 (blue ●), R134a (red ■), R1234yf (purple ▲), R1234ze(E) (brown ▼), and CO_2 (dashed line). (For interpretation of the references to color in this figure legend, the reader is referred to the web version of this article.)

Table 10
Values of α and β for different refrigerant gases at 303 K.

T/K	Parameter	R32	R134a	R125	R1234yf	R1234ze(E)
303	α	1.56	1.08	0.98	1.60	1.59
	β	1358	1900	2771	2918	1755
298	α	1.87		1.49		
	β	893		2746		

similar accuracy to the NRTL model. Mainly, the UNIFAC group contribution method, for which Dong et al. [156] fitted 16 new group interaction parameters to describe the interaction between fluorinated segments and ILs from VLE data of 18 HFC—IL mixtures, and to a lesser degree, a new version of the e-NRTL equation developed to consider the size difference of the molecules and ions in the solution [157].

Cubic EoS, which treat the IL as a whole molecule with a certain volume and cohesive energy [152], have also been extensively used to model the VLE and to predict the VLLE of fluorinated refrigerants and ILs. However, ILs have no measurable critical properties, so their pseudocritical properties have to be predicted applying different methods. Nevertheless, Morais et al. [86] demonstrated that the van der Waals EoS was not sensitive to the IL critical parameters above a certain critical pressure, a hypothesis that should be tested for other cubic EoS. The Redlich-Kwong EoS and the van der Waals EoS modified by

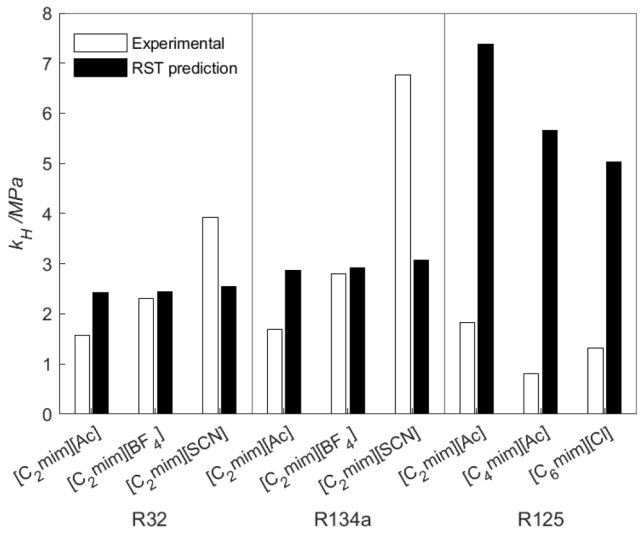

Fig. 15. Deviations from RST in the absorption of R32, R134a, and R125 with a selection of ILs.

Yokozeki [158] were originally applied to model the solubility of refrigerants in lubricant oils, and then used to model 33 F-gas—IL systems [64,76,80,82,85,95,126,128,129,159,160] and 13 F-gas—IL systems [86,161], respectively. The Soave-Redlich-Kwong and the Peng-Robinson EoS with typical van der Waals-two parameter mixing rules are other cubic EoS used for modeling systems of HFCs and ILs (5 F-gas—IL systems were modeled using that approach [89,162]). In addition, the Peng-Robinson EoS has also been applied combined with either the Wong-Sandler (17 F-gas—IL systems [163]) or the Adachi and Sugie (R23 + $[C_2mim][PF_6]$ [131]) mixing rules. Additionally, the cubic EoS of Peng-Robinson and Valderrama-Patel-Teja modified by Kwak and Mansoori have been used to model the VLE equilibrium of 19 and 13 F-gas—IL mixtures, respectively [153,164,165]. All these cubic EoS and the associated mixing rules are collected in Tables 11 and 12, respectively.

Statistical mechanics EoS are molecular-based approaches that describe the physics of the system, which enhances the model predictive ability and extends its range of application [152]. Both lattice models and chain fluid theories have been used for the description of the equilibrium of refrigerants and ILs. Regarding lattice models, Hekayati et al. used the Sanchez-Lacombe and the ε^*-modified Sanchez-Lacombe EoS to model 14 refrigerant—IL mixtures [166]. The ε^*-modified EoS treat the interaction energy as a temperature-dependent parameter, an approach that reported great improvements in the calculation of liquid densities of polar fluids and ILs, especially at high pressures [167]. Shojaeian and Fatoorehchi [168] developed a relatively simple cubic plus association EoS named Peng-Robinson-two state EoS and modeled 20 refrigerant—IL mixtures. The rest of the statistical mechanics EoS used for modeling the equilibrium of refrigerant—IL mixtures belongs to the family of the Statistical Associating Fluid Theory (SAFT), of which the soft-SAFT version has been the most widely applied. The soft-SAFT EoS, which is written in terms of the residual Helmholtz free energy of the system using a Lennard-Jones intermolecular potential as the reference fluid, has shown accurate descriptions of the mixture phase behavior and VLLE predictions [56,79,169]. Other SAFT type equations are the perturbed chain PC-SAFT, which has been implemented to calculate absorption refrigeration cycles [170], the truncated PC-SAFT (tPC-SAFT), only used to model the system R23—$[C_4mim][PF_6]$ [171], and the critical-point-based modified PC-SAFT (CP-PC-SAFT), used to purely predict the solubility of R134a and R1234ze(E) in $[C_6mim][Tf_2N]$ based on the pure-compound critical properties [172].

The conductor-like screening model for real solvents (COSMO-RS) has been used to predict the VLE of refrigerant—IL mixtures. COSMO-RS

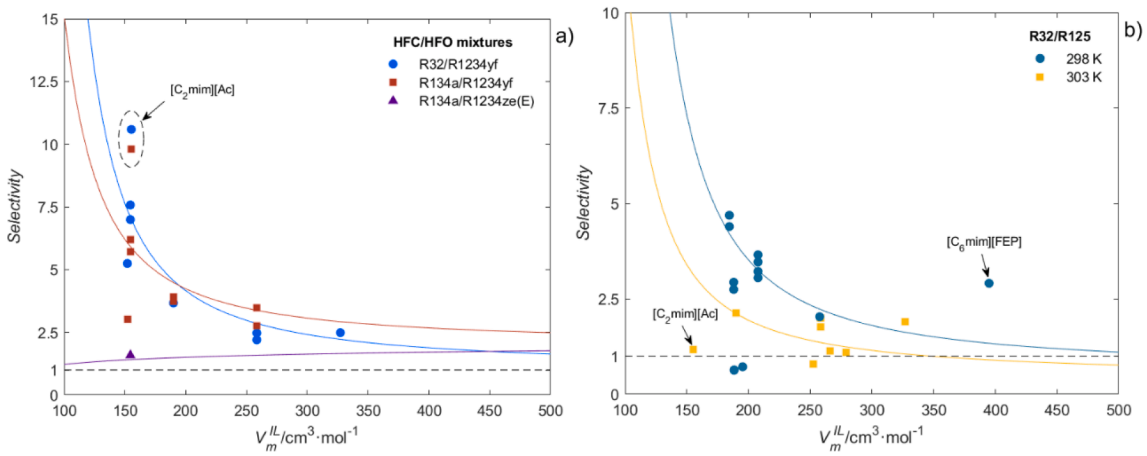

Fig. 16. Absorption selectivity for mixtures of (a) R32 and R1234yf (blue ●), R134a and R1234yf (red ■), R134a and R1234ze(E) at 303 K (purple ▲), and (b) R32 and R125 at 298 K (blue ●) and 303 K (yellow ■). The points present the ideal selectivity calculated from experimental data. Continuous lines present the selectivity calculated using the RST model. (For interpretation of the references to color in this figure legend, the reader is referred to the web version of this article.)

calculates the equilibrium using molecular surface polarity distributions obtained from quantum chemical calculations of the pure compounds of the mixture [152]. For the case of refrigerant absorption in ILs, COSMO-RS was used to screen the Henry's law constants of three fluorocarbons (R134a, R125, and R1234ze(E)) in 900 ILs [173]. The estimated solubility of R134a and R125 in ILs was pretty accurate considering that this is a fully predictive approach, but the absorption of R1234ze(E) was very much overestimated. Furthermore, COSMO-RS has been used to

Table 11
Cubic equations of state used to model F-gas—IL mixtures.

Equation	Expression	Parameters	References
Modified van der Waals	$P = \frac{RT}{V_m - b} - \frac{a}{V_m^2}$	$a = \frac{0.421875R^2T_c^2}{P_c}\alpha(T)$ $b = \frac{0.125RT_c}{P_c}$ $\alpha = \sum_{k=0}^{\leq 3}\beta_k\left(\frac{1}{T_r} - T_r\right)^k T_r \leq 1$ $\alpha = \beta_0 + \beta_1 \exp(2(1 - T_r) - 1)T_r \geq 1$	[86,161]
Modified Redlich-Kwong	$P = \frac{RT}{V_m - b} - \frac{a}{V_m^2 + bV_m}$	$a = \frac{0.42748R^2T_c^2}{P_c}\alpha(T)$ $b = \frac{0.08664RT_c}{P_c}$ α equal to that of the modified van der Waals EoS	[64,76,80,82,85,95,126,128,129,159,160]
Soave-Redlich-Kwong	$P = \frac{RT}{V_m - b} - \frac{a}{V_m^2 + bV_m}$	$a = \frac{0.42748R^2T_c^2}{P_c}\left(1 + \kappa\left(1 - \sqrt{T_r}\right)\right)^2$ $b = \frac{0.08664RT_c}{P_c}$ $\kappa = 0.480 + 1.574\omega - 0.176\omega^2$	[162]
Peng-Robinson	$P = \frac{RT}{V_m - b} - \frac{a}{V_m^2 + 2bV_m - b^2}$	$a = \frac{0.45724R^2T_c^2}{P_c}\left(1 + \kappa\left(1 - \sqrt{T_r}\right)\right)^2$ $b = \frac{0.07780RT_c}{P_c}$ $\kappa = 0.37464 + 1.54226\omega - 0.26992\omega^2$	[89,131,162,163]
Peng-Robinson/ Kwak-Mansoori	$P = \frac{RT}{V_m - b} - \frac{a + RTd - 2\sqrt{RTad}}{V_m^2 + 2bV_m - b^2}$	$a = a_c(1 + \kappa)^2$ $b = \frac{0.07780RT_c}{P_c}$ $d = \frac{a_c\kappa^2}{RT_c}$ $a_c = \frac{0.45724R^2T_c^2}{P_c}$ $\kappa = 0.37464 + 1.54226\omega - 0.26992\omega^2$	[164]

(continued on next page)

Table 12
Mixing rules used with the cubic equations of state.

Mixing rule	Parameters	Ref.
van der Waals 2–parameter	$a = \sum_{ij} \sqrt{a_i a_j}(1-k_{ij})x_i x_j$ $b = \frac{1}{2}\sum_{ij}(b_i+b_j)(1-l_{ij})x_i x_j$ $k_{ij}=k_{ji} \quad l_{ij}=l_{ji} \quad k_{ii}=l_{ii}=0$	[89,162]
Yokozeki	$a = \sum_{ij} \sqrt{a_i a_j} f_{ij}(1-k_{ij})x_i x_j$ $b = \frac{1}{2}\sum_{ij}(b_i+b_j)(1-k_{ij})(1-m_{ij})x_i x_j$ $f_{ij} = 1+\frac{\tau_{ij}}{T}$ $k_{ij} = \frac{l_{ij}l_{ji}(x_i+x_j)}{l_{ji}x_i + l_{ij}x_j}$ $l_{ij}=l_{ji} \quad m_{ij}=m_{ji} \quad \tau_{ij}=\tau_{ji} \quad l_{ii}=m_{ii}=\tau_{ii}=0$	[64,76,80,82,85,86,95,126,128,129,159–161]
Kwak-Mansoori	$a = \sum_{ij} \sqrt{a_i a_j} f_{ij}(1-k_{ij})x_i x_j$ $M = \sum_{ij}\left(\frac{M_i^{1/3}+M_j^{1/3}}{2}\right)^3 (1-\mu_{ij})x_i x_j$ $M \equiv b,c,d \quad \mu \equiv l,m,n \quad k_{ij}=k_{ji} \quad l_{ij}=l_{ji}$ $m_{ij}=m_{ji} \quad k_{ii}=l_{ii}=m_{ii}=0$	[153,164,165]
Wong-Sandler	$b-\frac{a}{RT} = \sum_{ij}\left(b-\frac{a}{RT}\right)_{ij}(1-k_{ij})x_i x_j$ $b = \frac{\sum_{ij}\left(b-\frac{a}{RT}\right)_{ij}x_i x_j}{1-\frac{G^{ex}}{CRT}-\sum_i x_i\frac{a_i}{b_i RT}}$ $a = b\left(\frac{G^{ex}}{C}+\sum_i x_i\frac{a_i}{b_i}\right)$ $\left(b-\frac{a}{RT}\right)_{ij} = \frac{1}{2}\left(\left(b_i-\frac{a_i}{RT}\right)+\left(b_j-\frac{a_j}{RT}\right)\right)$ $k_{ij}=k_{ji} \quad k_{ii}=0$ For Peng-Robinson, $C = -0.62322$. G^{ex} can be calculated with NRTL: $\frac{G^{ex}}{RT} = x_1 x_2\left(\frac{\tau_{21}G_{21}}{x_1+x_2G_{21}}+\frac{\tau_{12}G_{12}}{x_2+x_1G_{12}}\right)$	[163]
Adachi and Sugie	$a = \sum_{ij}\sqrt{a_i a_j}(1-k_{ij}-\lambda_{ij}(x_i-x_j))x_i x_j$ $b = \frac{1}{2}\sum_{ij}(b_i+b_j)(1-l_{ij})x_i x_j$ $k_{ij}=k_{ji} \quad l_{ij}=l_{ji} \quad \lambda_{ij}=\lambda_{ji} \quad k_{ii}=l_{ii}=\lambda_{ii}=0$	[131]

predict the R32 and R134a solubility in ILs in order to address the initial stages of the conceptual design of separation processes [174].

Artificial neural networks have also been applied to calculate the solubility of R32 in 17 ILs [175], a work recently extended to cover the solubility of 10 F-gases in 8 ILs for a total of 22 systems [176]. Considering the good results achieved, these networks could be used as a pre-screening tool for the selection of adequate IL solvents.

7.3. Process design for separating fluorinated refrigerants using ionic liquids

In addition to systematically describing the phase equilibria of refrigerant gases and ILs and modeling this equilibrium following different approaches, some studies have evaluated the potential use of ILs as entrainers in extractive distillation processes, showing they are promising solvents for separating complex mixtures [32,177].

Two works simulated extractive distillation columns for separating R410A into R32 and R125 using equilibrium models [169,178]. Both articles used the NRTL model to describe the phase equilibrium and simulated 28 column stages at 1 MPa with two flashes connected in series as shown in Fig. 17. Comparing the results of the two articles reveals that similar purities can be achieved using [C_4mim][PF_6] and [C_2mim][Tf_2N], while [C_4mim][PF_6] resulted in a lower IL flow rate and a reduced reboiler heat duty thanks to its greater solubility selectivity. Further aspects related to the scale-up and the influence of feed composition were evaluated in a patent by Shiflett and Yokozeki [179].

One recent article simulated the capture of either R134a or R32 from streams with 98% argon in an absorption column using equilibrium and rate-based models [174]. In that work, the phase equilibrium was calculated using the COSMO-SAC property model of Aspen Plus v10 treating the ILs as independent ions. Also, the viscosity of the IL was fitted from experimental data using an Arrhenius-like expression. The simulated absorption column (with no reboiler) was operated at 1 bar and the IL was regenerated in another column with a reboiler operating at 423.15 K. For low viscosity ILs, the separation performance predicted by rate-based models was 40% lower than that of equilibrium-based

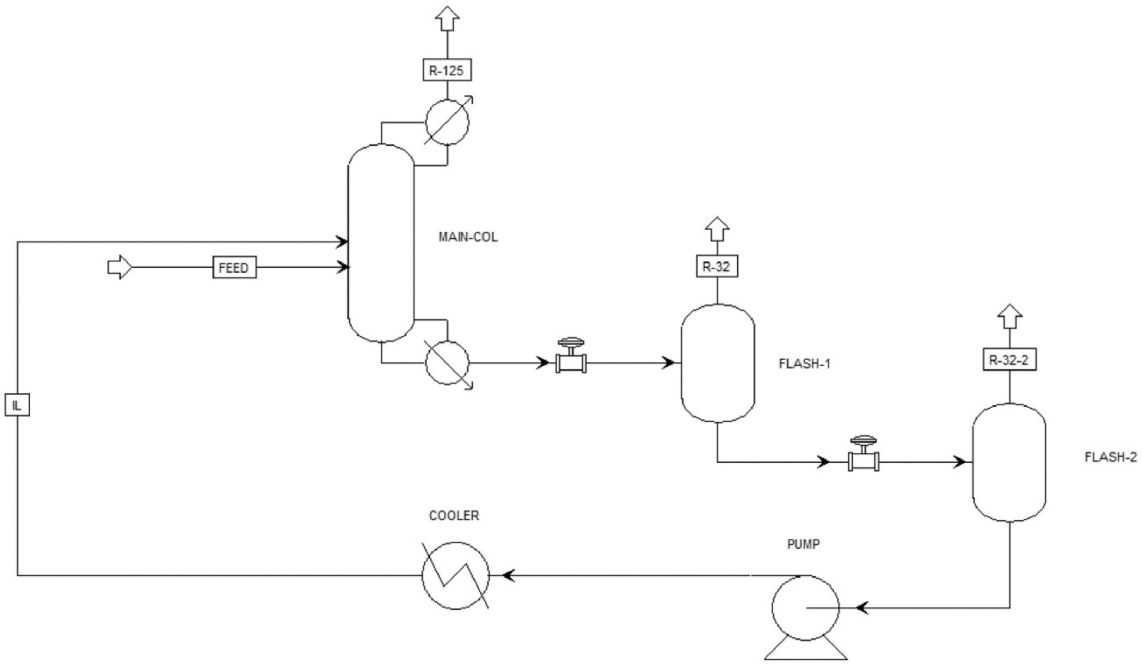

Fig. 17. Process flowsheet of a R410A separation unit using ILs as entrainer. Reprinted with permission from reference [169]. Copyright 2020 Elsevier.

simulations at low temperatures, the difference being attributed to mass transfer limitations. For highly viscous ILs, the rate-based models indicated that the operation would be extremely hindered by the mass transfer limitations at any temperature. Additionally, our review on the viscosity of refrigerant—IL mixtures presented in Section 6.1 suggests that the mixture viscosity does not follow ideal behavior, and therefore, the rate-based models should also consider the non-ideal mixture behavior to obtain more accurate simulation results.

Performing simulations using rate-based models is a step further towards accounting for the reduced separation efficiency caused by the high viscosity of ILs [134,180]. In fact, kinetics and mass transfer have been demonstrated to play a key role in absorption and extractive distillation processes where rate-based models produce accurate descriptions of pilot plant studies [134,136,180,181]. However, these models may require additional data such as mixture viscosities and surface tensions, which are often not available, in order to increase their accuracy. In the absence of mass transfer data, equilibrium model simulations are the best alternative for assessing the performance of extractive distillation columns considering that high viscosity ILs may have low applicability. However, setting a maximum viscosity value above which the IL is not even considered may be too drastic, especially if the sharp decrease expected in the viscosity of the mixture is taken into account.

Another IL property that must be considered in process design is the thermal stability of ILs, particularly regarding the regeneration stages. Typically, short-term ramped temperature analyses are performed to determine the point of thermal degradation, that is, the onset temperature (T_{onset}). However, this information should be complemented with long-term isothermal measurements which have proved that significant IL weight losses may occur at temperatures lower than T_{onset} [182–184]. In general, pyrrolidinium cation cores are more temperature resistant than their imidazolium, pyridinium and tetraalkyl ammonium counterparts; whereas the influence of the anion type has been well correlated to the anion hydrophobicity [182]. For instance, acetate- and halide-based anions significantly reduce the thermal stability while the [Tf_2N] anion can withstand much higher temperatures [185–187].

So far, the selection of an appropriate IL entrainer with high absorption capacity and selectivity has been the principal approach followed for the design of F-gases separation processes using ILs. Further steps should evaluate the optimal column design and the IL regeneration stage to minimize the energy requirements and the amount of IL solvent used, while maximizing the final product purity and recovery of the value-added refrigerant gases, as well as perform the cost analysis. In addition, theoretical studies should be validated by experimental work and case studies. In this sense, the phase equilibria of ternary mixtures should be researched experimentally to check whether the equilibrium models provide an accurate description. Also, the first steps should be given to evaluate the separation process at bench scale, as this would provide relevant information about whether the performance of conventional pressure drop and mass transfer correlations for column internals can be extrapolated to IL solvents, especially those with higher viscosity [32,188].

7.4. Refrigerant separations with IL-based membranes

Research into ILs combined with polymer materials has become increasingly important for gas separation using membrane technology. Such hybrid materials can be prepared in different ways: in the form of supported ionic liquid membranes (SILMs); physically blended into composite ionic liquid and polymer membranes (CILPMs); or as polymerizable ionic liquids (PILs) that may contain non-polymerizable ILs (PIL-IL membranes) [189,190]. To date, numerous studies have reported noticeable improvements in the separation of CO_2/N_2, CO_2/CH_4 and CO_2/H_2 gas pairs, commonly exceeding the so-called Robeson's upper bounds given by conventional polymers [191–193]. These types of IL-based hybrid membranes take advantage of the superior CO_2 solubility in the IL, with respect to that of $H_2/N_2/CH_4$, to yield membranes that in most cases exhibit improved solubility selectivity values and higher permeability than the base polymer membranes.

The separation of refrigerant mixtures using IL-based membranes has recently been addressed by Pardo et al. [21,22,194–196]. In these works, CILPMs are fabricated by immobilizing the ILs [C_2mim][SCN], [C_2mim][BF_4], [C_2mim][OTf], and [C_2mim][Tf_2N] within the thermoplastic elastomer Pebax®1657, a block copolymer comprising interlinked polyethylene oxide and polyamide-6 segments. In these works, the constituents of the mixtures R410A (50 wt% R32 and R125) and two

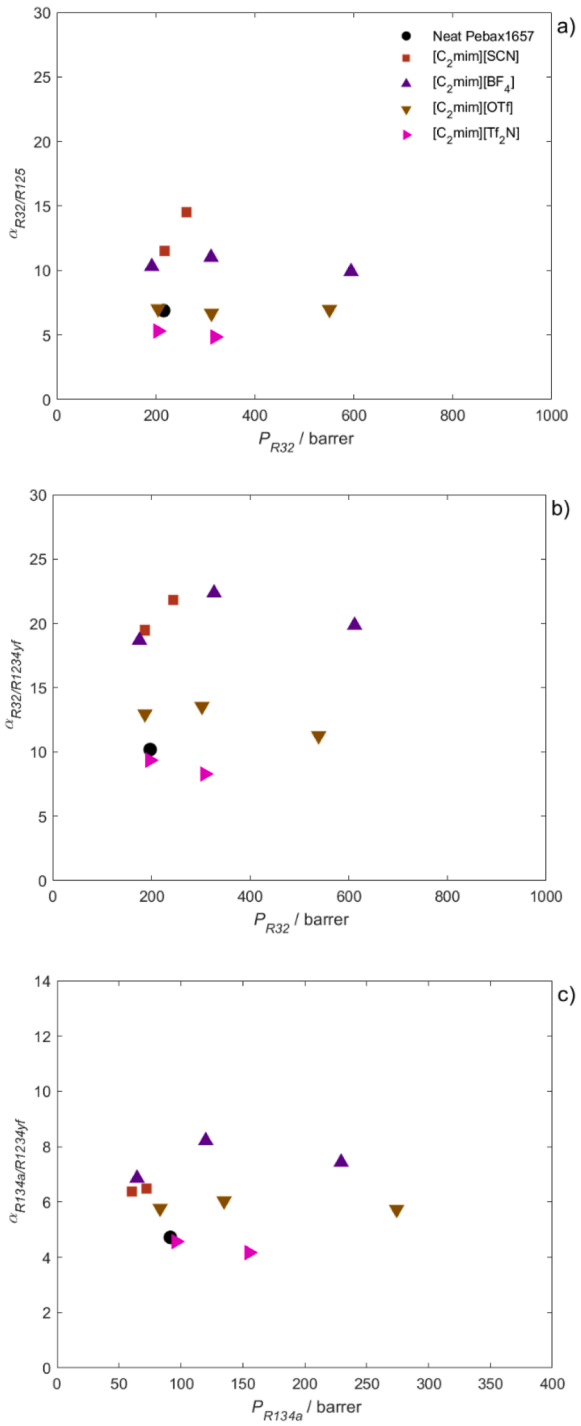

Fig. 18. Non-competitive selectivity vs single gas permeability of the fastest gas in neat Pebax® 1657 and CILPMs with [C_2mim][SCN], [C_2mim][BF_4], [C_2,mim][OTf] and [C_2mim][Tf_2N] for the gas pairs: a) R32/R125 (T = 303 K, P = 1.86 bar), b) R32/R1234yf (T = 303 K, P = 1.3 bar) and c) R134a/R1234yf (T = 303 K, P = 1.3 bar). Data are taken with permissions from references [22] and [161].

different HFC/HFO mixtures, namely R454B (68.9 wt% R32 and 31.1 wt % R1234yf) and R513A (44 wt% R134a and 56 wt% R1234yf), are separated. The results are shown in Fig. 18, where the ideal (non-competitive) permeability selectivity is plotted against the permeability of the most permeable compound for each separation. In all cases, the CILPMS prepared with the small molar volume ILs [C_2mim][SCN] and [C_2mim][BF_4] significantly improved the ideal selectivity for the gas pairs R32/R125, R32/R1234yf and R134a/R1234yf over the neat polymer membrane.

On the other hand, the ILs [C_2mim][OTf] and [C_2mim][Tf_2N] did not remarkably improve the permeability selectivity. These results agree well with the observed sorption behavior (Fig. 16), indicating that small molar volume ILs generally favor the solubility difference between pairs of gases. In addition, for both HFC/HFO separations, it was observed that a differential advantage provided by CILPMs containing [C_2mim][SCN] and [C_2mim][BF_4] is that the permeability of R1234yf is blocked due to a sharp solubility decrease in the composite matrix that improves the separation performance towards the recovery of either R32 or R134a. This behavior agrees very well with the predicted R1234yf solubility in small molar volume ILs using the RST (Fig. 14b).

In regard to the IL content of CILPMs, although the increased IL content in this type of hybrid materials significantly increases gas permeability, the mechanical stability of the membrane is compromised. For example, the authors reported that CILPMs with 60 wt% [C_2mim][BF_4] did not withstand continuous operation at pressures higher than 4 bar, whereas CILPMs containing 40 wt% [C_2mim][SCN] were tested for almost one month at pressures up to 12 bar [22].

In conclusion, given that the combined application of IL and polymer membranes currently represent a relatively unexplored field for F-gas separations, it is expected that future studies will focus on the search for novel materials using new polymers and ILs. Those studies should also test the mechanical and functional properties of the composite membranes over long operational periods and at process conditions close to those of the intended applications. Furthermore, the possibility of manufacturing IL-based composite membranes with industrial scale configurations, such as hollow fiber or spiral wound membrane modules, should be explored to determine the real separation potential of these novel materials [197–199].

8. Conclusions and prospective view

The international consensus on the negative contribution of HFCs to climate change led to the formulation of several agreements and regulations aimed at reducing the emissions of fluorinated gases. Among others, the global Kigali Amendment to the Montreal Protocol, the SNAP program in the US, and European Regulation 517/2014 schedule 85% reductions in the emission of HFCs by the late 2040s and propose the reclamation of fluorinated gases. This reclamation consists of reprocessing the refrigerant gas recovered during maintenance or prior to disposal to match the equivalent performance of a virgin substance. This context favors the recovery of HFC blends from end-of-life equipment, to then separate the mixtures into their pure components, which would allow those with lower environmental impact to be reused in new, more eco-friendly blends. However, most refrigerant blends behave as azeotropic or close-boiling mixtures that mimic pure compound behavior in terms of vapor–liquid equilibria, complicating the separation and recovery.

ILs are promising as entrainers in the separation process, so this review exhaustively compiles and analyzes the absorption of synthetic fluorinated refrigerants in ILs to act as a reference document for the future design of extractive distillation processes. The wide scope of this review covers the analysis of experimental results of thermodynamic and mass transport properties and the design of refrigerant separations based on the use of ILs in extractive distillation and membrane processes. We have proposed various milestones and guidelines to help authors make decisions with regard to future studies on the absorption of fluorinated gases in ILs:

- The UC-RAIL database provided as Supplementary Information in this review compiles all the experimental data published up to February 2021 on the absorption of fluorinated refrigerants in ILs. This includes 4444 vapor–liquid equilibrium points for 193 absorption pairs comprising 52 ILs and 26 F-gases, 86 vapor–liquid-liquid equilibrium points of 25 absorption pairs comprising 3 ILs and 16 gases, 249 F-gas—IL mixture viscosity points for 4 systems and 908 diffusion coefficients for 81 absorption pairs comprising 31 ILs and 14 F-gases.
- Our analysis using Henry's law constants establishes that ILs with low molar volumes are the most promising for achieving high selectivity values. Also, one option worth exploring involves those ILs that have strong interactions with fluorinated gases, as is the case of carboxylate anions that deviate from the Regular Solution Theory.
- The mass transport properties have also been compiled, but there is much less information on this, and it should be assessed again in the future. Particularly, the viscosity decay of ILs when they contain absorbed F-gas should be assessed, as the dissolution of refrigerant gases sharply decreases IL viscosity. This means that ILs which are *a priori* too viscous for operation may still be interesting for the design of extractive distillation processes. This information should also be implemented in process simulators, enabling the process design using robust results that consider the important positive values in excess mixture viscosity.
- There are some examples of process simulations for separating and purifying HFCs from blends in gas–liquid absorption configurations. However, further work is needed to define process integration and optimal design. Furthermore, given the high viscosity of many ILs, the use of rate-based models is recommended.
- Incipient results are available showing the potential of using ILs in membrane processes. Further assessment is needed to determine the optimal operating conditions for separating the refrigerant systems of interest. In addition, although the results are promising, IL-based membranes are still at an early stage of development and more efforts are required to build robust and compact membrane modules with large surface areas and to synthesize IL-based membranes with thin-film selective layers.

Overall, the knowledge of the thermodynamic properties of mixtures of F-gases and ILs is sufficient to allow educated guesses in terms of selecting ILs with potentially high selectivity that could be used to separate many different refrigerant mixtures. Future efforts should focus on evaluating mass transport properties and process design to pave the way to pilot plants and the upscaling of separation process based on the use of ILs, and to shift the refrigeration sector towards a more circular economy model.

Declaration of Competing Interest

The authors declare that they have no known competing financial interests or personal relationships that could have appeared to influence the work reported in this paper.

Acknowledgements

The authors fully acknowledge the financial support received from Project KET4F-Gas-SOE2/P1/P0823, which is co-financed by the European Regional Development Fund within the framework of Interreg Sudoe Programme, and project PID2019-105827RB-I00 – Agencia Estatal de Investigación, Spain. S. A.-D. and F. P. acknowledge the FPU grant (18/03939) and the post-doctoral fellowship (FJCI-2017-32884 Juan de la Cierva Formación), respectively, awarded by the Spanish Ministry of Science and Innovation. Marta Romay's graphical abstract is gratefully acknowledged.

Appendix A. Supplementary material

Supplementary data to this article can be found online at https://doi.org/10.1016/j.seppur.2021.119363.

References

[1] C. Booten, S. Nicholson, M. Mann, O. Abdelaziz, Refrigerants: Market Trends and Supply Chain Assessment, Golden, Colorado, 2020.
[2] J.M. Calm, The next generation of refrigerants - Historical review, considerations, and outlook, Int. J. Refrig. 31 (7) (2008) 1123–1133, https://doi.org/10.1016/j.ijrefrig.2008.01.013.
[3] A.J. Sicard, R.T. Baker, Fluorocarbon Refrigerants and their Syntheses: Past to Present, Chem. Rev. 120 (17) (2020) 9164–9303, https://doi.org/10.1021/acs.chemrev.9b00719.
[4] M.O. McLinden, M.L. Huber, (R)Evolution of Refrigerants, J. Chem. Eng. Data. 65 (9) (2020) 4176–4193, https://doi.org/10.1021/acs.jced.0c00338.
[5] United Nations, Montreal Protocol on Substances that Deplete the Ozone Layer, USA, 1987. https://treaties.un.org/Pages/ViewDetails. aspx?src=TREATY&mtdsg_no=XXVII-2-a&Chapter=27&lang=en.

[6] European Environment Agency, Annual European Union greenhouse gas inventory 1990-2018 and inventory report 2020, Brussels, 2020. https://www.eea.europa.eu/publications/european-union-greenhouse-gas-inventory-2020.
[7] United States Environmental Protection Agency, Inventory of U.S. greenhouse gas emissions and sinks: 1990-2018, 2020. https://www.epa.gov/ghgemissions/inventory-us-greenhouse-gas-emissions-and-sinks-1990-2018.
[8] P. Purohit, L. Höglund-Isaksson, J. Dulac, N. Shah, M. Wei, P. Rafaj, W. Schöpp, Electricity savings and greenhouse gas emission reductions from global phase-down of hydrofluorocarbons, Atmos. Chem. Phys. 20 (19) (2020) 11305–11327, https://doi.org/10.5194/acp-20-11305-2020.
[9] European Environment Agency, EEA greenhouse gas- data viewer, (n.d.). https://www.eea.europa.eu/data-and-maps/data/data-viewers/greenhouse-gases-viewer (accessed September 25, 2020).
[10] G.J.M. Velders, D.W. Fahey, J.S. Daniel, M. McFarland, S.O. Andersen, The large contribution of projected HFC emissions to future climate forcing, Proc. Natl. Acad. Sci. U. S. A. 106 (27) (2009) 10949–10954, https://doi.org/10.1073/pnas.0902817106.
[11] United Nations, Amendment to the Montreal protocol on substances that deplete the ozone layer, (2016).
[12] E.A. Heath, Amendment to the Montreal Protocol on Substances that Deplete the Ozone Layer (Kigali Amendment), Int. Leg. Mater. 56 (1) (2017) 193–205, https://doi.org/10.1017/ilm.2016.2.
[13] European Parliament and Council, EU 517/2014, (2014) 195–230.
[14] A. Mota-Babiloni, J. Navarro-Esbrí, Á. Barragán-Cervera, F. Molés, B. Peris, Analysis based on EU Regulation No 517/2014 of new HFC/HFO mixtures as alternatives of high GWP refrigerants in refrigeration and HVAC systems, Int. J. Refrig. 52 (2015) 21–31, https://doi.org/10.1016/j.ijrefrig.2014.12.021.
[15] A. Mota-Babiloni, J. Navarro-Esbrí, F. Molés, Á.B. Cervera, B. Peris, G. Verdú, A review of refrigerant R1234ze(E) recent investigations, Appl. Therm. Eng. 95 (2016) 211–222, https://doi.org/10.1016/j.applthermaleng.2015.09.055.
[16] M.O. McLinden, J.S. Brown, R. Brignoli, A.F. Kazakov, P.A. Domanski, Limited options for low-global-warming-potential refrigerants, Nat. Commun. 8 (2017) 1–9, https://doi.org/10.1038/ncomms14476.
[17] M.O. McLinden, C.J. Seeton, A. Pearson, New refrigerants and system configurations for vapor-compression refrigeration, Science (80-.) 370 (2020) 791–796, https://doi.org/10.1126/science.abe3692.
[18] A. Mota-Babiloni, P. Makhnatch, R. Khodabandeh, Recent investigations in HFCs substitution with lower GWP synthetic alternatives: Focus on energetic performance and environmental impact, Int. J. Refrig. 82 (2017) 288–301, https://doi.org/10.1016/j.ijrefrig.2017.06.026.
[19] G. Morrison, M.O. McLinden, Azeotropy in refrigerant mixtures, Int. J. Refrig. 16 (1993) 129–138, https://doi.org/10.1016/0140-7007(93)90069-K.
[20] D.K.J.A. Wanigarathna, J. Gao, B. Liu, Metal organic frameworks for adsorption-based separation of fluorocompounds: a review, Mater. Adv. 1 (3) (2020) 310–320, https://doi.org/10.1039/D0MA00083C.
[21] F. Pardo, G. Zarca, A. Urtiaga, Separation of Refrigerant Gas Mixtures Containing R32, R134a, and R1234yf through Poly(ether- block -amide) Membranes, ACS Sustain. Chem. Eng. 8 (6) (2020) 2548–2556, https://doi.org/10.1021/acssuschemeng.9b0719510.1021/acssuschemeng.9b07195.s001.
[22] F. Pardo, G. Zarca, A. Urtiaga, Effect of feed pressure and long-term separation performance of Pebax-ionic liquid membranes for the recovery of difluoromethane (R32) from refrigerant mixture R410A, J. Memb. Sci. 618 (2021) 118744, https://doi.org/10.1016/j.memsci.2020.118744.
[23] J.D. Seader, E.J. Henley, D.K. Roper, Separation process principles, 3rd ed, John Wiley & Sons Ltd, New Jersey, USA, 2010.
[24] D. Han, K.H. Row, Recent Applications of Ionic Liquids in Separation Technology, Molecules 15 (2010) 2405–2426, https://doi.org/10.3390/molecules15042405.
[25] T. Welton, Room-Temperature Ionic Liquids. Solvents for Synthesis and Catalysis, Chem. Rev. 99 (8) (1999) 2071–2084, https://doi.org/10.1021/cr980032t.
[26] V.I. Pârvulescu, C. Hardacre, Catalysis in Ionic Liquids, Chem. Rev. 107 (6) (2007) 2615–2665, https://doi.org/10.1021/cr050948h.
[27] D.R. MacFarlane, N. Tachikawa, M. Forsyth, J.M. Pringle, P.C. Howlett, G. D. Elliott, J.H. Davis, M. Watanabe, P. Simon, C.A. Angell, Energy Applications of Ionic Liquids, Energy Environ. Sci. 7 (1) (2014) 232–250, https://doi.org/10.1039/C3EE42099J.
[28] T.D. Ho, C. Zhang, L.W. Hantao, J.L. Anderson, Ionic liquids in analytical chemistry: Fundamentals, advances, and perspectives, Anal. Chem. 86 (1) (2014) 262–285, https://doi.org/10.1021/ac4035554.
[29] S. Zhang, Q. Zhang, Y. Zhang, Z. Chen, M. Watanabe, Y. Deng, Beyond solvents and electrolytes: Ionic liquids-based advanced functional materials, Prog. Mater. Sci. 77 (2016) 80–124, https://doi.org/10.1016/j.pmatsci.2015.10.001.
[30] G. Zarca, I. Ortiz, A. Urtiaga, Novel solvents based on thiocyanate ionic liquids doped with copper(I) with enhanced equilibrium selectivity for carbon monoxide separation from light gases, Sep. Purif. Technol. 196 (2018) 47–56, https://doi.org/10.1016/j.seppur.2017.06.069.
[31] Z. Lei, C. Dai, B. Chen, Gas Solubility in Ionic Liquids, Chem. Rev. 114 (2) (2014) 1289–1326, https://doi.org/10.1021/cr300497a.
[32] Z. Lei, C. Dai, J. Zhu, B. Chen, Extractive Distillation with Ionic Liquids: A Review, AIChE J. 60 (9) (2014) 3312–3329, https://doi.org/10.1002/aic.v60.910.1002/aic.14537.
[33] R. and A.-C.E. American Society of Heating, ASHRAE Refrigerant Designations, (n.d.). https://www.ashrae.org/technical-resources/standards-and-guidelines/ashrae-refrigerant-designations (accessed September 25, 2020).
[34] U.K. Deiters, Some remarks on the nomenclature of refrigerants, Fluid Phase Equilib. 132 (1-2) (1997) 265–270, https://doi.org/10.1016/S0378-3812(96)03232-3.
[35] European Fluorocarbons Technical Committee, Refrigerants Subject To The F-Gas Regulation 517/2014, (n.d.). https://www.fluorocarbons.org/library/ (accessed September 25, 2020).
[36] C. Kondou, D. BaBa, F. Mishima, S. Koyama, Flow boiling of non-azeotropic mixture R32/R1234ze(E) in horizontal microfin tubes, Int. J. Refrig. 36 (8) (2013) 2366–2378, https://doi.org/10.1016/j.ijrefrig.2013.07.009.
[37] Y. Maalem, A. Zarfa, Y. Tamene, S. Fedali, H. Madani, Prediction of thermodynamic properties of the ternary azeotropic mixtures, Fluid Phase Equilib. 517 (2020) 112613, https://doi.org/10.1016/j.fluid.2020.112613.
[38] Y. Zhao, Z. Li, X. Zhang, X. Wang, X. Dong, B. Gao, M. Gong, J. Shen, Azeotropic refrigerants and its application in vapor compression refrigeration cycle, Int. J. Refrig. 108 (2019) 1–13, https://doi.org/10.1016/j.ijrefrig.2019.08.024.
[39] B.O. Bolaji, Performance investigation of ozone-friendly R404A and R507 refrigerants as alternatives to R22 in a window air-conditioner, Energy Build. 43 (11) (2011) 3139–3143, https://doi.org/10.1016/j.enbuild.2011.08.011.
[40] Y. Zhao, M. Gong, X. Dong, H. Zhang, H. Guo, J. Wu, Prediction of ternary azeotropic refrigerants with a simple method, Fluid Phase Equilib. 425 (2016) 72–83, https://doi.org/10.1016/j.fluid.2016.05.010.
[41] R. Privat, J.-N. Jaubert, Classification of global fluid-phase equilibrium behaviors in binary systems, Chem. Eng. Res. Des. 91 (10) (2013) 1807–1839, https://doi.org/10.1016/j.cherd.2013.06.026.
[42] B.G. Lee, J.Y. Park, J.S. Lim, S.Y. Cho, K.Y. Park, Phase Equilibria of Chlorofluorocarbon Alternative Refrigerant Mixtures, J. Chem. Eng. Data. 44 (2) (1999) 190–192, https://doi.org/10.1021/je980180g.
[43] L. Kou, Z. Yang, X. Tang, W. Zhang, J. Lu, Experimental measurements and correlation of isothermal vapor-liquid equilibria for HFC-32 + HFO-1234ze(E) and HFC-134a + HFO-1234ze(E) binary systems, J. Chem. Thermodyn. 139 (2019), 105798, https://doi.org/10.1016/j.jct.2019.04.020.
[44] M. Nagel, K. Bier, Vapour-liquid equilibrium of ternary mixtures of the refrigerants R32, R125 and R134a, Int. J. Refrig. 18 (8) (1995) 534–543, https://doi.org/10.1016/0140-7007(96)81780-4.
[45] J.S. Lim, J.Y. Park, B.G. Lee, Y.W. Lee, Phase equilibria of 1,1,1-trifluoroethane (HFC-143a) + 1,1,1,2-tetrafluoroethane (HFC-134a), and + 1,1-difluoroethane (HFC-152a) at 273.15, 293.15, 303.15, and 313.15 K, Fluid Phase Equilib. 193 (2002) 29–39, https://doi.org/10.1016/S0378-3812(01)00632-X.
[46] L.-X. Chen, P. Hu, W.-B. Zhu, L. Jia, Z.-S. Chen, Vapor-liquid equilibria of fluoroethane (HFC-161) + 2,3,3,3-tetrafluoroprop-1-ene (HFO-1234yf), Fluid Phase Equilib. 392 (2015) 19–23, https://doi.org/10.1016/j.fluid.2015.02.014.
[47] X. Meng, X. Hu, T. Yang, J. Wu, Vapor liquid equilibria for binary mixtures of difluoromethane (R32) + fluoroethane (R161) and fluoroethane (R161) + trans-1,3,3,3-tetrafluoropropene (R1234ze(E)), J. Chem. Thermodyn. 118 (2018) 43–50, https://doi.org/10.1016/j.jct.2017.10.015.
[48] R. Stryjek, P.S. Chappelear, R. Kobayashi, Low-Temperature Vapor-Liquid Equilibria of Nitrogen-Methane System, J. Chem. Eng. Data. 19 (1974) 334–339, https://doi.org/10.1021/je60063a023.
[49] S.G. Levy, M.F. Doherty, A simple exact method for calculating tangent pinch points in multicomponent nonideal mixtures by bifurcation theory, Chem. Eng. Sci. 41 (12) (1986) 3155–3160, https://doi.org/10.1016/0009-2509(86)85052-7.
[50] C.N. Kim, Y.M. Park, Vapor-liquid equilibria for the difluoromethane (HFC-32)+ 1,1,1-trifluoroethane (HFC-143a) system, J. Chem. Eng. Data. 45 (1) (2000) 34–37, https://doi.org/10.1021/je9901379.
[51] T. Kamiaka, C. Dang, E. Hihara, Vapor-liquid equilibrium measurements for binary mixtures of R1234yf with R32, R125, and R134a, Int. J. Refrig. 36 (3) (2013) 965–971, https://doi.org/10.1016/j.ijrefrig.2012.08.016.
[52] M.H. Barley, J.D. Morrison, A. O'Donnel, I.B. Parker, S. Petherbridge, R. W. Wheelhouse, Vapour-liquid equilibrium data for binary mixtures of some new refrigerants, Fluid Phase Equilib. 140 (1-2) (1997) 183–206, https://doi.org/10.1016/S0378-3812(97)00146-5.
[53] S. Horstmann, M. Wilken, K. Fischer, J. Gmehling, Isothermal vapor-liquid equilibrium and excess enthalpy data for the binary systems propylene oxide + 2-methylpentane and difluoromethane (R32) + pentafluoroethane (R125), J. Chem. Eng. Data. 49 (6) (2004) 1504–1507, https://doi.org/10.1021/je034253u.
[54] M.B. Shiflett, S.I. Sandler, Modeling fluorocarbon vapor-liquid equilibria using the Wong-Sandler model, Fluid Phase Equilib. 147 (1-2) (1998) 145–162, https://doi.org/10.1016/S0378-3812(98)00253-2.
[55] Y. Higashi, Vapor-Liquid Equilibrium, Coexistence Curve, and Critical Locus for Pentafluoroethane +1,1,1-Trifluoroethane (R125/R143a), J. Chem. Eng. Data. 44 (1999) 333–337, https://doi.org/10.1021/je980266+.
[56] C.G. Albà, L.F. Vega, F. Llovell, Assessment on Separating Hydrofluoroolefins from Hydrofluorocarbons at the Azeotropic Mixture R513A by Using Fluorinated Ionic Liquids: A Soft-SAFT Study, Ind. Eng. Chem. Res. 59 (29) (2020) 13315–13324, https://doi.org/10.1021/acs.iecr.0c02331.
[57] S. Peper, J.M.S. Fonseca, R. Dohrn, High-pressure fluid-phase equilibria: Trends, recent developments, and systems investigated (2009–2012), Fluid Phase Equilib. 484 (2019) 126–224, https://doi.org/10.1016/j.fluid.2018.10.007.
[58] B.R. Mellein, A.M. Scurto, M.B. Shiflett, Gas Solubility in Ionic Liquids, Curr. Opin. Green Sustain. Chem. 28 (2021) 100425, https://doi.org/10.1016/j.cogsc.2020.100425.
[59] M.B. Shiflett, A. Yokozeki, Solubilities and Diffusivities of Carbon Dioxide in Ionic Liquids: [bmim][PF6] and [bmim][BF4], Ind. Eng. Chem. Res. 44 (2005) 4453–4464, https://doi.org/10.1021/ie058003d.
[60] J.E. Sosa, R.P.P.L. Ribeiro, P.J. Castro, J.P.B. Mota, J.M.M. Araújo, A.B. Pereiro, Absorption of Fluorinated Greenhouse Gases Using Fluorinated Ionic Liquids, Ind.

Eng. Chem. Res. 58 (45) (2019) 20769–20778, https://doi.org/10.1021/acs.iecr.9b0464810.1021/acs.iecr.9b04648.s001.
[61] W. Ren, A.M. Scurto, High-pressure phase equilibria with compressed gases, Rev. Sci. Instrum. 78 (12) (2007) 125104, https://doi.org/10.1063/1.2814025.
[62] I.M.A. Fonseca, J.P.B. Almeida, H.C. Fachada, Automated apparatus for gas solubility measurements, J. Chem. Thermodyn. 39 (10) (2007) 1407–1411, https://doi.org/10.1016/j.jct.2007.05.013.
[63] Z. Lei, J. Yuan, J. Zhu, Solubility of CO2 in Propanone, 1-Ethyl-3-methylimidazolium Tetrafluoroborate, and Their Mixtures, J. Chem. Eng. Data. 55 (10) (2010) 4190–4194, https://doi.org/10.1021/je100343v.
[64] M.B. Shiflett, A. Yokozeki, Vapor-Liquid-Liquid Equilibria of Pentafluoroethane and Ionic Liquid [bmim][PF6] Mixtures Studied with the Volumetric Method, J. Phys. Chem. B. 110 (29) (2006) 14436–14443, https://doi.org/10.1021/jp062437k.
[65] Y. Zhang, X. Wang, J. Yin, Viscosity of saturated mixtures of 1-hexyl-3-methylimidazolium bis(trifluoromethylsulfonyl)amide with R600a and R152a, J. Chem. Thermodyn. 141 (2020) 105970, https://doi.org/10.1016/j.jct.2019.105970.
[66] A. Ahosseini, W. Ren, L.R. Weatherley, A.M. Scurto, Viscosity and self-diffusivity of ionic liquids with compressed hydrofluorocarbons: 1-Hexyl-3-methyl-imidazolium bis(trifluoromethylsulfonyl)amide and 1,1,1,2-tetrafluoroethane, Fluid Phase Equilib. 437 (2017) 34–42, https://doi.org/10.1016/j.fluid.2016.11.022.
[67] D. Camper, C. Becker, C. Koval, R. Noble, Diffusion and solubility measurements in room temperature ionic liquids, Ind. Eng. Chem. Res. 45 (1) (2006) 445–450, https://doi.org/10.1021/ie0506668.
[68] J. Crank, in: The Mathematics of Diffusion, 2nd ed, Clarendon Press, Oxford, UK, 1975, https://doi.org/10.1016/0306-4549(77)90072-X.
[69] M.B. Shiflett, A. Yokozeki, Solubility and Diffusivity of Hydrofluorocarbons in Room-Temperature Ionic Liquids, AIChE J. 52 (3) (2006) 1205–1219, https://doi.org/10.1002/aic.v52:310.1002/aic.10685.
[70] M.B. Shiflett, M.A. Harmer, C.P. Junk, A. Yokozeki, Solubility and Diffusivity of Difluoromethane in Room-Temperature Ionic Liquids, J. Chem. Eng. Data. 51 (2) (2006) 483–495, https://doi.org/10.1021/je050386z.
[71] M.B. Shiflett, A. Yokozeki, J.P. Knapp, Process for the separation of fluorocarbons using ionic liquids, US Patent 7,964,760 B2, 2011.
[72] M.B. Shiflett, M.A. Harmer, C.P. Junk, A. Yokozeki, Solubility and diffusivity of 1,1,1,2-tetrafluoroethane in room-temperature ionic liquids, Fluid Phase Equilib. 242 (2) (2006) 220–232, https://doi.org/10.1016/j.fluid.2006.01.026.
[73] S. Asensio-Delgado, F. Pardo, G. Zarca, A. Urtiaga, Vapor−Liquid Equilibria and Diffusion Coefficients of Difluoromethane, 1,1,1,2-Tetrafluoroethane, and 2,3,3,3-Tetrafluoropropene in Low-Viscosity Ionic Liquids, J. Chem. Eng. Data. 65 (9) (2020) 4242–4251, https://doi.org/10.1021/acs.jced.0c00224.
[74] G. Yu, Y. Jiang, Z. Lei, Pentafluoroethane Dehydration with Ionic Liquids, Ind. Eng. Chem. Res. 57 (36) (2018) 12225–12234, https://doi.org/10.1021/acs.iecr.8b02790.
[75] L.i. Dong, D. Zheng, G. Sun, X. Wu, Vapor-Liquid Equilibrium Measurements of Difluoromethane + [Emim]OTf, Difluoromethane + [Bmim]OTf, Difluoroethane + [Emim]OTf, and Difluoroethane + [Bmim]OTf Systems, J. Chem. Eng. Data. 56 (9) (2011) 3663–3668, https://doi.org/10.1021/je2005566.
[76] M.B. Shiflett, A. Yokozeki, Absorption cycle utilizing ionic liquid as working fluid, US Patent 8715521 B2 (2014).
[77] S. Asensio-Delgado, F. Pardo, G. Zarca, A. Urtiaga, Enhanced absorption separation of hydrofluorocarbon/hydrofluoroolefin refrigerant blends using ionic liquids, Sep. Purif. Technol. 249 (2020) 117136, https://doi.org/10.1016/j.seppur.2020.117136.
[78] J.M.M.V. Sousa, J.F.O. Granjo, A.J. Queimada, A.G.M. Ferreira, N.M.C. Oliveira, I.M.A. Fonseca, Solubilities of hydrofluorocarbons in ionic liquids: Experimental and modelling study, J. Chem. Thermodyn. 73 (2014) 36–43, https://doi.org/10.1016/j.jct.2013.07.013.
[79] D. Jovell, S. B. Gómez, M.E. Zakrzewska, A.V.M. Nunes, J.M.M. Araújo, A. B. Pereiro, F. Llovell, Insight on the Solubility of R134a in Fluorinated Ionic Liquids and Deep Eutectic Solvents, J. Chem. Eng. Data. 65 (10) (2020) 4956–4969, https://doi.org/10.1021/acs.jced.0c0058810.1021/acs.jced.0c00588.s001.
[80] M.B. Shiflett, D.R. Corbin, B.A. Elliott, A. Yokozeki, Sorption of trifluoromethane in zeolites and ionic liquid, J. Chem. Thermodyn. 64 (2013) 40–49, https://doi.org/10.1016/j.jct.2013.04.018.
[81] D.L. Minnick, M.B. Shiflett, Solubility and Diffusivity of Chlorodifluoromethane in Imidazolium Ionic Liquids: [emim][Tf2N], [bmim][BF4], [bmim][PF6], and [emim][TFES], Ind. Eng. Chem. Res. 58 (25) (2019) 11072–11081, https://doi.org/10.1021/acs.iecr.9b02419.
[82] M.B. Shiflett, A. Yokozeki, Solubility Differences of Halocarbon Isomers in Ionic Liquid [emim][Tf2N], J. Chem. Eng. Data. 52 (5) (2007) 2007–2015, https://doi.org/10.1021/je700295e.
[83] W. Ren, A.M. Scurto, M.B. Shiflett, A. Yokozeki, Phase behavior and equilibria of ionic liquids and refrigerants: 1-ethyl-3-methyl-imidazolium bis (trifluoromethylsulfonyl)imide ([EMIm][Tf2N]) and R-134a, in: Gas-Expanded Liq. Near-Critical Media, 2009, pp. 112–128. https://doi.org/10.1021/bk-2009-1006.ch006.
[84] L.F. Lepre, D. Andre, S. Denis-Quanquin, A. Gautier, A.A.H. Pádua, M. Costa Gomes, Ionic liquids can enable the recycling of fluorinated greenhouse gases, ACS Sustain, Chem. Eng. 7 (19) (2019) 16900–16906, https://doi.org/10.1021/acssuschemeng.9b04214.
[85] M.B. Shiflett, A. Yokozeki, Binary Vapor-Liquid and Vapor–Liquid–Liquid Equilibria of Hydrofluorocarbons (HFC-125 and HFC-143a) and Hydrofluoroethers (HFE-125 and HFE-143a) with Ionic Liquid [emim][Tf2N], J. Chem. Eng. Data. 53 (2) (2008) 492–497, https://doi.org/10.1021/je700588d.
[86] A.R.C. Morais, A.N. Harders, K.R. Baca, G.M. Olsen, B.J. Befort, A.W. Dowling, E. J. Maginn, M.B. Shiflett, Phase Equilibria, Diffusivities, and Equation of State Modeling of HFC-32 and HFC-125 in Imidazolium- based Ionic Liquids for the Separation of R-410A, Ind. Eng. Chem. Res. 59 (40) (2020) 18222–18235, https://doi.org/10.1021/acs.iecr.0c0282010.1021/acs.iecr.0c02820.s001.
[87] M.B. Shiflett, A. Yokozeki, Gaseous Absorption of Fluoromethane, Fluoroethane, and 1,1,2,2-Tetrafluoroethane in 1-Butyl-3-Methylimidazolium Hexafluorophosphate, Ind. Eng. Chem. Res. 45 (18) (2006) 6375–6382, https://doi.org/10.1021/ie060192s.
[88] M. He, S. Peng, X. Liu, P. Pan, Y. He, Diffusion coefficients and Henry's constants of hydrofluorocarbons in [HMIM][Tf2N], [HMIM][TfO], and [HMIM][BF4], J. Chem. Thermodyn. 112 (2017) 43–51, https://doi.org/10.1016/j.jct.2017.04.009.
[89] W. Ren, A.M. Scurto, Phase equilibria of imidazolium ionic liquids and the refrigerant gas, 1,1,1,2-tetrafluoroethane (R-134a), Fluid Phase Equilib. 286 (1) (2009) 1–7, https://doi.org/10.1016/j.fluid.2009.07.007.
[90] X. Liu, M.Q. Nguyen, S. Xue, C. Song, M. He, Vapor-Liquid Equilibria and Inter-Diffusion Coefficients for Working Pairs for Absorption Refrigeration Systems Composed of [HMIM][BF4] and Fluorinated Propanes, Int. J. Refrig. 104 (2019) 34–41, https://doi.org/10.1016/j.ijrefrig.2019.04.023.
[91] X. Liu, P. Pan, M. He, Vapor-liquid equilibrium and diffusion coefficients of R32 + [HMIM][FEP], R152a + [HMIM][FEP] and R161 + [HMIM][FEP], J. Mol. Liq. 253 (2018) 28–35, https://doi.org/10.1016/j.molliq.2018.01.032.
[92] X. Liu, M. He, N. Lv, X. Qi, C. Su, Vapor−Liquid Equilibrium of Three Hydrofluorocarbons with [HMIM][Tf2N], J. Chem. Eng. Data. 60 (5) (2015) 1354–1361, https://doi.org/10.1021/je501069b.
[93] X. Liu, M. He, N. Lv, X. Qi, C. Su, Solubilities of R-161 and R-143a in 1-Hexyl-3-methylimidazolium bis (trifluoromethylsulfonyl)imide, Fluid Phase Equilib. 388 (2015) 37–42, https://doi.org/10.1016/j.fluid.2014.12.026.
[94] X. Liu, P. Pan, F. Yang, M. He, Solubilities and diffusivities of R227ea, R236fa and R245fa in 1-hexyl-3-methylimidazolium bis(trifluoromethylsulfonyl)imide, J. Chem. Thermodyn. 123 (2018) 158–164, https://doi.org/10.1016/j.jct.2018.04.004.
[95] M.B. Shiflett, D.R. Corbin, A. Yokozeki, Comparison of the sorption of trifluoromethane (R-23) on zeolites and in an ionic liquid, Adsorpt. Sci. Technol. 31 (1) (2013) 59–83, https://doi.org/10.1260/0263-6174.31.1.59.
[96] J.M.M.V. Sousa, J.F.O. Granjo, A.J. Queimada, A.G.M. Ferreira, N.M.C. Oliveira, I.M.A. Fonseca, Solubility of hydrofluorocarbons in phosphonium-based ionic liquids: Experimental and modelling study, J. Chem. Thermodyn. 79 (2014) 184–191, https://doi.org/10.1016/j.jct.2014.08.001.
[97] X. Liu, N. Lv, C. Su, M. He, Solubilities of R32, R245fa, R227ea and R236fa in a phosphonium-based ionic liquid, J. Mol. Liq. 218 (2016) 525–530, https://doi.org/10.1016/j.molliq.2016.02.041.
[98] X. Liu, X. Qi, N. Lv, M. He, Gaseous absorption of fluorinated ethanes by ionic liquids, Fluid Phase Equilib. 405 (2015) 1–6, https://doi.org/10.1016/j.fluid.2015.07.001.
[99] L.F. Lepre, L. Pison, I. Otero, A. Gautier, J. Dévemy, P. Husson, A.A.H. Pádua, M. Costa Gomes, Using hydrogenated and perfluorinated gases to probe the interactions and structure of fluorinated ionic liquids, Phys. Chem. Chem. Phys. 21 (17) (2019) 8865–8873, https://doi.org/10.1039/C9CP00593E.
[100] B.J. Costa Cabral, R.C. Guedes, R.S. Pai-Panandiker, C.A. Nieto de Castro, Hydrogen bonding and the dipole moment of hydrofluorocarbons by density functional theory, Phys. Chem. Chem. Phys. 3 (2001) 4200–4207, https://doi.org/10.1039/b102879k.
[101] E. Kryachko, S. Scheiner, CH···F hydrogen bonds. Dimers of fluoromethanes, J. Phys. Chem. A. 108 (2004) 2527–2535, https://doi.org/10.1021/Jp0365108.
[102] M. Karamoddin, F. Varaminian, Solubility of R22, R23, R32, R134a, R152a, R125 and R744 refrigerants in water by using equations of state, Int. J. Refrig. 36 (6) (2013) 1681–1688, https://doi.org/10.1016/j.ijrefrig.2013.04.013.
[103] Q.R. Sheridan, W.F. Schneider, E.J. Maginn, Role of Molecular Modeling in the Development of CO_2-Reactive Ionic Liquids, Chem. Rev. 118 (2018) 5242–5260, https://doi.org/10.1021/acs.chemrev.8b00017.
[104] T. Endo, Y. Nishisaka, Y. Kin, Y. Kimura, Systematic estimation and interpretation of fractional free volume in 1-alkyl-3-methylimidazolium-based ionic liquids, Fluid Phase Equilib. 498 (2019) 144–150, https://doi.org/10.1016/j.fluid.2019.06.027.
[105] X. Liu, K.E. O'Harra, J.E. Bara, C.H. Turner, Molecular Insight into the Anion Effect and Free Volume Effect of CO2 Solubility in Multivalent Ionic Liquids, Phys. Chem. Chem. Phys. 22 (36) (2020) 20618–20633, https://doi.org/10.1039/D0CP03424J.
[106] M.S. Shannon, J.M. Tedstone, S.P.O. Danielsen, M.S. Hindman, A.C. Irvin, J. E. Bara, Free volume as the basis of gas solubility and selectivity in imidazolium-based ionic liquids, Ind. Eng. Chem. Res. 51 (15) (2012) 5565–5576, https://doi.org/10.1021/ie202916e.
[107] P.J. Carvalho, K.A. Kurnia, J.A.P. Coutinho, Dispelling some myths about the CO2 solubility in ionic liquids, Phys. Chem. Chem. Phys. 18 (22) (2016) 14757–14771, https://doi.org/10.1039/C6CP01896C.
[108] Y. Sun, Y. Zhang, G. Di, X. Wang, J.M. Prausnitz, L. Jin, Vapor-Liquid Equilibria for R1234ze(E) and Three Imidazolium-Based Ionic Liquids as Working Pairs in Absorption-Refrigeration Cycle, J. Chem. Eng. Data. 63 (8) (2018) 3053–3060, https://doi.org/10.1021/acs.jced.8b0031410.1021/acs.jced.8b00314.s001.
[109] D.L. Minnick, M.B. Shiflett, Solubility and Diffusivity of Bromodifluoromethane (Halon-1201) in Imidazolium Ionic Liquids: [C2C1im][Tf2N], [C4C1im][BF4], and [C4C1im][PF6], J. Chem. Eng. Data. 65 (7) (2020) 3277–3286, https://doi.org/10.1021/acs.jced.0c00022.

[110] Y. Zhang, J. Yin, X. Wang, Vapor-liquid equilibrium of 2,3,3,3-tetrafluoroprop-1-ene with 1-butyl-3-methylimidazolium hexafluorophosphate, 1-hexyl-3-methyl imidazolium hexafluorophosphate, and 1-octyl-3-methylimidazolium hexafluorophosphate, J. Mol. Liq. 260 (2018) 203–208, https://doi.org/10.1016/j.molliq.2018.03.112.
[111] M. He, P. Pan, F. Yang, T. Wang, X. Liu, Gaseous Absorption of trans-1-Chloro-3,3,3-trifluoropropene in Three Immidazolium-Based Ionic Liquids, J. Chem. Eng. Data. 63 (5) (2018) 1780–1788, https://doi.org/10.1021/acs.jced.8b00110.
[112] X. Liu, L. Bai, S. Liu, M. He, Vapor−Liquid Equilibrium of R1234yf/[HMIM][Tf2N] and R1234ze (E)/[HMIM][Tf2N] Working Pairs for the Absorption Refrigeration Cycle, J. Chem. Eng. Data. 61 (11) (2016) 3952–3957, https://doi.org/10.1021/acs.jced.6b00731.
[113] J.L. Anthony, E.J. Maginn, J.F. Brennecke, Solubilities and thermodynamic properties of gases in the ionic liquid 1-n-butyl-3-methylimidazolium hexafluorophosphate, J. Phys. Chem. B. 106 (29) (2002) 7315–7320, https://doi.org/10.1021/jp020631a.
[114] M.F. Costa Gomes, Low-pressure solubility and thermodynamics of solvation of carbon dioxide, ethane, and hydrogen in 1-hexyl-3-methylimidazolium bis (trifluoromethylsulfonyl) amide between temperatures of 283 K and 343 K, J. Chem. Eng. Data. 52 (2) (2007) 472–475, https://doi.org/10.1021/je0604129.
[115] C.M. Sanchez, T. Song, J.F. Brennecke, B.D. Freeman, Hydrogen Stable Supported Ionic Liquid Membranes with Silver Carriers: Propylene and Propane Permeability and Solubility, Ind. Eng. Chem. Res. 59 (12) (2020) 5362–5370, https://doi.org/10.1021/acs.iecr.9b04886.
[116] D. Camper, C. Becker, C. Koval, R. Noble, Low pressure hydrocarbon solubility in room temperature ionic liquids containing imidazolium rings interpreted using regular solution theory, Ind. Eng. Chem. Res. 44 (6) (2005) 1928–1933, https://doi.org/10.1021/ie049312r.
[117] F.A.M.M. Gonçalves, C.S.M.F. Costa, C.E. Ferreira, J.C.S. Bernardo, I. Johnson, I. M.A. Fonseca, A.G.M. Ferreira, Pressure-volume-temperature measurements of phosphonium-based ionic liquids and analysis with simple equations of state, J. Chem. Thermodyn. 43 (6) (2011) 914–929, https://doi.org/10.1016/j.jct.2011.01.009.
[118] Y. Sun, Y. Zhang, X. Wang, J.M. Prausnitz, L. Jin, Gaseous absorption of 2,3,3,3-tetrafluoroprop-1-ene in three imidazolium-based ionic liquids, Fluid Phase Equilib. 450 (2017) 65–74, https://doi.org/10.1016/j.fluid.2017.07.013.
[119] X. Wang, Y. Zhang, D. Wang, Y. Sun, Phase Equilibria of trans-1,3,3,3-Tetrafluoropropene with Three Imidazolium Ionic Liquids, J. Chem. Eng. Data. 62 (6) (2017) 1825–1831, https://doi.org/10.1021/acs.jced.7b00047.
[120] Y.F. Hu, Z.C. Liu, C.M. Xu, X.M. Zhang, The molecular characteristics dominating the solubility of gases in ionic liquids, Chem. Soc. Rev. 40 (2011) 3802–3823, https://doi.org/10.1039/c0cs00006j.
[121] Y. Sun, G. Di, J. Wang, Y. Hu, X. Wang, M. He, Gaseous solubility and thermodynamic performance of absorption system using R1234yf / IL working pairs, Appl. Therm. Eng. 172 (2020) 115161, https://doi.org/10.1016/j.applthermaleng.2020.115161.
[122] X. Liu, Z. Ye, L. Bai, M. He, Performance comparison of two absorption-compression hybrid refrigeration systems using R1234yf/ionic liquid as working pair, Energy Convers. Manag. 181 (2019) 319–330, https://doi.org/10.1016/j.enconman.2018.12.030.
[123] K. Kontomaris, N.C. Moull, M.B. Shiflett, Compositions comprising ionic liquids and fluoroolefins and use thereof in absorption cycle systems, US Patent Application 2011/0088418 A1, 2011.
[124] A. Mota-Babiloni, M. Mastani Joybari, J. Navarro-Esbrí, C. Mateu-Royo, Á. Barragán-Cervera, M. Amat-Albuixech, F. Molés, Ultralow-temperature refrigeration systems: Configurations and refrigerants to reduce the environmental impact, Int. J. Refrig. 111 (2020) 147–158, https://doi.org/10.1016/j.ijrefrig.2019.11.016.
[125] L. Pison, J.N. Canongia Lopes, L.P.N. Rebelo, A.A.H. Padua, M.F. Costa Gomes, Interactions of fluorinated gases with ionic liquids: Solubility of CF4, C2F6, and C3F8 in trihexyltetradecylphosphonium bis(trifluoromethylsulfonyl)amide, J. Phys. Chem. B. 112 (39) (2008) 12394–12400, https://doi.org/10.1021/jp8051714.
[126] J. Kumełan, Á. Pérez-Salado Kamps, D. Tuma, A. Yokozeki, M.B. Shiflett, G. Maurer, Solubility of tetrafluoromethane in the ionic liquid [hmim][Tf2N], J. Phys. Chem. B. 112 (10) (2008) 3040–3047, https://doi.org/10.1021/jp076737t.
[127] W. Ren, A.M. Scurto, Global phase behavior of imidazolium ionic liquids and compressed 1,1,1,2-tetrafluoroethane (R-134a), AIChE J. 55 (2) (2009) 486–493, https://doi.org/10.1002/aic.v55:210.1002/aic.11657.
[128] A. Yokozeki, M.B. Shiflett, Global phase behaviors of trifluoromethane in ionic liquid [bmim][PF6], AIChE J. 52 (11) (2006) 3952–3957, https://doi.org/10.1002/(ISSN)1547-590510.1002/aic.v52:1110.1002/aic.11007.
[129] M.B. Shiflett, A. Yokozeki, Vapor-Liquid-Liquid Equilibria of Hydrofluorocarbons + 1-Butyl-3-methylimidazolium Hexafluorophosphate, J. Chem. Eng. Data. 51 (5) (2006) 1931–1939, https://doi.org/10.1021/je060275f10.1021/je060275f.s001.
[130] M.B. Shiflett, A. Yokozeki, Hydrogen substitution effect on the solubility of perhalogenated compounds in ionic liquid [bmim][PF6], Fluid Phase Equilib. 259 (2) (2007) 210–217, https://doi.org/10.1016/j.fluid.2007.07.035.
[131] A. Shariati, C.J. Peters, High-pressure phase behavior of systems with ionic liquids: measurements and modeling of the binary system fluoroform + 1-ethyl-3-methylimidazolium hexafluorophosphate, J. Supercrit. Fluids. 25 (2) (2003) 109–117, https://doi.org/10.1016/S0896-8446(02)00160-2.
[132] A. Shariati, K. Gutkowski, C.J. Peters, Comparison of the Phase Behavior of Some Selected Binary Systems with Ionic Liquids, AIChE J. 51 (5) (2005) 1532–1540, https://doi.org/10.1002/aic.v51:510.1002/aic.10384.
[133] K. Dong, X. Liu, H. Dong, X. Zhang, S. Zhang, Multiscale Studies on Ionic Liquids, Chem. Rev. 117 (10) (2017) 6636–6695, https://doi.org/10.1021/acs.chemrev.6b00776.
[134] M.T. Mota-Martinez, P. Brandl, J.P. Hallett, N. Mac Dowell, Challenges and opportunities for the utilisation of ionic liquids as solvents for CO_2 capture, Mol. Syst. Des. Eng. 3 (3) (2018) 560–571, https://doi.org/10.1039/C8ME00009C.
[135] K. Li, W. Wu, J. Wu, H. Liang, H. Zhang, Experiments on vapour-liquid equilibrium of CO_2-ionic liquid under flow conditions and influence on its refrigeration cycle, Appl. Therm. Eng. 180 (2020) 115865, https://doi.org/10.1016/j.applthermaleng.2020.115865.
[136] J. Palomar, M. Larriba, J. Lemus, D. Moreno, R. Santiago, C. Moya, J. de Riva, G. Pedrosa, Demonstrating the key role of kinetics over thermodynamics in the selection of ionic liquids for CO_2 physical absorption, Sep. Purif. Technol. 213 (2019) 578–586, https://doi.org/10.1016/j.seppur.2018.12.059.
[137] J. Wang, Z. Song, H. Cheng, L. Chen, L. Deng, Z. Qi, Multilevel screening of ionic liquid absorbents for simultaneous removal of CO_2 and H_2S from natural gas, Sep. Purif. Technol. 248 (2020) 117053, https://doi.org/10.1016/j.seppur.2020.117053.
[138] J. Wang, Z. Song, H. Cheng, L. Chen, L. Deng, Z. Qi, Computer-Aided Design of Ionic Liquids as Absorbent for Gas Separation Exemplified by CO_2 Capture Cases, ACS Sustain. Chem. Eng. 6 (9) (2018) 12025–12035, https://doi.org/10.1021/acssuschemeng.8b0232110.1021/acssuschemeng.8b02321.s001.
[139] M.G. Freire, A.R.R. Teles, M.A.A. Rocha, B. Schröder, C.M.S.S. Neves, P. J. Carvalho, D.V. Evtuguin, L.M.N.B.F. Santos, J.A.P. Coutinho, Thermophysical Characterization of Ionic Liquids Able To Dissolve Biomass, J. Chem. Eng. Data. 56 (12) (2011) 4813–4822, https://doi.org/10.1021/je200790q.
[140] J.A. Widegren, J.W. Magee, Density, viscosity, speed of sound, and electrolytic conductivity for the ionic liquid 1-hexyl-3-methylimidazolium bis (trifluoromethylsulfonyl)imide and its mixtures with water, J. Chem. Eng. Data. 52 (6) (2007) 2331–2338, https://doi.org/10.1021/je700329a.
[141] Y. Zhang, X. Jia, X. Wang, Experimental investigation on the viscosity of [Hmim][Tf2N] saturated with R1234ze(E) or R1234yf, Int. J. Refrig. 117 (2020) 338–345, https://doi.org/10.1016/j.ijrefrig.2020.04.018.
[142] I.H. Bell, J. Wronski, S. Quoilin, V. Lemort, Pure and Pseudo-pure Fluid Thermophysical Property Evaluation and the Open-Source Thermophysical Property Library CoolProp, Ind. Eng. Chem. Res. 53 (6) (2014) 2498–2508, https://doi.org/10.1021/ie4033999.
[143] J. Kendall, K.P. Monroe, The viscosity of liquids. II. The viscosity-composition curve for ideal liquid mixtures, J. Am. Chem. Soc. 39 (1917) 1787–1802, https://doi.org/10.1021/cen-v023n003.p224.
[144] S. Atashrouz, M. Zarghampour, S. Abdolrahimi, G. Pazuki, B. Nasernejad, Estimation of the viscosity of ionic liquids containing binary mixtures based on the Eyring's theory and a modified Gibbs energy model, J. Chem. Eng. Data. 59 (11) (2014) 3691–3704, https://doi.org/10.1021/je500572t.
[145] D. Camper, J. Bara, C. Koval, R. Noble, Bulk-fluid solubility and membrane feasibility of Rmim-based room-temperature ionic liquids, Ind. Eng. Chem. Res. 45 (18) (2006) 6279–6283, https://doi.org/10.1021/ie060177n.
[146] S. Zeng, X. Zhang, L.u. Bai, X. Zhang, H. Wang, J. Wang, D.i. Bao, M. Li, X. Liu, S. Zhang, Ionic-Liquid-Based CO2 Capture Systems: Structure, Interaction and Process, Chem. Rev. 117 (14) (2017) 9625–9673, https://doi.org/10.1021/acs.chemrev.7b00072.
[147] G. Zarca, I. Ortiz, A. Urtiaga, Recovery of carbon monoxide from flue gases by reactive absorption in ionic liquid imidazolium chlorocuprate(I): Mass transfer coefficients, Chinese J. Chem. Eng. 23 (5) (2015) 769–774, https://doi.org/10.1016/j.cjche.2014.06.040.
[148] S.S. Moganty, R.E. Baltus, Diffusivity of carbon dioxide in room-temperature ionic liquids, Ind. Eng. Chem. Res. 49 (19) (2010) 9370–9376, https://doi.org/10.1021/ie101260j.
[149] T. Wang, X. Liu, J. Chu, Y. Shi, J. Li, M. He, Molecular dynamics simulation of diffusion and interaction of [bmim][Tf2N] + HFO-1234yf mixture, J. Mol. Liq. 312 (2020), 113390, https://doi.org/10.1016/j.molliq.2020.113390.
[150] J.E. Bara, T.K. Carlisle, C.J. Gabriel, D. Camper, A. Finotello, D.L. Gin, R.D. Noble, Guide to CO_2 separations in imidazolium-based room-temperature ionic liquids, Ind. Eng. Chem. Res. 48 (6) (2009) 2739–2751, https://doi.org/10.1021/ie8016237.
[151] S.S. Moganty, R.E. Baltus, Regular solution theory for low pressure carbon dioxide solubility in room temperature ionic liquids: Ionic liquid solubility parameter from activation energy of viscosity, Ind. Eng. Chem. Res. 49 (12) (2010) 5846–5853, https://doi.org/10.1021/ie901837k.
[152] L.F. Vega, O. Vilaseca, F. Llovell, J.S. Andreu, Modeling ionic liquids and the solubility of gases in them: Recent advances and perspectives, Fluid Phase Equilib. 294 (1-2) (2010) 15–30, https://doi.org/10.1016/j.fluid.2010.02.006.
[153] C.A. Faúndez, J.O. Valderrama, R.A. Campusano, Henry's law constant as a function of temperature and pressure to calculate the solubility of difluoromethane (R-32) in ionic liquids, Int. J. Refrig. 119 (2020) 401–409, https://doi.org/10.1016/j.ijrefrig.2020.05.024.
[154] W. Wu, T. You, H. Zhang, X. Li, Comparisons of different ionic liquids combined with trans-1,3,3,3-tetrafluoropropene (R1234ze(E)) as absorption working fluids, Int. J. Refrig. 88 (2018) 45–57, https://doi.org/10.1016/j.ijrefrig.2017.12.011.
[155] Y.J. Kim, S. Kim, Y.K. Joshi, A.G. Fedorov, P.A. Kohl, Thermodynamic analysis of an absorption refrigeration system with ionic-liquid/refrigerant mixture as a working fluid, Energy. 44 (1) (2012) 1005–1016, https://doi.org/10.1016/j.energy.2012.04.048.
[156] L.i. Dong, D. Zheng, X. Wu, Working pair selection of compression and absorption hybrid cycles through predicting the activity coefficients of hydrofluorocarbon +

ionic liquid systems by the UNIFAC model, Ind. Eng. Chem. Res. 51 (12) (2012) 4741–4747, https://doi.org/10.1021/ie202029d.
[157] L. Bai, M. He, X. Liu, Z. Ye, A new activity coefficient model for the solution of molecular solute + ionic liquid, Fluid Phase Equilib. 493 (2019) 144–152, https://doi.org/10.1016/j.fluid.2019.04.016.
[158] A. Yokozeki, Solubility of refrigerants in various lubricants, Int. J. Thermophys. 22 (2001) 1057–1071, https://doi.org/10.1023/A:1010695705260.
[159] S. Kim, P.A. Kohl, Analysis of [hmim][PF6] and [hmim][Tf2N] ionic liquids as absorbents for an absorption refrigeration system, Int. J. Refrig. 48 (2014) 105–113, https://doi.org/10.1016/j.ijrefrig.2014.09.003.
[160] S. Kim, N. Patel, P.A. Kohl, Performance simulation of ionic liquid and hydrofluorocarbon working fluids for an absorption refrigeration system, Ind. Eng. Chem. Res. 52 (19) (2013) 6329–6335, https://doi.org/10.1021/ie400261g.
[161] A. Yokozeki, M.B. Shiflett, Gas solubilities in ionic liquids using a generic van der Waals equation of state, J. Supercrit. Fluids. 55 (2) (2010) 846–851, https://doi.org/10.1016/j.supflu.2010.09.015.
[162] A.C.D. Freitas, L.P. Cunico, M. Aznar, R. Guirardello, Modeling vapor liquid equilibrium of ionic liquids + gas binary systems at high pressure with cubic equations of state, Brazilian J. Chem. Eng. 30 (1) (2013) 63–73, https://doi.org/10.1590/S0104-66322013000100008.
[163] K. Parvaneh, A. Rasoolzadeh, A. Shariati, Modeling the phase behavior of refrigerants with ionic liquids using the QC-PC-SAFT equation of state, J. Mol. Liq. 274 (2019) 497–504, https://doi.org/10.1016/j.molliq.2018.10.116.
[164] C.A. Faúndez, L.A. Barrientos, J.O. Valderrama, Modeling and thermodynamic consistency of solubility data of refrigerants in ionic liquids, Int. J. Refrig. 36 (8) (2013) 2242–2250, https://doi.org/10.1016/j.ijrefrig.2013.06.006.
[165] J.O. Valderrama, C.A. Faúndez, R. Campusano, An overview of a thermodynamic consistency test of phase equilibrium data. Application of the versatile VPT equation of state to check data of mixtures containing a gas solute and an ionic liquid solvent, J. Chem. Thermodyn. 131 (2019) 122–132, https://doi.org/10.1016/j.jct.2018.09.019.
[166] J. Hekayati, A. Roosta, J. Javanmardi, Thermodynamic modeling of refrigerants solubility in ionic liquids using original and ε*-Modified Sanchez-Lacombe equations of state, Fluid Phase Equilib. 403 (2015) 14–22, https://doi.org/10.1016/j.fluid.2015.05.046.
[167] H. Machida, Y. Sato, R.L. Smith, Simple modification of the temperature dependence of the Sanchez-Lacombe equation of state, Fluid Phase Equilib. 297 (2) (2010) 205–209, https://doi.org/10.1016/j.fluid.2010.03.024.
[168] A. Shojaeian, H. Fatoorehchi, Modeling solubility of refrigerants in ionic liquids using Peng Robinson-Two State equation of state, Fluid Phase Equilib. 486 (2019) 80–90, https://doi.org/10.1016/j.fluid.2019.01.003.
[169] S. Asensio-Delgado, D. Jovell, G. Zarca, A. Urtiaga, F. Llovell, Thermodynamic and process modeling of the recovery of R410A compounds with ionic liquids, Int. J. Refrig. 118 (2020) 365–375, https://doi.org/10.1016/j.ijrefrig.2020.04.013.
[170] I. Sujatha, G. Venkatarathnam, Comparison of performance of a vapor absorption refrigeration system operating with some hydrofluorocarbons and hydrofluoroelfins as refrigerants along with ionic liquid [hmim][Tf2N] as the absorbent, Int. J. Refrig. 88 (2018) 370–382, https://doi.org/10.1016/j.ijrefrig.2018.03.004.
[171] E.K. Karakatsani, I.G. Economou, M.C. Kroon, C.J. Peters, G.J. Witkamp, tPC-PSAFT modeling of gas solubility in imidazolium-based ionic liquids, J. Phys. Chem. C. 111 (2007) 15487–15492, https://doi.org/10.1021/jp070556+.
[172] I. Polishuk, Implementation of CP-PC-SAFT for Predicting Thermodynamic Properties and Gas Solubility in 1-Alkyl-3-methylimidazolium Bis (trifluoromethylsulfonyl)imide Ionic Liquids without Fitting Binary Parameters, Ind. Eng. Chem. Res. 56 (27) (2017) 7845–7857, https://doi.org/10.1021/acs.iecr.7b0184610.1021/acs.iecr.7b01846.s001.
[173] D. Moreno, V.R. Ferro, J. de Riva, R. Santiago, C. Moya, M. Larriba, J. Palomar, Absorption refrigeration cycles based on ionic liquids: Refrigerant/absorbent selection by thermodynamic and process analysis, Appl. Energy. 213 (2018) 179–194, https://doi.org/10.1016/j.apenergy.2018.01.034.
[174] J.E. Sosa, R. Santiago, D. Hospital-Benito, M.F. Costa Gomes, J.M.M. Araújo, A. B. Pereiro, J. Palomar, Process Evaluation of Fluorinated Ionic Liquids as F-Gases Absorbents, Environ. Sci. Technol. (2020), https://doi.org/10.1021/acs.est.0c05305.
[175] C.A. Faúndez, R.A. Campusano, J.O. Valderrama, Misleading results on the use of artificial neural networks for correlating and predicting properties of fluids. A case on the solubility of refrigerant R-32 in ionic liquids, J. Mol. Liq. 298 (2020) 112009, https://doi.org/10.1016/j.molliq.2019.112009.
[176] E.N. Fierro, C.A. Faúndez, A.S. Muñoz, Influence of thermodynamically inconsistent data on modeling the solubilities of refrigerants in ionic liquids using an artificial neural network, J. Mol. Liq. 337 (2021) 116417, https://doi.org/10.1016/j.molliq.2021.116417.
[177] A.B. Pereiro, J.M.M. Araújo, J.M.S.S. Esperança, I.M. Marrucho, L.P.N. Rebelo, Ionic liquids in separations of azeotropic systems - A review, J. Chem. Thermodyn. 46 (2012) 2–28, https://doi.org/10.1016/j.jct.2011.05.026.
[178] M.B. Shiflett, A. Yokozeki, Separation of difluoromethane and pentafluoroethane by extractive distillation using ionic liquid, Chem. Today. 24 (2006) 28–30.
[179] M.B. Shiflett, A. Yokozeki, Utilizing ionic liquids for hydrofluorocarbon separation, US Patent 8,628,644 B2, 2014.
[180] E. Quijada-Maldonado, T.A.M. Aelmans, G.W. Meindersma, A.B. de Haan, Pilot plant validation of a rate-based extractive distillation model for water-ethanol separation with the ionic liquid [emim][DCA] as solvent, Chem. Eng. J. 223 (2013) 287–297, https://doi.org/10.1016/j.cej.2013.02.111.
[181] E. Quijada-Maldonado, G.W. Meindersma, A.B. De Haan, Pilot plant study on the extractive distillation of toluene-methylcyclohexane mixtures using NMP and the ionic liquid [hmim][TCB] as solvents, Sep. Purif. Technol. 166 (2016) 196–204, https://doi.org/10.1016/j.seppur.2016.04.041.
[182] C. Maton, N. De Vos, C.V. Stevens, Ionic liquid thermal stabilities: Decomposition mechanisms and analysis tools, Chem. Soc. Rev. 42 (2013) 5963–5977, https://doi.org/10.1039/c3cs60071h.
[183] Y. Huang, Z. Chen, J.M. Crosthwaite, S. N.V.K. Aki, J.F. Brennecke, Thermal Stability of Ionic Liquids in Nitrogen and Air Environments, J. Chem. Thermodyn. 161 (2021) 106560, https://doi.org/10.1016/j.jct.2021.106560.
[184] N. Meine, F. Benedito, R. Rinaldi, Thermal stability of ionic liquids assessed by potentiometric titration, Green Chem. 12 (2010) 1711–1714, https://doi.org/10.1039/c0gc00091d.
[185] E. Fabre, S.M.S. Murshed, A review of thermophysical properties and potential of ionic liquids for thermal applications, J. Mater. Chem. A. (2021), https://doi.org/10.1039/d1ta03656d.
[186] Y. Cao, T. Mu, Comprehensive investigation on the thermal stability of 66 ionic liquids by thermogravimetric analysis, Ind. Eng. Chem. Res. 53 (20) (2014) 8651–8664, https://doi.org/10.1021/ie5009597.
[187] M. Villanueva, A. Coronas, J. García, J. Salgado, Thermal stability of ionic liquids for their application as new absorbents, Ind. Eng. Chem. Res. 52 (45) (2013) 15718–15727, https://doi.org/10.1021/ie401656e.
[188] V. Gerbaud, I. Rodriguez-Donis, L. Hegely, P. Lang, F. Denes, X.Q. You, Review of extractive distillation. Process design, operation, optimization and control, Chem. Eng. Res. Des. 141 (2019) 229–271, https://doi.org/10.1016/j.cherd.2018.09.020.
[189] K. Friess, P. Izák, M. Kárászová, M. Pasichnyk, M. Lanč, D. Nikolaeva, P. Luis, J. C. Jansen, A review on ionic liquid gas separation membranes, Membranes (Basel). 11 (2021) 1–58, https://doi.org/10.3390/membranes11020097.
[190] G. Zarca, W.J. Horne, I. Ortiz, A. Urtiaga, J.E. Bara, Synthesis and gas separation properties of poly(ionic liquid)-ionic liquid composite membranes containing a copper salt, J. Memb. Sci. 515 (2016) 109–114, https://doi.org/10.1016/j.memsci.2016.05.045.
[191] P. Bernardo, J.C. Jansen, F. Bazzarelli, F. Tasselli, A. Fuoco, K. Friess, P. Izák, V. Jarmarová, M. Kačírková, G. Clarizia, Gas transport properties of Pebax®/room temperature ionic liquid gel membranes, Sep. Purif. Technol. 97 (2012) 73–82, https://doi.org/10.1016/j.seppur.2012.02.041.
[192] J.E. Bara, E.S. Hatakeyama, D.L. Gin, R.D. Noble, Improving CO_2 permeability in polymerized room-temperature ionic liquid gas separation membranes through the formation of a solid composite with a room-temperature ionic liquid, Polym. Adv. Technol. (2008) 229–236, https://doi.org/10.1002/pat.1209.
[193] P. Scovazzo, D. Havard, M. McShea, S. Mixon, D. Morgan, Long-term, continuous mixed-gas dry fed CO_2/CH_4 and CO_2/N_2 separation performance and selectivities for room temperature ionic liquid membranes, J. Memb. Sci. 327 (1-2) (2009) 41–48, https://doi.org/10.1016/j.memsci.2008.10.056.
[194] F. Pardo, S.V. Gutiérrez-Hernández, G. Zarca, A. Urtiaga, Toward the recycling of low-GWP hydrofluorocarbon/hydrofluoroolefin refrigerant mixtures using composite ionic liquid-polymer membranes, ACS Sustain. Chem. Eng. 9 (20) (2021) 7012–7021, https://doi.org/10.1021/acssuschemeng.1c0066810.1021/acssuschemeng.1c00668.s001.
[195] C. Hermida-Merino, F. Pardo, G. Zarca, J.M.M. Araújo, A. Urtiaga, M.M. Piñeiro, A.B. Pereiro, Integration of stable ionic liquid-based nanofluids into polymer membranes, Part I: Membrane synthesis and characterization, Nanomaterials. 11 (2021) 607–623, https://doi.org/10.3390/nano11030607.
[196] F. Pardo, S. Gutiérrez-Hernández, C. Hermida-Merino, J.M.M. Araújo, M. M. Piñeiro, A.B. Pereiro, G. Zarca, A. Urtiaga, Integration of Stable Ionic Liquid-Based Nanofluids into Polymer Membranes. Part II: Gas Separation Properties toward Fluorinated Greenhouse Gases, Nanomaterials 11 (2021) 1–19, https://doi.org/10.3390/nano11030607.
[197] W. Fam, J. Mansouri, H. Li, V. Chen, Improving CO2 separation performance of thin film composite hollow fiber with Pebax®1657/ionic liquid gel membranes, J. Memb. Sci. 537 (2017) 54–68, https://doi.org/10.1016/j.memsci.2017.05.011.
[198] Z. Dai, L.u. Bai, K.N. Hval, X. Zhang, S. Zhang, L. Deng, Pebax®/TSIL blend thin film composite membranes for CO2 separation, Sci. China Chem. 59 (5) (2016) 538–546, https://doi.org/10.1007/s11426-016-5574-3.
[199] G. Zarca, A. Urtiaga, L.T. Biegler, I. Ortiz, An optimization model for assessment of membrane-based post-combustion gas upcycling into hydrogen or syngas, J. Memb. Sci. 563 (2018) 83–92, https://doi.org/10.1016/j.memsci.2018.05.038.